UNIVERSITY OF PRETORIA

FACULTY OF EBIT

DEPARTMENT OF MINING ENGINEERING

Name Surname	Jan Abram Maritz	Student nr	97245586

Course code   :   PYI 890

Name of supervisor   :   Prof DF Malan

Date of submission   :   June 2015

THE EFFECT OF SHEAR STRESSES ON PILLAR STRENGTH

JAN ABRAM MARITZ

Presented in fulfilment of the requirements for the degree

MAGISTER ENGINEERING (MINING ENGINEERING)

In the Faculty of Engineering, Built Environment and Information Technology

Department of Mining Engineering

UNIVERSITEIT VAN PRETORIA
UNIVERSITY OF PRETORIA
YUNIBESITHI YA PRETORIA

DECLARATION OF ORIGINALITY

I hereby declare that this project is my own unaided work and I have referenced all the sources I have used. It is being submitted in fulfilment of the requirements for the degree Magister Engineering (Mining Engineering) at the University of Pretoria, Pretoria. It has not been submitted before for any degree or examination at any other university. This document represents my own opinion and interpretation of information received from research or / and interviews. I thus accept the rules of assessment of the University and the consequences of transgressing them.

_____

Jan Abram Maritz

23 June 2015

Abstract

The effect of shear stresses on pillar strength

Jan Abram Maritz

Supervisor: Prof DF Malan

Department: Mining Engineering

University: University of Pretoria

Degree: Magister Engineering (Mining Engineering)

In mining, the loading environment on pillars is highly complex with combinations of normal and shear stresses. It is also understood that with an active and working face, constant redistribution of stresses will occur to maintain stress equilibrium.

A rock sample subjected to uniaxial loading conditions can fail in either indirect tension or shear. A pillar in the mining environment would react in much the same way. However, as "confinement" is created at the pillar and hanging wall or footwall contacts, shear failure is commonly observed in failed pillars.

A number of theories and equations have been derived trying to correctly calculate pillar strength in an underground design. These early attempts argued that the strength is only governed by the width of the pillar in relation to the mining height as well as a certain pillar "strength" constant (K-value). Both the coal and hard rock industries have adopted this design methodology for determining pillar sizes, all with relatively good success. Numerical analysis has shown that complex stress interaction occur between irregular shape pillars when not superimposed, highlighting the fact that superimposing of pillars should be treated with caution. As the stress environment changes, so does the loading on the pillar with preliminary results showing that the strength of the pillar will also be affected in the presence of shear stress.

The research presented in this document shows that loading conditions that may affect pillar strength should be considered and detailed and special treatment should be given during the design in cases where shear loading may exist.

ACKNOWLEDGEMENTS

I would like to acknowledge the following individuals who created the opportunity to conduct this research. Their guidance and support throughout this period of study is greatly appreciated;

- Professor Malan as supervisor of this research study and co-author of various publications.
- Professor Webber-Youngman as Head of the Department Mining Engineering and co-supervisor.
- Mr K le Bron for his assistance with the inelastic modelling.
- My wife and family, for supporting me during many nights and countless hours of research.

CONTENT

LIST OF FIGURES

LIST OF TABLES

LIST OF APPENDICES

LIST OF ABBREVIATIONS

APS	Average Pillar Stress
CMRCC	Coal Mines Research Controlling Council
COMRO	Chamber of Mines Research Organization
CSIR	Council for Scientific and Industrial Research
DRMS	Downgraded Rock Mass Strength
ESS	Excess shear Stress
FoG	Fall of Ground
FoS	Factor of Safety
K-value	Pillar strength constant
mbs	Meter below surface
PLAN	Pillar Loading Alteration Number
RCF	Rockwall Condition Factor
TEXAN	Tabular Excavation Analysis
UCS	Uniaxial Compressive Strength
w:h	Width-to-height

1 INTRODUCTION

The key aspect of any mining operation is to maximise extraction for optimum profit. In any pillar design layout, this opportunity is compromised as revenue is left untouched in the pillars, designed to ensure a safe working environment. Optimising of these pillar designs, or ultimately, substitution of pillars with artificial support, had become a big driving factor for new and established mines alike.

Historically, pillars were designed based on trial and error, and it was not until the early 20th century that the approach changed to be more scientific. An argument was made that the strength of pillars should exceed the load acting on the pillar. In this argument, determining the actual strength of a natural material and then estimating the load that will be applied to the pillar proved to be not so easily attainable.

As rock-related accidents and fatalities had been a major concern for the industry, strata control and rock engineering received increasingly more attention, especially since the disaster at Coalbrook Mine during the 1960s. Here, 437 mine workers lost their lives after a massive pillar collapse trapped them underground. Apart from the various coal-dust explosions (which are not rock-related disasters), the Coalbrook catastrophe has to be one of the largest single event rock-related disaster the mining industry has ever seen.

This led to a period where research in the coal industry enjoyed good funding while trying to fill the knowledge gap that existed in the design of safe workings with regard to room-and-pillar operations. Van der Merwe (2006), on p. 857, states that the "*strength of nominally square internal pillars is the one issue that received the most attention, but the strength of barrier pillars, overburden behaviour and loading systems is still largely unknown*".

1.1 Introduction to the research

Many factors influence the complex loading environment of any mine. It is also understood that with an active and advancing face, consistent redistribution of stresses occur to maintain equilibrium. It could therefore be expected that a pillar,

1

which is planned and designed to only experience normal loading conditions, will not always be in this "ideal" environment, and during some stages of mining, shear stresses would also form part of the loading system.

In the past, most of the fundamental research was conducted for the coal industry and especially on pillars and pillar designs. The reason for this focused field was mainly because the research funding was sourced from the coal mining industry. The Coal Mines Research Controlling Council (CMRCC) was formed with the Council for Scientific and Industrial Research (CSIR), and the Chamber of Mines Research Organization (COMRO) also channelled its priority into coal pillar design (Malan and Napier, 2011).

The Coalbrook disaster report (dated more than 50 years ago) commented on the uncertainty in determining the strength of pillars in a room-and-pillar layout. This uncertainty in the strength, together with the loading environment, is still not fully understood.

1.1.1 History and current understanding of pillar strength and loading system

This subsection will explain the history and progression in the understanding of pillar strength and loading system; it will also show that very little effort was focused on the influence of shear movement and stresses on pillars. Areas of research included failure modes in rock samples, the influence of direction of loading in laminated rock samples, pillar strength as a function of the pillar dimensions, and the loading environment of the pillar system.

Failure modes

When a rock sample is placed under uniaxial loading conditions, failure will occur in either one of the possible two modes, either in the form of indirect tension or shear. When the ends have a low friction angle and the sample can expand based on the sample's Poisson's ratio, indirect tension failure is observed. Shear failure occurs when the ends (or complete sample) are confined in some or other way, e.g. friction between platen and sample (Jaeger, Cook and Zimmerman, 2007).

2
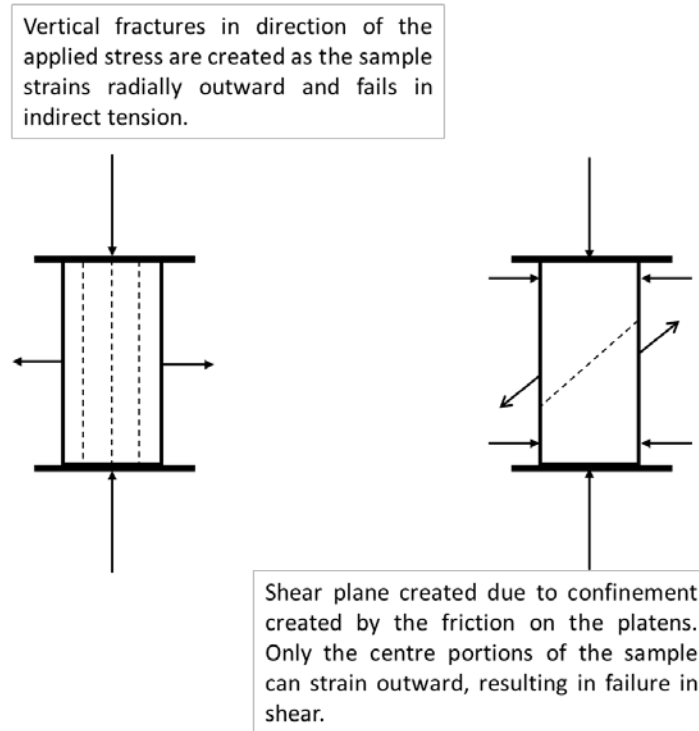
Figure 1-1: Failure modes in uniaxial compression

For a pillar underground, the same failure modes apply. However, as "confinement" is created at the pillar and hanging wall or footwall contacts, shear failure is commonly observed in failed pillars.

Scaling of pillars is also observed, yet this only applies for the pillar skin, and complete failure due to scaling is uncommon.

Loading direction

For a laminated rock sample, as the loading direction changes – measured relative to the direction of schistosity – the uniaxial compressive strength greatly differs as the angle changes (Salcedo, 1983). Figure 1-2 indicates the varying compressive stress levels for changing loading angle.
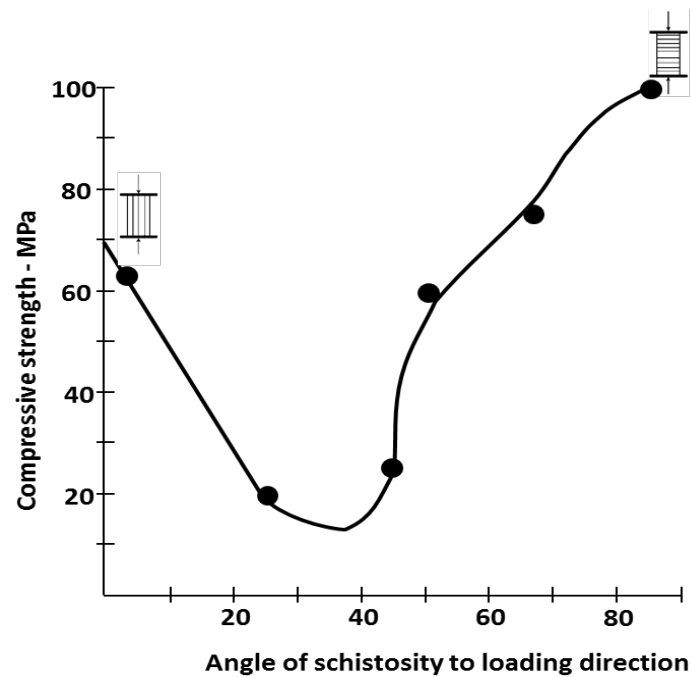
Figure 1-2: The effect of loading direction on the strength of graphitic phyllite (after Salcedo, 1983)

Hence, if the loading is not perpendicular to the pillar with a horizontal state of schistosity as predicted by the tributary area theory, the strength of the investigated pillar is suggested to be less than initially anticipated. The current understanding of the load is that it always acts vertically and perpendicularly to the bedding planes.

Pillar strength

Dating back as far as 1962, a number of equations have been derived, each trying to correctly calculate pillar strength. Initially, it was argued that the strength is only governed by the width of the pillar in relation to the mining height (Bieniawski, 1968) as well as a certain pillar "strength" constant (K-value). These strength formulae have been adjusted and revised several times during the few years which followed by various researchers adopting various methodologies. The K-value that is applied in these formulae is derived mainly from an adjusted or downgraded uniaxial compressive strength value for the particular rock type. As the nature of the intact rock is so complex, the value used in coal pillar designs ranged between 1.5 and 7.2 MPa, with those used in hard rock ranging between 33 and 54 MPa. With a change in the K-value, the power function of the width and height of the pillar was also adjusted so as to obtain a best fit to the investigated results.

Since 1967, the most frequently used pillar strength calculation equation has been the Salamon and Munro (1967) equation, which is proven by the resultant decrease in pillar collapses since using the equation (equation 1-1). Salmon and Munro had concluded that the pillar strength can be expressed as a power function that includes the pillar dimensions.

$$Strength_{(coal)} = k \frac{w^{0.46}}{h^{0.66}}$$

[1-1]

where *K* represents the pillar strength constant (the downgraded uniaxial compressive value), *w* represents the effective width of the pillar, and *h* represents the pillar height.

The hard rock industry has adopted this formula, together with adjustments to the constants and with relatively good success.

Pillar loading

After the strength of a pillar, the next parameter that should be determined is the loading on the pillar and pillar system. This loading is generally only calculated by means of the tributary area theory (TAT), which assumes the weight of the overburden before mining and which is to be carried by the pillar after mining. This can easily be calculated when a regular layout is assumed, whereby the pillar is square and the mining areas are constant. This would be a safe approach to take, since TAT predicts the maximum load acting on the pillar, assuming an infinitely large area has been mined, given the specific parameters.

Being a conservative approach, TAT overestimates the load on internal pillars as well as on barrier pillars. For the internal pillars, the abutment of adjacent mining areas and pillars' abilities to change the loading environment are ignored. In the case of the barrier pillars, the calculation assumes all internal pillars to be in a failed state and unable to add any support resistance to the system, which is not the case in this study.

TAT is limited to the vertical stress (for a flat deposit) due to the rock density and the earth gravitational forces and does not cater for any change in orientation of the applied stresses. Hence, on inclined deposits, the TAT represents the force that is normal to the pillar and not the force that is acting vertically down on the pillar.

With the TAT loading value now not parallel to the vertical load, it raises the question of the possible existence of a stress environment other than the normal stress condition acting on the pillar.

Another means of obtaining the load would be to conduct numerical modelling based on the layout of the proposed block of ground. By this, a complete stress regime acting on the pillar could be calculated based on the input parameters and influence from previously mined-out areas.

Salamon and Oravecz (1976) indicated by means of numerical modelling that stresses interact between the mining level and various benchmarks relative to the mining area. Based on their findings, they derived their 0.75C rule. This rule suggests the superimposing of pillars when multi-seam mining is to be done with a middling of less than 75 per cent of the distance between pillar centres.

Current design methodologies largely exploit the TAT, since the environment of application is generally flat, and in areas where multi-reefing applies, interaction is rarely a concern.

1.2 Project background

Considering the current assumption to pillar loading, the strength varies as the loading direction changes with the possible influence that multi-reef mining could have on the stress environment. It appears that the actual loading condition and orientation, and ultimately, the calculation of pillar stability in the underground environment are far more complex than what is generally accepted.

The assumption is that inclined reef planes mined on a pillar method or multi-reef pillar environments might be subjected to an additional stress component (shear stress) overlooked in the past when the strength equations were derived.

Following the success in the coal industry based on the application of the Salamon and Munro (1967) equation for coal, the hard rock industry tried to copy the success by adjusting the power factors for the pillar width and height in order to obtain a better fit to the available data. Research on hard rock pillar strength criteria started as early as 1972 (Hedley and Grant, 1972), and it again saw some variations in the parameters included and values used as benchmarks, as research continued.

The necessary research was unfortunately never conducted to develop and calibrate a formula for South African hard rock (platinum or gold) conditions. Instead, the Hedley and Grant (1972) formula developed for the Canadian uranium mines was adopted. Only the K-value was modified to reflect local rock strengths. This approach seemed to work well, and over the years, it became firmly entrenched. It will not be incorrect to state that it is currently the "industry-accepted" method for designing pillars in shallow hard rock mines in South Africa. A close examination of the original Hedley and Grant (1972) publication reveals that it is based on a large number of assumptions; however, the applicability of this formulation to design hard rock pillars in the Bushveld Complex in South Africa becomes highly questionable. It has nevertheless been used to design a large number of room-and-pillar layouts in the country with an appropriate modification of the K-value.

The most recent research pertaining to hard rock pillars is the work done by Watson, Rydert, Kataka, Kuijpers and Leteane (2008). With their research, they derived a formula to determine the value of the power parameters to best fit the Merensky pillars based on a back analysis on failed pillars. This formula has not yet been implemented nor tested by the mining industry.

The inherent dangers of using empirical design formulae for rock masses in which they were not originally designed for is the possibility of large-scale failure, such as the Coalbrook accident. Three case studies of mine collapses in South African were discussed by Malan (2010) in his keynote lecture on whether pillars can be designed with confidence in hard rock mines (Malan, 2010). The failure in all three cases was facilitated by the presence of weak partings (sometimes with clay infilling), which substantially weaken the pillars. Figure 1-3 illustrates such a weak parting at the pillar/hanging wall contact. The original empirical formulae were developed for different rock types and the application of these formulae outside the limits for which they were developed led to the large-scale collapses.

The issue of not being applicable to all scenarios could even be more aggravated by adding shear forces which were also not included in the original formula.

Figure 1-3: Scaling facilitated by a weak contact at the pillar/hanging wall contact

It is well known that a weak interface between the hanging wall and pillars may reduce pillar strength significantly. Wagner (1980) commented on this issue and noted that the strength of the pillar will be strongly affected by the friction and cohesion in the contact plane. Peng (1978) illustrated in a series of laboratory experiments prepared from the same rock type that the strength can vary by as much as 100% depending on the conditions at the interface of the rock-sample testing machine. Similar results were reported by Wagner (1980). His tests showed that the presence of a soft layer at the rock/platen interface not only reduces the strength of the rock sample but also changes the mode of failure of the specimen. The mode of failure changes from "hourglassing" and scaling on the edges of the higher friction angles to axial splitting of the lower contact friction angles.

In all the instances in determining the pillar strengths, two main parameters tend to drive the design strength. These are the pillar strength constant (K-value) and some variation on the ratio of the width to height of the pillar. All of these equations mainly assume that a single reef is being mined and that these reefs are flat or near horizontal.

The hypothesis is that inclined reef planes mined on a pillar method or multi-reef pillar environments might be subjected to an additional stress component (shear stress) overlooked in the past when the strength equations were derived.

8

1.3 Problem statement

As the loading environment of underground pillars is far more complex than what the derived strength equations assume, an investigation in required into the existence of shear stresses on pillars and the effect of these stresses on pillar strength. After confirmation of the stress environment and the influence on the pillar system, a procedure is required to provide guidelines for estimating factor of safety adjustment values for environments experiencing shear stress conditions.

1.4 Objectives

The research project is set out to achieve the following objectives:

   i.   Critically appraise the current pillar strength formulae.
   ii. Confirm the possible presence of shear stresses in a single reef room-and-pillar design.
   iii. Establish the possible effect shear stresses could have on the pillar strength.
   iv. Provide a guideline to be used when estimating the pillar strength factor.

1.5 Scope of the study

The study will be focused on shear stress around a room-and-pillar layout and especially the pillar area. Weak planes and other geological discontinuities will not necessarily be evaluated, except in numerical models where clear mention is made of such planes.

The numerical modelling will be based on typical room-and-pillar hard rock parameters. The comments would be made based on the findings from the layout(s) modelled; thus, the method more than the rock properties are to be taken as a guideline of where the recommendations would be applicable.

Numerical modelling will be done on an elastic, homogeneous model, whereafter an inelastic model would follow.

The study in no way considers cost and/or downstream effects associated to changing of pillar dimensions and extraction ratios. The recommendations will only be based on establishing a mining environment which is from a rock engineering judgment safe to mine.

1.6 Methodology

First, a literature survey was undertaken to gain an understanding of how the pillar strength equations were derived and used in the mining industry, especially in a room-and-pillar layout. This would also lead to an understanding into which parameters are included in the calculations of the intricate part of the pillar design methodology. The literature would highlight other factors that might be playing a significant role in the strength of the pillar in these layouts. This study would assist in the appraisal of the current and commonly used formulae.

The occurrence of shear stresses in pillars will be studied by using an elastic boundary element numerical modelling code in order to validate the presence of shear stresses in proposed mining environments.

The findings from the elastic model will further be analysed by means of an inelastic model in order to determine the influence shear stress has on pillar stability.

Results from the numerical models were used to evaluate the effect of the shear stresses on the pillar strengths and to derive a guideline to be followed in pillar designs where shear stresses are present. The aim is to increase the confidence in the strength criteria of the pillar system in totality.

1.7 References

Bieniawski, Z.T. (1968). The effect of specimen size on compressive strength of coal. Int. J. Rock Mech. Min. Sci., vol 5, pp. 325-335.

Hedley, D.G.F. and Grant, F. (1972). Stope-and-pillar design for Elliot Lake Uranium Mines. Bull. Can. Inst. Min. Metal., pp. 37-44.

Jaeger, J.C., Cook, N.G.W. and Zimmerman, R.W. (2007). Fundamentals in rock mechanics.

Malan, D. (2010). Keynote Lecture - Pillar design in hard rock mines: Can we do this with confidence? In P. Hagan, & S. Saydam (Ed.), Second Ground Control in Mining Conference, (pp. 15-30). Sydney.

Malan, D.F. and Napier, J.A.L. (2011). The design of stable pillars in the Bushveld Complex mines: a problem solved? The Journal of The Southern African Institute of Mining and Metallurgy, vol 111.

Peng, S. (1978). Coal mine ground control. pp. 181-182. New York: John Wiley and Sons.

Salamon, M.D.G. and Munro, A.H. (1967). A study of the strength of coal pillars. The Journal of The Southern African Institute of Mining and Metallurgy, pp. 56-67.

Salamon, M.D. and Oravecz, K.I. (1976). Rock Mechanics in Coal Mining. P.R.D. Series No 198.

Salcedo, D. (1983). Macizos Rocosos: Caracterización, Resistencia al Corte y Mecanismos de Rotura. 25 Aniversario Conferencia Soc. Venezolana de, (pp. 143-172). Caracas.

Van der Merwe, J.N. (2006). Beyond Coalbrook: What did we learn? The Journal of The Southern African Institute of Mining and Metallurgy, vol 106, pp. 857-868.

Wagner, H. (1980). Pillar design in coal mines. The Journal of The Southern African Institute of Mining and Metallurgy, pp. 37-45.

Watson, B.P., Rydert, J.A., Kataka, M.O., Kuijpers, J.S. and Leteane, F.P. (2008). Merensky pillar strength formulae based on back-analysis of pillar failures at Impala Platinum. The Southern African Institute of Mining and Metallurgy, vol 108, pp. 449-461.

2 LITERATURE SURVEY

A discussion on mining methods that exploit pillars as an integral part of the local and regional support strategy will lead the discussion on the pillar design parameters. The discussed methods include room-and-pillar and sequential grid. These two methods could cover a broad spectrum of reef dip angles from horizontal to steep (0° to 45°) as well as multi-reef mining environments.

Ample literature can be found on pillar design, formula establishment, layout optimisation and strength estimation back analysis. Although most of these build on the foundation set by previous work done in the field, a few main parameters could be defined: pillar strength, pillar load and the safety factor. These parameters are listed and summarised below and elaborated on in the following chapter.

i. Pillar strength: Size and shape play a significant role in the strength of a rock sample or pillar. As the ratio of width to height increases, it is assumed that the increase in volume supplies some sort of confinement, increasing strength.

Various other factors (e.g. jointing) also play a role in affecting the pillar strength. These factors are reported and highlighted below.

ii. Pillar loading: A complex loading environment exists around the mining faces and on the pillars as a support system. The direction of stresses, the magnitude of these stresses, and the presence of other structures all influence the resultant load on the supporting pillar. These load environments are either calculated based on empirical models or simulated by numerical analysis.

iii. Safety factor: Optimisation of the layout based on the ratio between the strength of and load exerted on the pillar system. As the safety factor is dependent on the accuracy of the pillar strength and load calculations, optimising the layout is greatly dependent on the first two parameters.

2.1 Existing mining layouts with pillar support

2.1.1 Room-and-pillar layout design

The common practice on flat, shallow to intermediate depth deposits in hard rock and coal with limited restriction to the mining width is to exploit the mineral resource by means of a room-and-pillar layout. This entails mining the deposit with a series of development ends and leaving behind areas of unmined resource (pillars). The design methodology is mainly based on that of a Factor of Safety (FoS) approach, where the strength of the pillar is compared to the effective load on the pillar. Equation 2-1 depicts the ratio of FoS.

$$\text{FoS} = \frac{\text{Pillar Strength}}{\text{Pillar Load}} \qquad\qquad [2\text{-}1]$$

Pillar safety factors of 1.6 are applied in coal engineering designs, and values at least as high as this are appropriate for hard rock non-yield pillar designs (Jager and Ryder, 1999). The value of 1.6 was selected for coal mines as it was found that this value corresponds to a probability of failure of 0.001. As discussed by Ryder and Jager (2002) page 279: "*For lack of anything else more substantial, the figure of 1.6 is generally used in hard rock pillar design in South Africa*". Owing to the uncertainty in pillar strength, in some cases, it may be prudent to use values as high as 2 for the FoS. As the planned layouts in general include substantial regional pillars and the pillar strength formula being conservative, a FoS of 1.5 to 1.6 is deemed to be acceptable for most projects.

The elements influencing this safety factor include the pillar height (generally associated to the mining height), the effective pillar width, a rock-specific strength factor, extraction ratio, and an applied load. Each of these will be discussed in the subsequent subsections below.

Mining environment

The room-and-pillar method is a common and widely used method for both coal and hard rock mines at shallow depth. The strategy aims at controlling the tensile zone on a regional basis so as to prevent large-scale mine collapses as in the case of Coalbrook and prevent local instability in the working areas. Design for regional stability pillars is such as to limit the spans to less than 50 per cent of the depth, with

pillars with a width-to-height ratio of not less than 10. This should ensure a long-term stable layout and design.

The method mainly exploits trackless machinery to extract the ore, leaving unmined ground (pillars) of predetermined dimensions and resulting in extraction ratios varying from as low as 40 per cent up to 80 per cent depending on depth and rock mass characteristics. A basic layout of a room-and-pillar design is shown in Figure 2-1 below depicting local, regional and main development protection pillars.
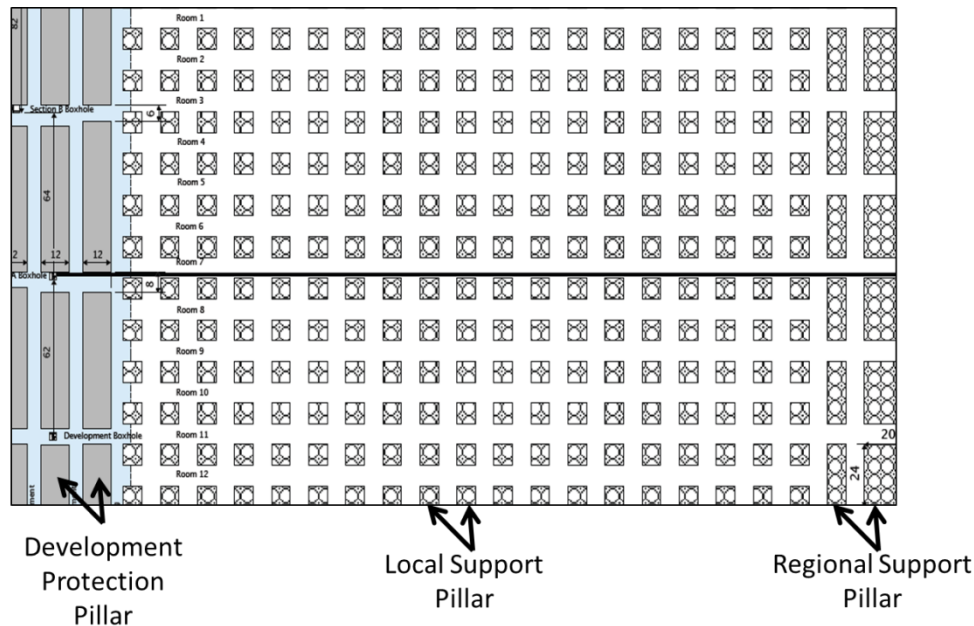
Figure 2-1: Basic layout for room-and-pillar mining method indicating regional stability pillar as well

As trackless equipment is used in some cases, limitations are set to the dip of the orebody, which should be less than 8º for effective utilisation. This is not to say that steeper dipping ore bodies cannot be mined on this method; however, adaptations should be made to the layout, and apparent dip layouts could be considered or else productivity of the equipment will be lost.

Ore handling and transportation to the surface metallurgical plant could be done via vertical shaft system(s), declines, trucking or continuous systems such as conveyor belts. The ore supply line only requires proper protection from Falls of Ground (FoG) and long-term stability.

14

In the South African context, the commodities exploiting the reserve by means of room-and-pillar layouts include platinum (Western and Eastern limb of Bushveld Igneous Complex), coal, nickel and manganese, to name but a few.

2.1.2 Sequential grid

In a sequential grid extraction layout, the regional pillars are spaced based on regular intervals so as to ensure low ERR levels and pillar stress (Applegate, 1997). Figure 2-2 depicts the basic layout of a typical sequential grid method. Development drives (normally 120 m deep to avoid stress interaction from the reef horizon) are blasted along the orebody strike, with cross-cuts developed at predetermined intervals to intersect the reef plane. As the reef horizon is reached, a raise is developed on reef (on dip), whereafter mining commences, extracting the block of ground between the pillars in either a strike advance direction or dip advance. If a strike advance approach is taken per stope, the panels are mined in an overhand fashion (the bottom faces leading the top faces of the raise) with the macro layout being mined and scheduled to achieve an underhand macro layout. A schematic (Handley, De Lange, Essrich and Banning, 2000) is shown in Figure 2-2.
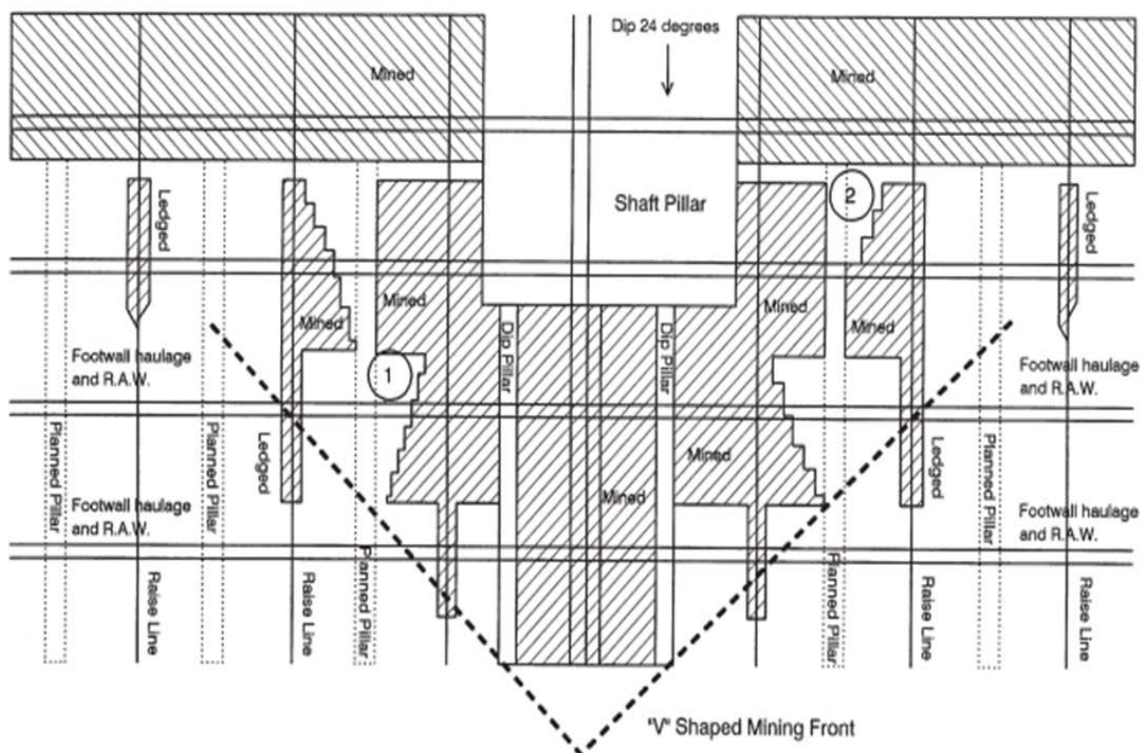
Figure 2-2: Basic layout of sequential grid mining method (after Handley et al. (2000))

This method is commonly applied in a dipping orebody that makes use of conventional hand-held machinery for drilling and blasting.

The orientation of the stability pillar could also be along strike, as in the case of long wall mining in the coal industry, where a coal plough or shearer advances along strike, or in hard rock mining, where the development follows the stoping faces in de-stressed areas.

2.2 Pillar strength

Kaiser, Kim, Bewick and Valley (n.d.) commented that the commonly adopted pillar strength estimation methodologies involve:

- Empirical formulae that are based on the best-fit equations related to observed pillar performance data.
- Use of numerical stress modelling tools such as:
  - Continuum numerical stress modelling and various rock mass strength criteria.
  - Displacement discontinuity methods.
  - Use of discrete numerical stress modelling codes to attempt to simulate the progressive failure of pillars.

Kaiser et al. (n.d.) also commented that the dataset is limited, even with a number of case studies recorded, and that no datasets exist for areas deeper than 1000 metres below surface.

Research into rock and pillar strengths dates as far back as the early 1940s (Greenwald, Howarth and Hartman, 1941). This early research was the predecessor to, among others, the well-known and applied Salamon and Munro formula that followed.

The pillar strength formula derived by Salamon and Munro (Salamon and Munro, 1967) was based on back analysis of stable and collapsed coal pillars. This commonly used formula is given by:

$$Strength_{(coal)} = 7.2 \frac{w^{0.46}}{h^{0.66}}$$

[2-2]

where *w* is the effective pillar width, *h* is the pillar or mining height, and the 7.2 MPa multiplier reflects the best-fit values fitted strength of 1 m cube coal. The 'power-law' formulation from equation 2-2 predicts only that the fitted strength value, pillar width and mining height are factors governing the strength of a pillar.

An alternative approach to the power formula was described by Bieniawski (1992) in a 'linear' form, which expresses the strength as a function of the width:height (w:h) ratio of the pillar and an *in situ* strength of the rock mass. Equation 2-3 depicts the pillar strength as a function of these parameters, where K is the strength of *in-situ* coal (6 MPa).

$$Strength_{(coal)} = K\left(0.64 + 0.36\frac{w}{h}\right)$$

[2-3]

A variation of equation 2 has been part of the design methodology for hard-rock pillar designs; however, the general applicability is still unclear. Hedley and Grant (1972) documented a back analysis on uranium pillar from a mine in Canada suggesting the same formula with a different set of constants. These pillars had a w:h ratio of around 2.5. The Hedley and Grant (1972) formula is given in equation 2-4.

$$Strength_{(uranium\ ore)} = K\frac{w^{0.5}}{h^{0.75}}$$

[2-4]

In the South African context, the values are commonly used in the design with values for the *in-situ* strength (K) ranging from 35 MPa to 60 MPa depending on the rock properties. Through the years, practical experience has indicated that a value of one third of the UCS of the rock mass is a good start for initial designs for pillar layouts. The typical rock strengths in the hard rock mines range between 100 and 180 MPa, hence, the range stated above.

The 'power-law' equations for both coal and hard rock imply that the strength of the pillar will decrease as the pillar volume increases (cube dimension). This can be seen in the two graphs in Figure 2-3.
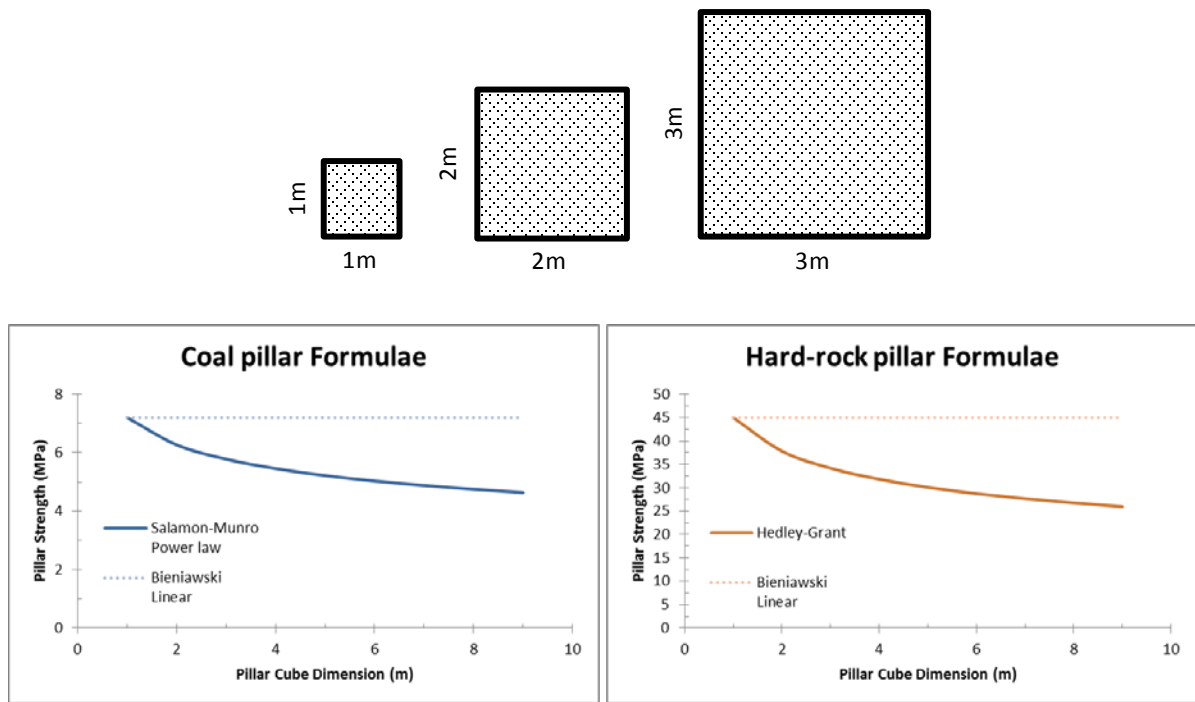
Figure 2-3: Pillar strength versus pillar cube volume

When the analysis is made on a study based on changing pillar width resulting in a volume increase, the opposite trend is observed. As the width increases at a constant mining height (1.0m), the pillar strength increases, suggesting a "stronger" pillar.
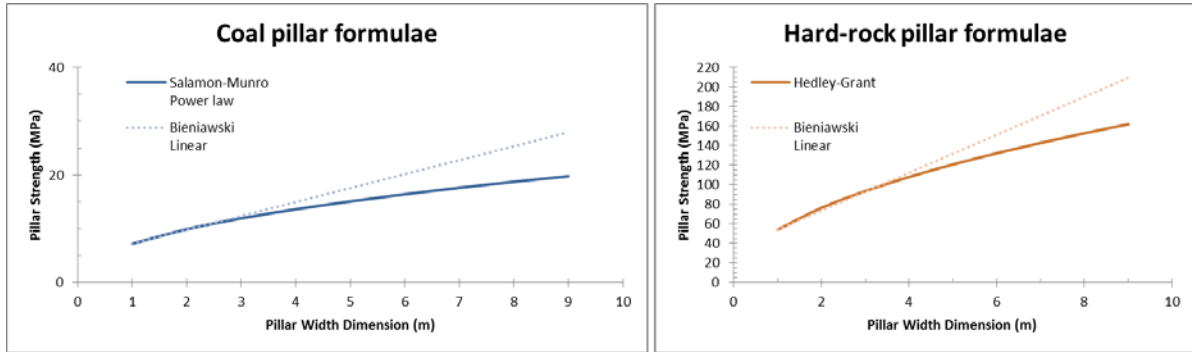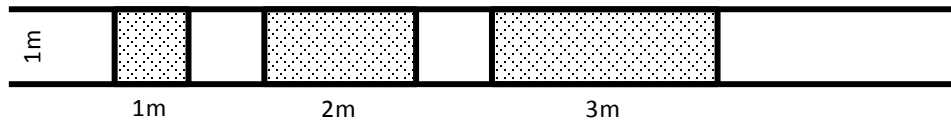
Figure 2-4: Pillar strength versus pillar volume (changing width with constant height)

The w:h ratio and power-law formula is considered acceptable up to a ratio of 5:1, whereafter the squat pillar equation (equation 2-5) becomes applicable (Madden, Canbulat and York, 1998).

$$\text{Squat Pillar Strength} = k \frac{R_0{}^b}{V^a}\left\{\frac{b}{\varepsilon}\left[\left(\frac{R}{R_0}\right)^\varepsilon - 1\right] + 1\right\} \qquad [2\text{-}5]$$

where R_0 is the critical width-to-height ratio

    R is the pillar width to mining height ratio

    ε is the rate of strength increase

    a is a constant 0.0667

    b is a constant 0.5933

    V is the pillar volume

ε is suggested to be taken as 2.5 and R_0 as 5.0 (Salamon and Wagner, 1985).

Equation 2-5 can therefore be rewritten as:

$$\text{Squat Pillar Strength} = \frac{0.0786}{V^{0.0667}}\{R^{2.5} + 181.6\} \qquad [2\text{-}6]$$

When plotting the pillar strength as a function of the volume and applying the squat formula for w:h ratios of greater than 5, the trend in Figure 2-5 is observed.
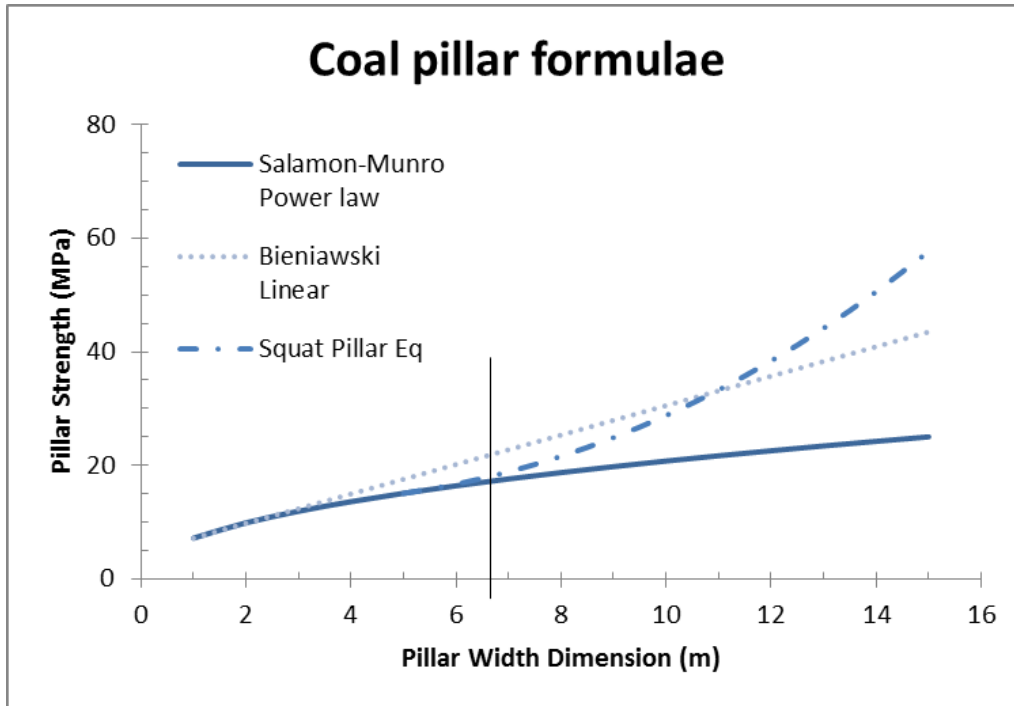
Figure 2-5: Pillar strength versus pillar volume (changing width at constant height)

As the power-law formula predicts a decrease in strength at w:h ratios that are greater than 5, the squat formulation predicts an increase with an increase in pillar width.

Similar to the discussion above with regard to the strength of pillars, Esterhuizen, Dolinar and Ellenberger (2011) established a strength equation (equation 2-7) for underground stone mines in the United States.

$$S = 0.65 \times UCS \times LDF \times \frac{w^{0.3}}{h^{0.59}} \qquad [2\text{-}7]$$

where *UCS* is the uniaxial compressive stress, *LDF* is the large discontinuity factor (0-1, where no discontinuity depicts 1), *w* is the width of the pillar and *h* is the height.

What is noteworthy in this formula is that the design strength used was revised as 65 per cent of the UCS. In their information circular, Esterhuizen et al. (2011) used the base equation (equation 2) with adjusted values for α and β, and made further adjustments with regard to the presence of large discontinuities, rectangular pillars and other geotechnical conditions.

By plotting this formula on a graph with changing widths and constant height, one can observe the same trend in the plots; still, the values are significantly higher, which is directly as a result of the much higher K-value (65% of UCS) used in

equation 7 compared to the value used in the hard rock mines of South Africa (33% of UCS).
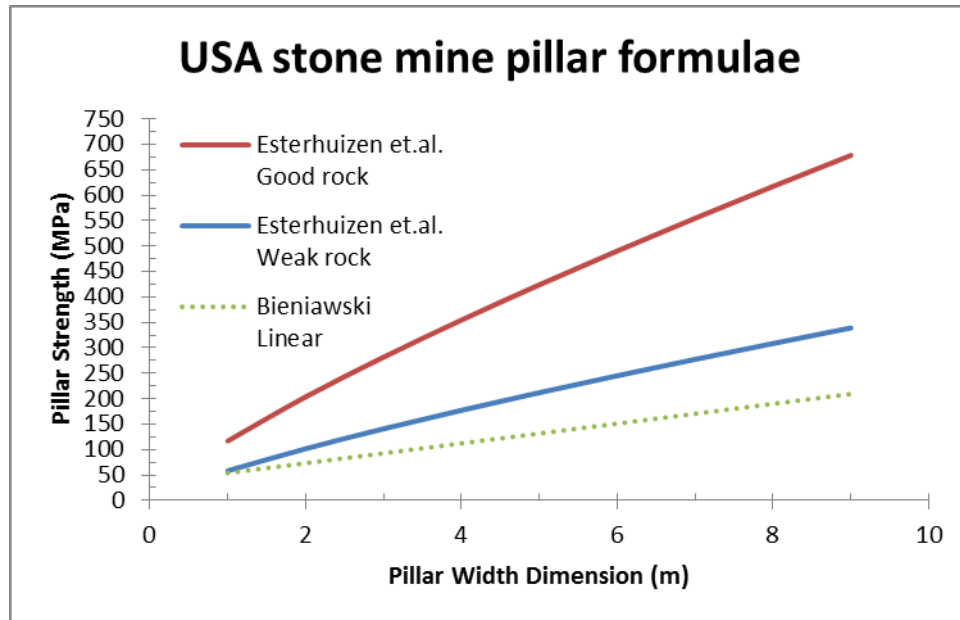
Figure 2-6: Pillar strength versus Pillar volume (changing width at constant height based on Esterhuizen equation)

It therefore appears that the used formulae in the current environment merely include the width and height of the pillar together with the rock strength when calculating the strength of a pillar.

2.2.1 Factors affecting pillar strength

As stated by York, Canbulat and Jack (2000), the strength of pillars is influenced by many factors, with the strength of the rock mass being the initial driver of the strength. They also suggest that other factors should be taken into account when deriving the strength of the pillar. The list of factors includes:

i. jointing within the pillar
ii. roof and floor conditions
iii. conditions of the contacts
iv. dip
v. total loading system
vi. virgin horizontal and vertical stress ratio (k-ratio)
vii. creep and time-dependent deformation

viii.   length to width ratio

ix.   pillar dimensions (inclusive of the pillar width and mining height)

This list could be divided into four groups of parameters, of which one would be the rock material characteristics (i – iii), the deposit characteristics (iv), the loading environment (v – vii) and, finally, the actual pillar design and shape (viii – ix).

York et al. (2000) advised on the loading to samples (or pillars) in a normal fashion, where the load is perpendicular to the rock surface. They also mentioned that of the two empirical formulae used, Salamon and Munro (1967) and Bieniawski (1968), the Salamon and Munro are more strongly based on *in-situ* data even though the pillar strength reduction factors have not explicitly been catered for in their analysis. It is further suggested that the empirical equation shows volume strength decay as a function of the pillar system factors rather than the properties of the rock mass material.

In earlier work done by Madden et al. (1998) and Roberts, Van der Merwe, Canbulat, Sellers and Coetzer (2002), the same was concluded. Madden's list of factors that influence the strength of coal pillars is as follows:

i.   factors including seam strength

ii.   surrounding strata properties

iii.   geology, discontinuities

iv.   loading rate

v.   time

vi.   weathering

If any of these factors becomes dominant, the use of the current pillar design methodology will result in incorrect values of pillar strength since the pillar strength formula does not take all these factors into account. Therefore, any deviation of the above-mentioned factors from the current empirical range must be given special treatment, which will yield more accurate results.

2.2.2 Pillar vs. Rock mass strength

Through the years, various empirical methods evolved trying to estimate the strength of a rock mass, with a set of rock mass properties exposed to a particular stress environment.

According to Hoek and Brown (1980), it was found that the peak tri-axial stress for a sample is driven by the magnitude of the confinement. The Hoek and Brown failure criterion is one of the most commonly used empirical formulae and is given in equation 2-8.

$$\sigma_1 = \sigma_3 + \sqrt{m_b \sigma_c \sigma_3 + s{\sigma_c}^2} \qquad [2\text{-}8]$$

where σ_3 is the confinement stress, *m* and *s* are rock constants depicting the rock mass quality and σ_c is the uniaxial compressive stress of the intact rock.

In their report on the strength of hard-rock pillars, Martin and Maybee (2000) commented that empirical formulas derived to calculate pillar stability suggest that the strength is directly related to the w:h ratio of the pillars and that pillars with a w:h ratio greater than 2.0 seldom fail. They further concluded that the conservative Hoek-Brown criteria overestimate the strength of hard-rock pillars due to a cohesion-loss process.

The essence of the Hoek and Brown criterion is based on the attributes of a rock sample that will increase in axial strength when a confining stress is applied to the sample. Hence, it can be concluded that the strength of a pillar will be dependent on the confinement of the rock at the pillar core.

2.3 Pillar load

The second parameter considered in the design of a pillar layout would be the pillar loading.

The stress acting on the pillar increases as the load of the overburden stays constant with a reduction in area. This can also be described with the general equation for stress calculation:

$$\text{Stress} = \frac{\text{Force}}{\text{Area}} \qquad [2\text{-}9]$$

Calculating the load on pillar can be done by either modelling the mining layout with an appropriate numerical modelling package or alternatively calculating the expected load using standard equations.

Pillar loading on a typical room-and-pillar layout is commonly simplified by using the tributary area theory (TAT). This theory assumes that the weight of the overburden immediately above the area is to be carried by the pillar after mining. This applies where the size of the pillar layout is uniform and where the depth to the extraction horizon is less than the panel width. This implies a large area when evaluating layouts at depths. The schematic in Figure 2-7 illustrates the discussion.
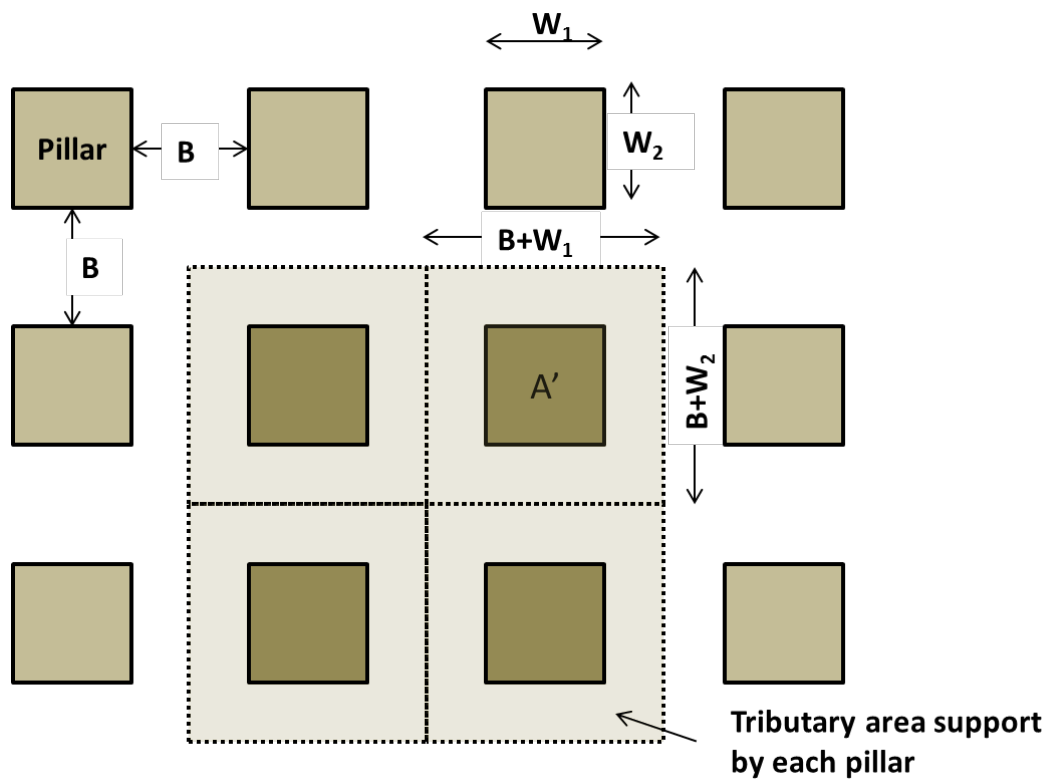
Figure 2-7: Tributary area schematic (plan view)
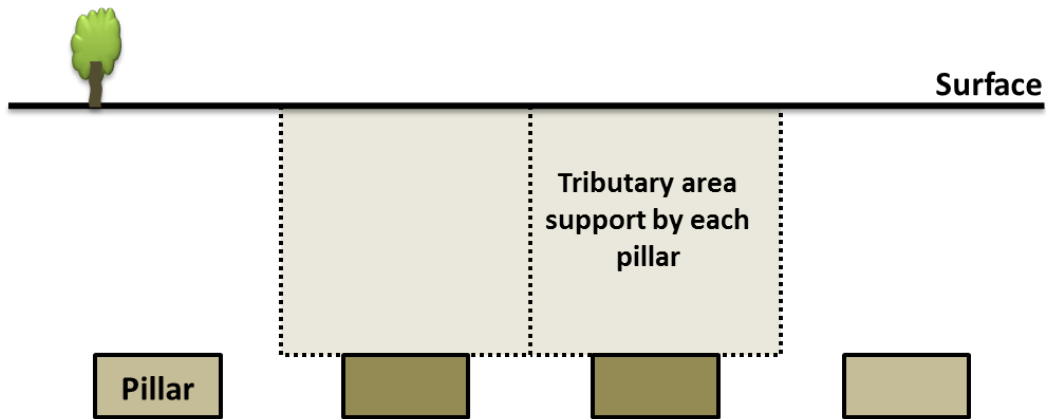
Figure 2-8: Tributary area schematic (section view)

The load is calculated (equation 10) as a function of the unit weight of the overburden (ρ), depth below surface (H), pillar centres (C), and the width of the pillar (w).

$$\text{Load} = \frac{\rho H C^2}{w^2} \text{ Pa} \qquad\qquad \text{[2-10]}$$

This theory also assumes that the extraction level is flat; hence, the load applied to the pillar is vertical, orientated perpendicular to the pillar surface area. If the extraction is at an angle (dip), the load applied to the pillar is still assumed to be perpendicular, yet not vertical.

TAT is generally used in the mining industry to calculate the empirical value for loading on the pillar based on the extraction ratio associated to that individual pillar. This assumes that all the pillars in a room-and-pillar layout are loaded in the same proportion (equal load) of the overlying overburden up to surface.

The extraction ratio can be calculated as:

$$e = \frac{(B+W_1)(B+W_2)-(W_1 W_2)}{(B+W_1)(B+W_2)} \qquad\qquad \text{[2-11]}$$

where *e* depicts the extraction ratio, B the width of the rooms, and W_1 and W_2, the width of the pillars.

By applying the reasoning around TAT, the Average Pillar Stress (APS) can be calculated using the following equation:

$$\text{APS} = \frac{\sigma_v}{(1-e)} \qquad\qquad \text{[2-12]}$$

where σ_v represents the virgin vertical stress.

The APS is then taken forward to the FoS calculations and compared against the strength of the pillar to determine pillar stability.

2.3.1 Limitations of TAT

Besides the fact that TAT makes it simpler to determine the axial stress state in a pillar, it has some limitations that have to be taken into account. It assumes that the pillars carry the uniform load of the overburden overlying them and of the areas which have been mined out. In its application, TAT ignores the fact that the presence of abutments in a mining area results in a different distribution of stresses, and it only assumes that the mining area has got a regular geometry. Apart from that, any deformations and failures occurring in the hanging wall because of the mining activities are not being addressed by TAT (Roberts et al., 2002).

According to Brady and Brown (2005), the use of TAT only focuses on the pre-mining component of normal stress, which acts in the same direction as the principal axis of the pillar support system. This means that it assumes that other components of the pre-mining stress are negligible and have no effect on the stability of the pillar.

Another limitation found in the use of TAT is that it does not take into consideration the effect that the location of the pillar within the layout has on the stress state of that particular pillar. TAT also ignores the overburden stiffness and seam stiffness, both of which have a significant effect on the pillar load.

2.4 Factor of Safety

As discussed under Section 2.1.1, the Factor of Safety (FoS) is calculated as a ration of strength of the pillar to the stress on acting on the pillar.

An example of the use of these equations is presented below.

The room-and-pillar layout is given as having a 2 m mining height, 8 m bord width, 8 m square pillars and 400 m below surface. The rock density is on average 3000 kg/m³. Determine the factor of safety of these pillars. K-value equals 50 MPa.

Table 2-1: Factor of safety calculation – example

		Unit	Value	
Pillar dimension	(w_1)	m	8	
	(w_2)		8	
Bord		m	8	
Depth		m	400	
Density		kg/m^3	3000	
Extraction	(e)	%	75	Equation 2-11
Average Pillar Stress (TAT)		MPa	47.1	Equation 2-12
Strength (Hedley and Grant)		MPa	84.1	Equation 2-4
Factor of Safety			1.8	Equation 2-1

2.4.1 Factor of safety incorporating shear stresses

Swart, Keyter, Wesseloo, Stacey and Joughin (2000) investigated the effect of surface topography (natural and man-made) in order to quantify the effect on loading of pillars. They state that the overall FoS (the state where all stress orientations are included) will always be less than the FoS for the pillars when only the compressive stresses are considered. This entails the use of normal stress acting on the pillar and the normal compressive strength of the pillar. They imply that the calculated FoS which is commonly perceived as being conservative might in actual fact be less conservative in scenarios where significant shear stresses are present and act on the pillar area.

Graphical representation of the stress state within a pillar, showing all the stresses acting on the pillar, can be viewed in the Mohr plot below.
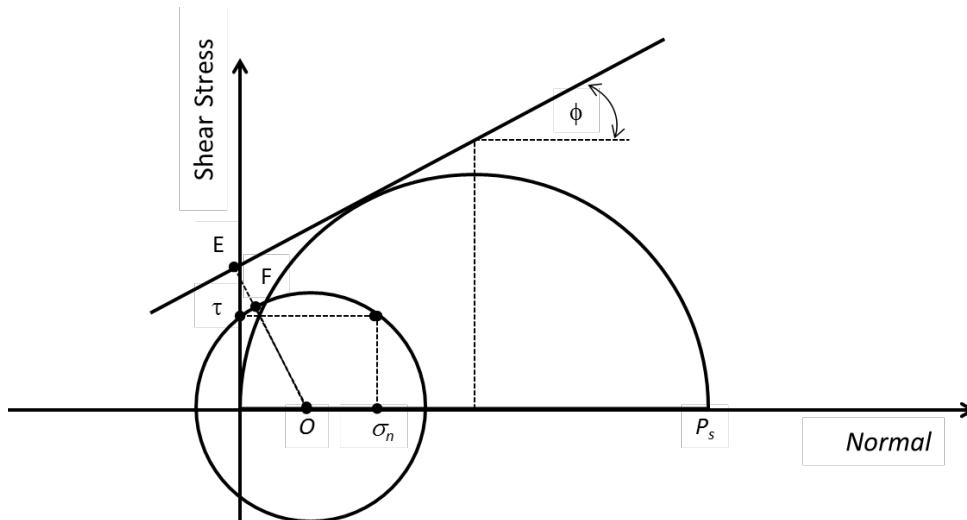
Figure 2-9: Mohr circles of stresses acting on a pillar (after Swart et al. (2000))

In Figure 2-9, P_s depicts the stress value at which the pillar will be for maximum compressive stress. The σ_n value is the state of stress used in the standard equations as the load or Average Pillar Stress (APS). The ratio between these two values is calculated by $FoS = \frac{Pillar\ strength}{Pillar\ load}$, assuming only principle stresses (no shear components) are present.

If a shear component does exist in the pillar, Swart et al. (2000) proposed that the FoS should be reconsidered as being the ration between the radius of the acting stress circle, OF, to the perpendicular distance to the failure Mohr-Coulomb failure envelope, OE. This ratio can be written as:

$$FoS = \frac{OE}{OF} = \frac{c \cdot \cos(\phi) + \frac{1}{2} \cdot \sigma_n \cdot \sin(\phi)}{\sqrt{\frac{\sigma_n^2}{4} + \tau^2}} \qquad [2\text{-}13]$$

with c being the cohesion and ϕ the friction angle. The stresses are given by σ_n for the normal and τ for the shear component.

The design downgraded strength for the rock mass (DRMS) can be included in the equation for calculating the cohesion (equation 2-13).

$$c = \frac{1}{2} \cdot DRMS \cdot \frac{W_{eff}^{\alpha}}{H^{\beta}} \cdot \left(\frac{1 - \sin(\phi)}{\cos(\phi)}\right) \qquad [2\text{-}14]$$

2.4.2 Effect of dip on pillar safety factor

In the South African mining context, most room-and-pillar operations – coal or hard rock – are roughly horizontal. This entails that the dip of the mining horizon is less

than 5°. Steeper areas are also mined by means of this method, with the upper limit governed by mechanical mining equipment's capabilities. As stated by Van der Merwe and Madden (2002), a dip can affect the pillar stability in coal pillar designs by:

i.   A reduction in effective pillar area.
ii. Spalling of down dip side of pillar as a result of gravity.
iii. Ride in the roof strata.
iv. Non-symmetrical stress distribution may result in increased load on the down dip side.

The impact the dip has mainly pertains to effective pillar width as well as mining height. Figure 2-10 illustrates the variances between the parameters for flat and inclined coal seams.
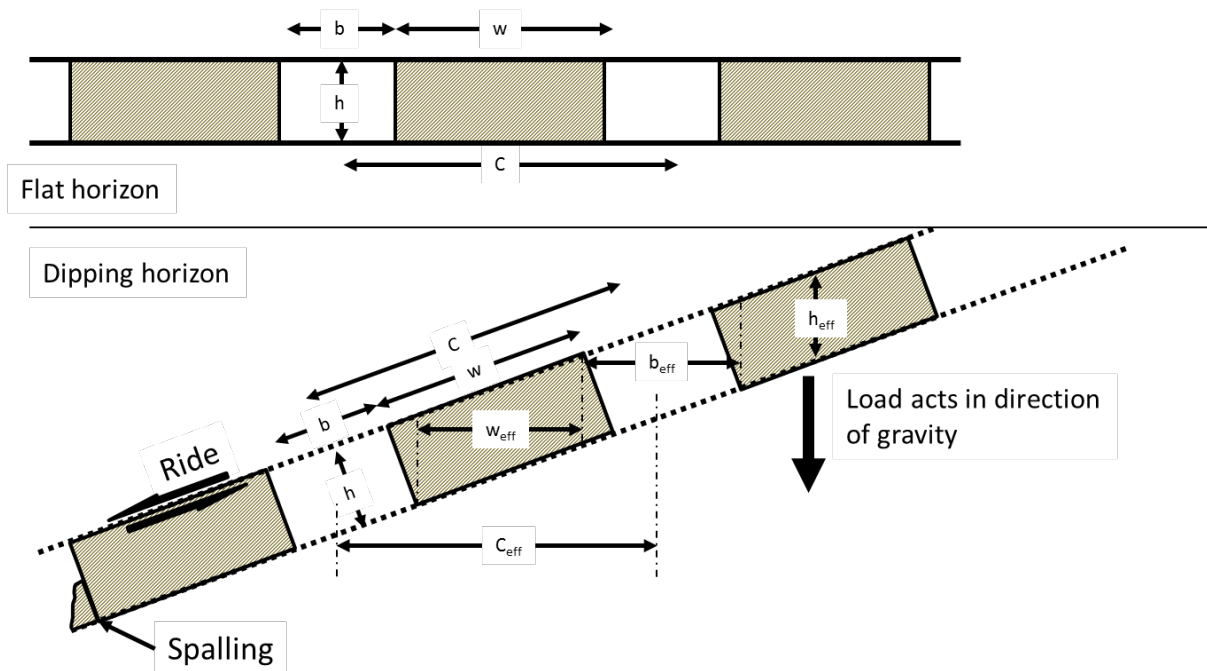
Figure 2-10: Effect of gradient on pillar dimensions (after Van der Merwe and Madden (2002))

The effective dimensions can be presented by:

Effective pillar height, $h_{eff} = \dfrac{h}{\cos\theta}$ [2-15]

Effective pillar width along dip, $w_{eff} = (w - h\tan\theta)\cos\theta$ [2-16]

Effective bord width along dip, $b_{eff} = (b + h\tan\theta)\cos\theta$ [2-17]

Effective pillar centres along dip, $c_{eff} = (b + w)\cos\theta$ [2-18]

Effective depth, $\quad h_{eff} = h$ at pillar effective mid width $(\frac{w_{eff}}{2})$ [2-19]

Van der Merwe and Madden (2002) recommend numerical modelling for pillar designs for horizons dipping steeper than 11° due to the adverse effects of shear induced by a ride on the pillar corners.

Consider as an example, a mine with a bord width of 8 m, mining height of 3 m and pillar width of 14 m at 120 m below surface.

Table 2-2: Factor of safety calculation – example

	Flat	10°
Effective width (m)	14	13.3
Effective height (m)	3	3.05
Effective bord (m)	8	8.4
Effective depth (m)	120	120
Effective centres (m)	22	21.7
Strength (MPa)	11.7	11.4
Load (MPa)	7.4	7.7
Factor of Safety	1.58	1.49

From this safety factor adjustment, it can be seen that an increase in dip will increase the load acting on the pillar and decrease the strength.

2.5 Internal friction

As the internal friction of the rock mass could not be altered by the practising Rock Engineer, it has been shown that this rock property could greatly influence the stability of the immediate hanging wall (Maritz and Malan, 2011).

With a special combination of reef dip and internal friction of a particular plane, slip could occur on that plane and can be calculated by using the Mohr-Coulomb criteria (equation 2-20).

$$\tau_{max} = \mu\sigma_n + c \qquad\qquad \text{[2-20]}$$

where μ is the tan of the friction angle ($\mu=tan(\phi)$), σ_n is the normal stress on the plane and c being the cohesion.

It is commonly assumed that the parting planes have very low cohesion value; hence, the cohesion is assumed to be zero. Equation 2-20 can then be rewritten as:

$$\phi = \tan^{-1}\frac{\tau_{max}}{\sigma_n} \qquad\qquad \text{[2-21]}$$

that one could use to calculate the minimum friction angle required at which a plane would mobilise for a given stress tensor. This is presented by Maritz and Malan (2011) in the plot in Figure 2-11.
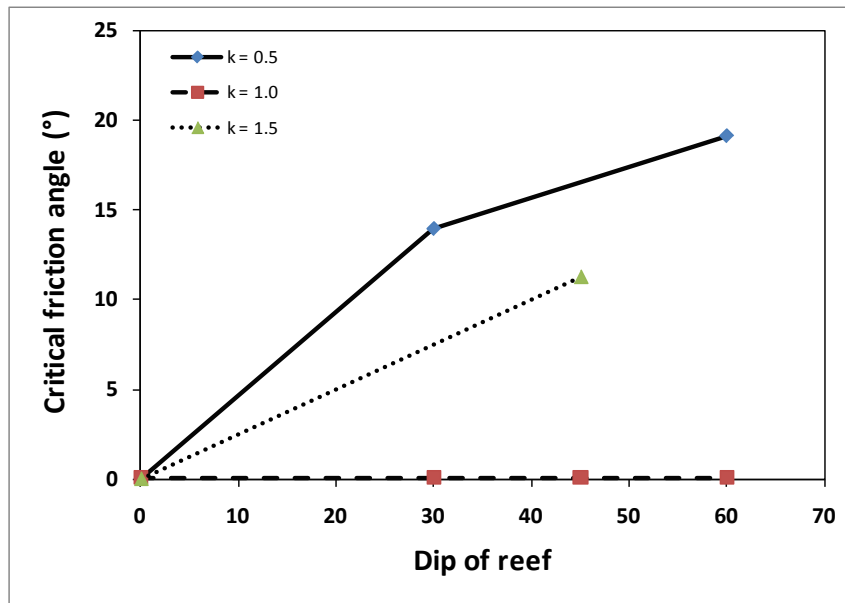
Figure 2-11: Relationship between critical friction angle and dip of the reef (after Maritz and Malan (2011))

Taking a general mining environment for room-and-pillar platinum layout in South African conditions, the interpretation of the graph would be that with a 5° dip of the reef horizon and a horizontal to vertical stress ratio of 1.5, a minimum friction angle of 2.5° would be required to maintain stability.

Also from the plot, one can conclude that in mining scenarios where the k-ratio is near unity, the influence of the friction angle could be ignored as any angle would result in stable conditions based on this discussion.

Proving that there needs to be other failure mechanisms that drive the failure, failures are observed on weak partings even with very small reef dip.

2.6 Inclined pillars

Lorig and Cabrera (2013) noted that pillar curves used in the mining industry worldwide do not necessarily cater for pillars in the case of foliated or inclined orebodies. This is attributed to the fact that all the formulae have been based on environments with brittle isotropic rocks.

Their analysis indicate that brittle type failure occurs in pillars, of which the width-to-height ratio is less than or equals to 1.0, whereas a more ductile (strain softening – hardening) type failure is expected in pillars with a ratio that is greater than 1.0. Slim pillars appear to be failing inside the pillar only, whereas the squat pillars fail both in the pillar and hanging wall contact of the pillar.

Figure 2-12 represents the contours of shear strain at peak load, which indicate failure at the critical 0.4% strain. The change from brittle to plastic failure can be seen in Figure 2-13.
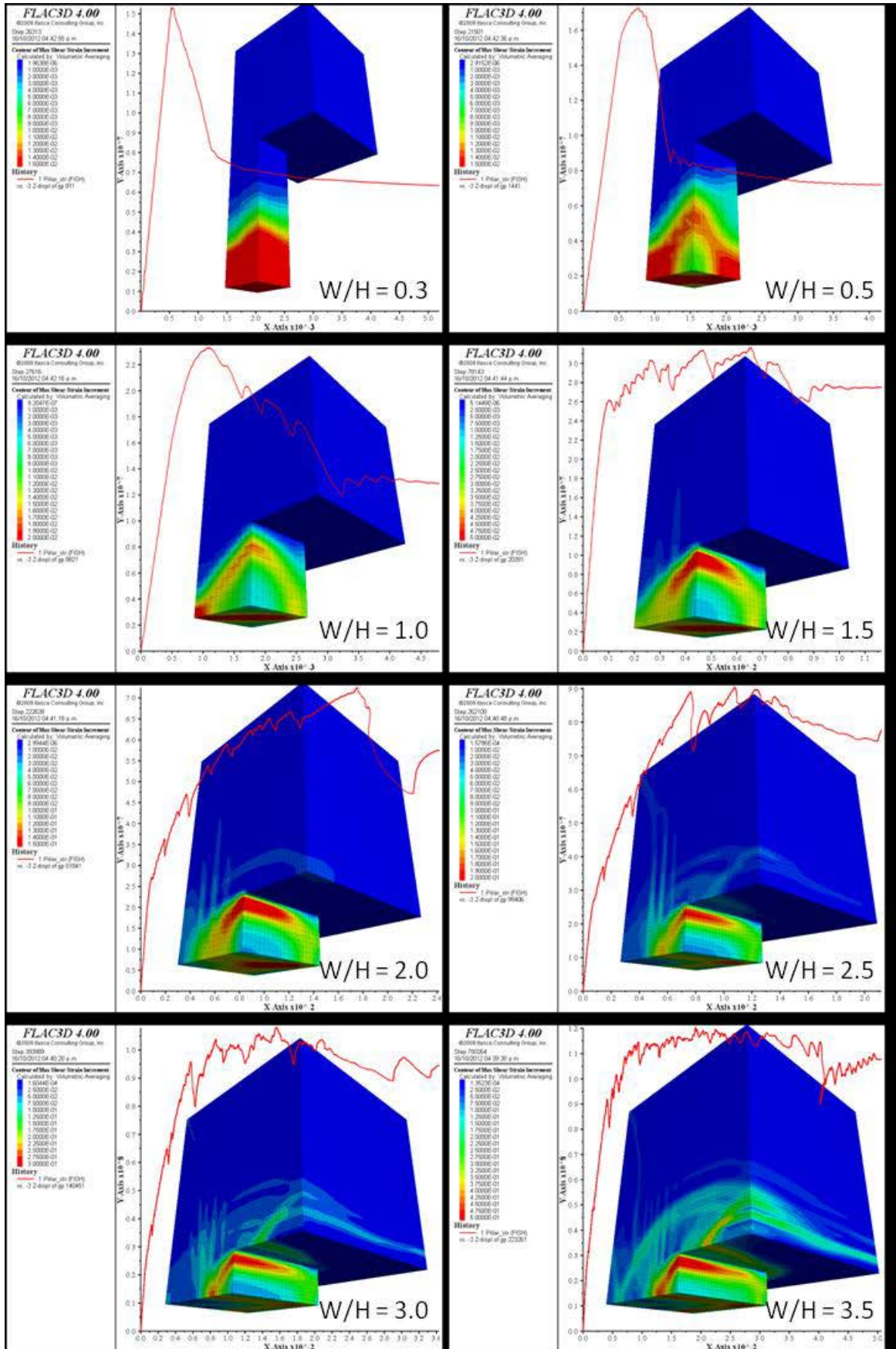
Figure 2-12: Contours of shear strain at peak load for each model analysed. Load vs. axial strain is superimposed (after Lorig and Cabrera (2013))
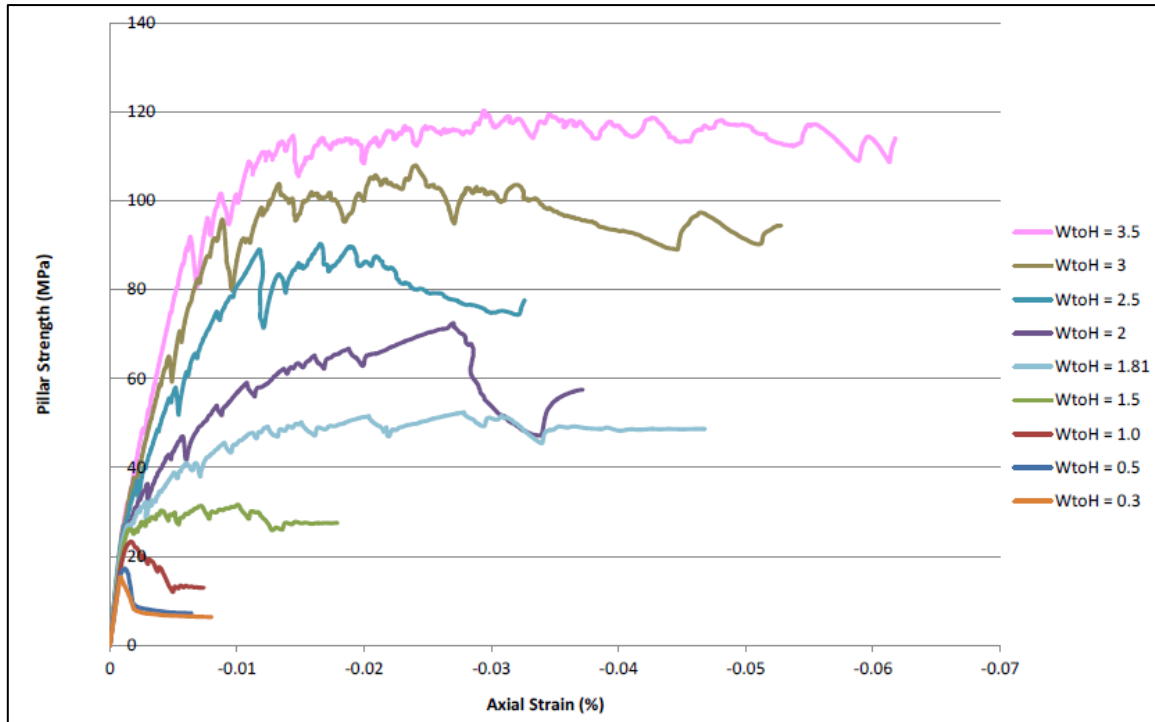
Figure 2-13: Relationship between pillar strength and pillar axial strain for vertical pillars (after Lorig and Cabrera (2013))

On their analysis of inclined pillars, they found:

"*Spalling and punching in peak situations without causing a pillar failure are observed. Thus, the pillar failure is developed from degraded conditions of the pillar system, caused by the punching mechanism, resulting in a shear failure.*" – Lorig and Cabrera (2013).

Their findings with respect to the shear strains are presented in Figure 2-14.
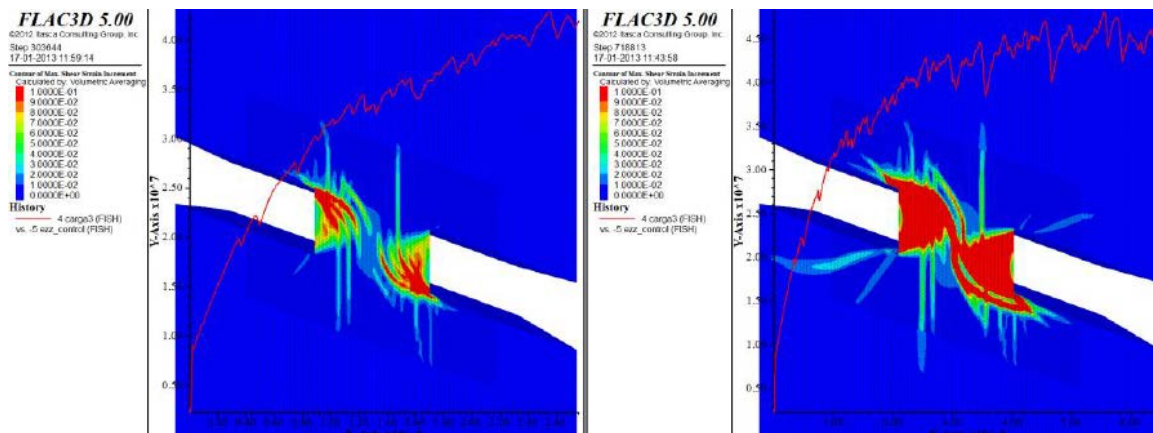
Figure 2-14: Shear strains for the analysed model in a status prior to peak (left) and in the post-peak status (right). Load history applied on the inclined pillar is superimposed (after Lorig and Cabrera (2013)

35

The analysis supported the expected reduction in strength triggered by the inclination of pillars. The reduction observed was in the order of 10 per cent for pillars with a width-to-height ratio of 1.8. Steeper dipping reef planes and pillar inclination is suggested to have an even higher reduction value. Lorig and Cabrera (2013) noted that the assumptions and boundary conditions applied to the model will notably affect the reduction numbers since real-life displacements are not only a constraint to the vertical but normal to the extracted ore.

2.7 Summary

Room-and-pillar and sequential grid are the two most commonly used extraction methods which strongly rely on stability of pillars as the primary support system. These layouts are traditionally designed based on the Factor of Safety methodology, where the ratio between the strength of the pillar and the load on the pillar should exceed acceptable levels (typically safety factor ratios of between 1.6 and 2.0).

The pillar strength can be calculated in two ways: first, by applying empirical formulae and secondly, by means of displacement discontinuity numerical modelling. The formulae proved to be highly dependent on the dimensions of the pillar and a reduced rock mass strength value. It is concluded that the pillar strength is influenced by the rock material characteristics, the deposit characteristics, loading environment and pillar design and shape. It appears that all these factors are combined in the reduced strength value (k-value). All authors submit that if a scenario exists that deviate from the assumed conditions from where the formulae were derived, special treatment should be given to the specific condition.

Loading on the pillar is currently simplified by applying the tributary area theory. It assumes the loading of the pillar based on the primitive stress before mining and the extraction ratio associated to the individual pillar. It is known that the calculated load would be higher than that of the numerical model since the tributary area theory does not take into consideration the effect of nearby pillars and abutments.

The common factor of safety is calculated by comparing the load to the strength. It is common practice to use the normal load on the pillar (from tributary area theory or numerical modelling) as the load and the strength from the equations for calculating the safety factor. This method excludes any influence of the shear stresses that

might exist on the pillar. Variations were made to the standard factor of safety formula, yet had not been implemented by industry. In the coal mining industry, adjustment to the input parameters are made when a deposit is mined which exceeds a 5° inclination, reducing the safety factor.

Latest studies on pillar width-to-height ratios indicate that slim pillars with ratios less than 1.0 indicate shear failure in the pillar only when compared to squat pillars, which indicate shear failure in the pillar and hanging wall contact of the pillar.

2.8 References

Applegate, J. (1997). The successful introduction of sequential grid mining at Elandsrand G.M. Co.Ltd. Paper and discussions, 132-145. Ass. Mine Managers of South Africa.

Bieniawski, Z.T. (1968). The effect of specimen size on compressive strength of coal. Int. J. Rock Mech. Min. Sci., vol 5, pp. 325-335.

Bieniawski, Z.T. (1992). A method revised: coal pillar strength formula based on filed investigations. Proc. Workshop on coal pillar mechanics and design. US Bureau of Mines IC.

Brady, B. and Brown, E. (2005). Rock Mechanics for underground mining (3rd ed.). New York, United States of America: Springer Science and Business Media, Kluwer Academic Publishers.

Esterhuizen, G.S., Dolinar, D.R. and Ellenberger, J.L. (2011). Pillar strength in underground stone mines in the United States. International Journal of Rock Mechanics & Mining Sciences, vol 48, pp. 42-50.

Greenwald, H., Howarth, H. and Hartman, I. (1941). Progress report: Experiments on strength of small pillars of coal in the Pittsburgh bed. USBM, R.I. 3575.

Handley, M., De Lange, J., Essrich, F. and Banning, J. (2000). A review of the sequential grid mining method employed at Elandsrand Gold Mine. The Journal of The South African Insitute of Mining and Metallurgy, pp. 157-168.

Hedley, D.G.F. and Grant, F. (1972). Stope-and-pillar design for Elliot Lake Uranium Mines. Bull. Can. Inst. Min. Metal., pp. 37-44.

Hoek, E. and Brown, E.T. (1980). Underground Excavations in Rock. Instn Min. Metall. London.

Jager, A.J. and Ryder, J.A. (1999). A handbook on rock engineering pratice for tabular hard rock mines. Johannesburg: The Safety in Mines Research Advisory Committee.

Kaiser, P., Kim, B., Bewick, R. and Valley, B. (n.d.). Rock mass strength at depth and implications for pillar design.

Lorig, L.J. and Cabrera, A. (2013). Pillar strength estimates for foliated and inclined pillars in schistose material. In Zhu, Detournay, Hart, & Nelson (Ed.), Continuum and Distinct Element Numerical Modeling in Geomechanics. Minneapolis.

Madden, B., Canbulat, I. and York, G. (1998). Current South African coal pillar research. The Journal of The South African Institute of Mining and Metallurgy, pp. 7-10.

Maritz, J.A. and Malan, D.F. (2011). The influence of shear stress and weak contacts on pillar behaviour. 12th ISRM International Congress on Rock Mechanics. Beijing.

Martin, C.D. and Maybee, W.G. (2000). The strength of hard-rock pillars. International Journal of Rock Mechanics & Mining Sciences, vol 37, pp. 1239-1246.

Ryder, J.A. and Jager, A.J. (2002). A textbook on rock engineering for tabular hard rock mines. Johannesburg: The Safety in Mines Research Advisory Committee.

Roberts, D., Van der Merwe, J., Canbulat, I., Sellers, E. and Coetzer, S. (2002). Development of a method to estimate coal pillar loading. Safety in Mines Research Advisory Committee.

Salamon, M.D.G. and Munro, A.H. (1967). A study of the strength of coal pillars. The Journal of The Southern African Institute of Mining and Metallurgy, pp. 56-67.

Salamon, M.D.G. and Wagner, H. (1985). Practical experiences in the design of coal pillars. Safety in Mines Research, Proceedings of the 21st International Conference. Sydney.

Swart, A., Keyter, G., Wesseloo, J., Stacey, T. and Joughin, W. (2000). Influence of surface topography on the loading of pillar workings in near surface and shallow mines – OTH 501. SIMRAC.

Van der Merwe, J.N. and Madden, B.J. (2002). Rock Engineering for underground coal mining. Johannesburg: The South African Institute of Mining and Metallurgy.

York, G., Canbulat, I. and Jack, B. (2000). Coal pillar design procedures COL 337. SIMRAC.

3 PILLAR LOADING ENVIRONMENTS

As complex as the mining environment itself, the pillar loading environment proves to challenge the engineer at various levels during the design and implementation phase. From the literature survey, it was found that the generally assumed vertical and normal stress could experience variations based on the dip of the reef horizon in relation to other excavations (stress changes in multi-reef mining) and even the orientation of the pillars. This section will address the study and investigation into the incidence of stresses other than the normal stresses and the influence of these stresses on the loading environment.

Mining of multi-reef tabular orebodies with a small middling between the reefs has gained more prominence in recent years. Although multi-seam mining in the coal industry has been practised for many years (Van der Merwe and Madden, 2002), mining of multi-reef horizons in the chrome and platinum industries has only seen significant growth in recent times. Complex stress situations arise in these mining environments, and no clear design rules are available for these layouts. Hence, a need was identified to investigate superimposing of pillars in multi-reef conditions.

Excess shear stress (ESS) is commonly used in the rock engineering discipline to calculate stability on possible failure planes. This methodology is applied on the pillar hangingwall contact to gauge first if shear stresses are present on such planes and, secondly, to determine the influence of these driving forces on the loading system.

3.1 Superimposed pillars

Multi seaming is no new term for coal miners who have been practising this over many years. The burning issue when doing multi-seam mining is the position of pillars for the various mining horizons relative to the other horizon. Guidelines were developed by Salamon and Oravecz (1976) in which they put down the 0.75C rule. This rule entails that seams with a middling of less than 75 per cent of the pillar centre distance would experience stress interaction between pillars on an RP layout; hence, pillars should be superimposed (place in line with each other).
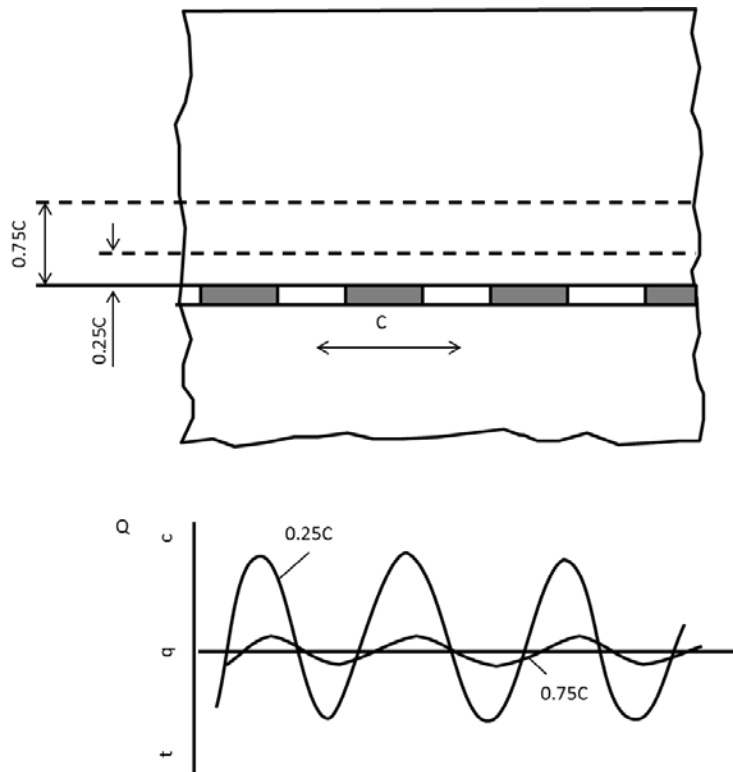
Figure 3-1: Stresses above room-and-pillar workings (after Salamon and Oravecz (1976))

Even though this was established by numerically modelling a single reef scenario, Maritz, Malan and Piper (2012) confirmed this with the modelling of two reef horizons. In the report, it was concluded that the superimposing of pillars might give a false sense of security since the position of the pillars might see a reduction in stress level. However, an additional component arises in the form of shear stresses on the pillar areas. The layout of the room-and-pillar model can be seen in Figure 3-2.
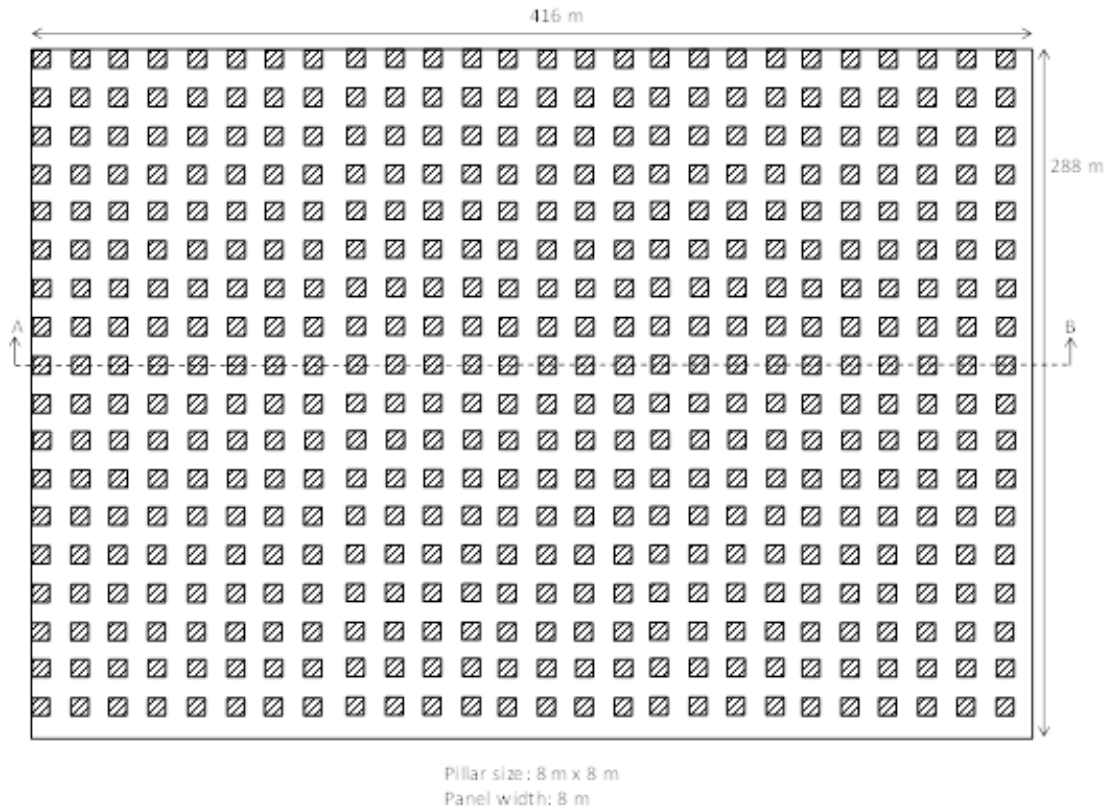
Figure 3-2: A room-and-pillar layout simulated using the TEXAN code (Maritz et. al. (2012))

The data values used in the report were relative density of 3.0, depth of mining at 1000 meters, and extraction of 75%.

The results of the interaction studies are plotted in Figure 3-3, indicating that there is a definitive change in stresses as one calculates stress levels closer to the mining horizon. In the case where the benchmark level is placed 12 m below the reef (0.75 times the 16 m pillar centres), the interaction is remarkable.
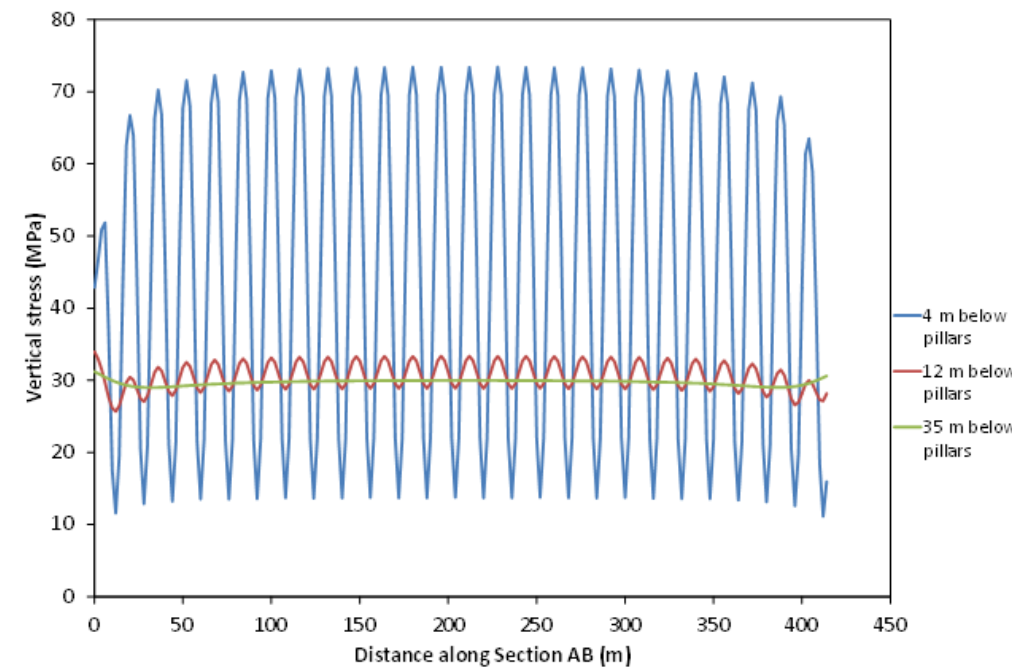
Figure 3-3: Simulated vertical stress along Section AB (Figure 3-3) at various distance below Reef A (after Maritz and Malan (2012))

Further studies of the stress levels on the individual pillars on Reef A showed that when these stresses are plotted, it becomes apparent that the stress levels on the pillars in actual fact decreased (see Figure 3-4) when multi-reef mining was introduced (middling of 35 m).
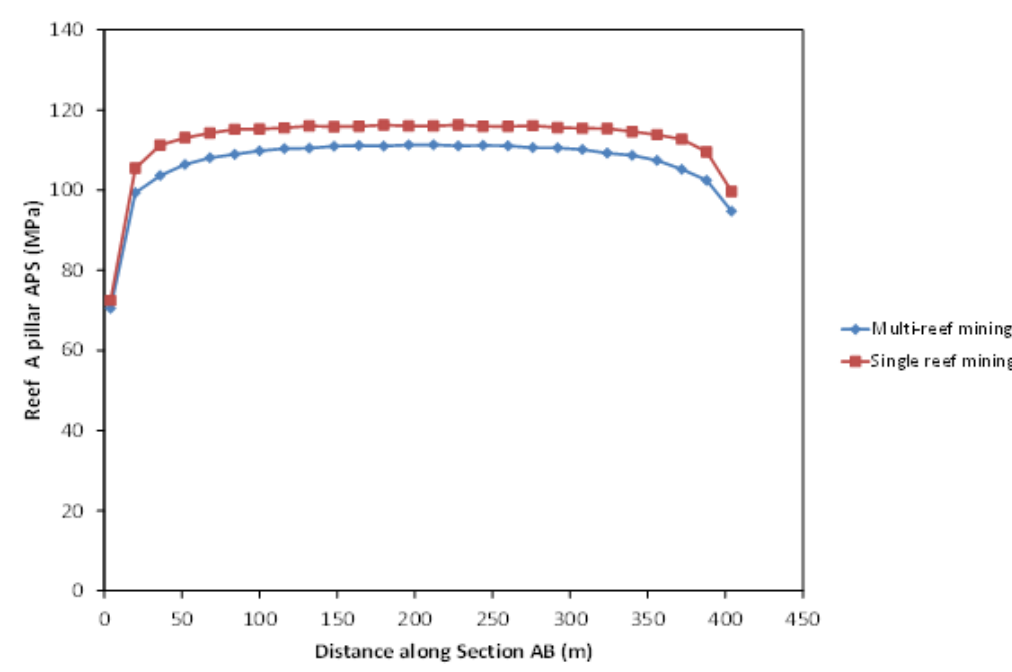
Figure 3-4: Simulated APS for the Reef A pillars for single reef and multi-reef mining – 35 m middling (after Maritz and Malan (2012))

The foregoing values along strike compare well against the theoretical value calculated by using the TAT, which results in an APS of 117 MPa.

In further studies into the added shear stress component (Maritz and Malan, 2012) in the simulation of a single pillar configuration at 0° dip, it was found that no shear stresses were induced on the pillar with a single reef scenario. The layout of this model can be viewed in Figure 3-5.
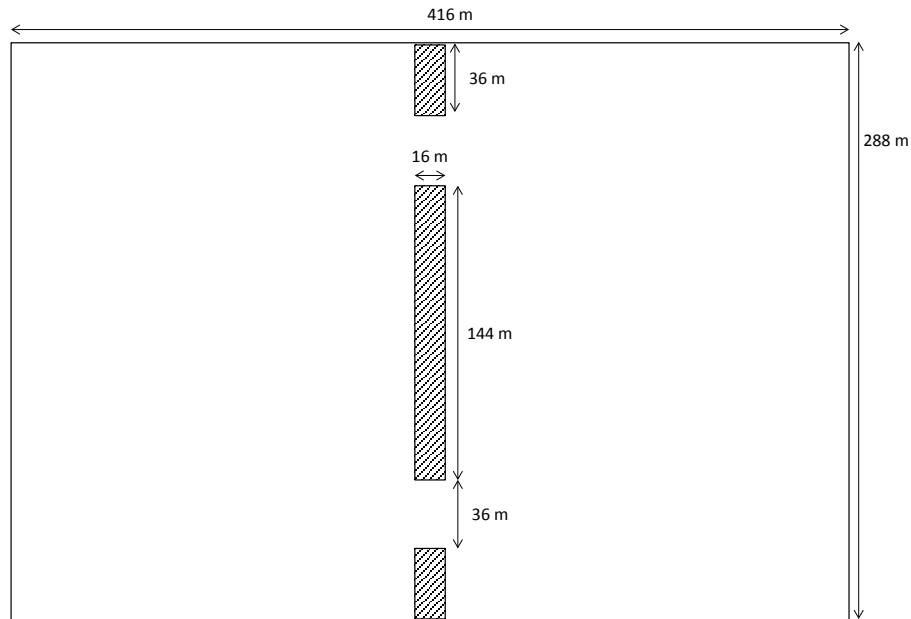
Figure 3-5: Simulated layout with regional pillar (after Maritz and Malan (2012))

When a second reef was introduced into the model (Reef B being simulated with a 35 m middling to Reef A), shear stresses were induced on the modelled pillar, even at 0° dip.

The following table presents the reduction in pillar loading (APS) when the two reefs are modelled compared to single reef mining.

Table 3-1: Simulated APS (after Maritz and Malan (2012))

Mining scenario	Reef A pillar width (m)	Reef B pillar width (m)	Reef A pillar APS (MPa)	Reef B pillar APS (MPa)
Reef A mining only	16	-	211.8	-
Reef B mining only	-	16	-	219.2
Multi-reef mining	16	16	158.4	173.8

Table 3-1 clearly shows the reduction in APS when the second reef is introduced. However, the model also indicates the shear component on the pillar on Reef A (see Figure 3-6).
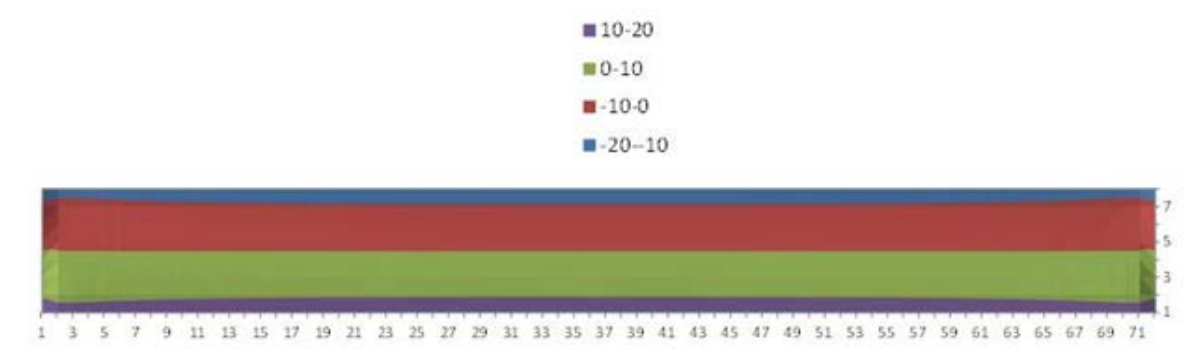
Figure 3-6: Shear stress contours on 16 m by 144 m pillar – Reef A (after Maritz and Malan (2012))

Note: The negative values in the modelling results are only indicative of the direction of the shear stress.

The figure on the shear stresses indicates an increase in shear stress towards the pillar sides and a 0 MPa shear stress value at the pillar core at which point a directional shift is observed.

3.1.1 CASE STUDY: Multi-reef pillar mining

Multi-reef mining at a mine in the Eastern Bushveld was also investigated. Historically, only the lower MG1 reef was mined, but mining on the upper MG2 Reef has now commenced. As the middling between the reefs is only approximately 9 m and the depth below surface is 100 m, a study into the stability of the pillars and the

middling was required. For the TEXAN simulation, the mining outlines were approximated with polygons to enable the area to be discretised with triangular elements. The outline for MG1 is shown in Figure 3-7 and MG2 in Figure 3-8.
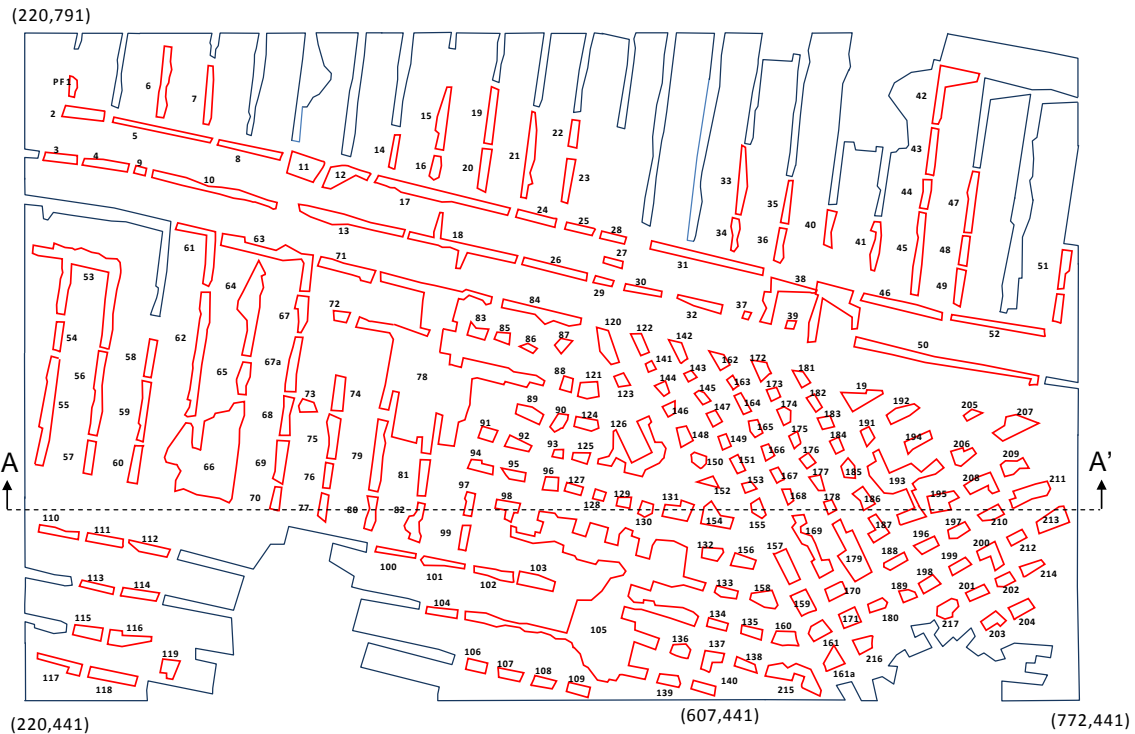
Figure 3-7: Extent of the MG1 area simulated in detail with TEXAN
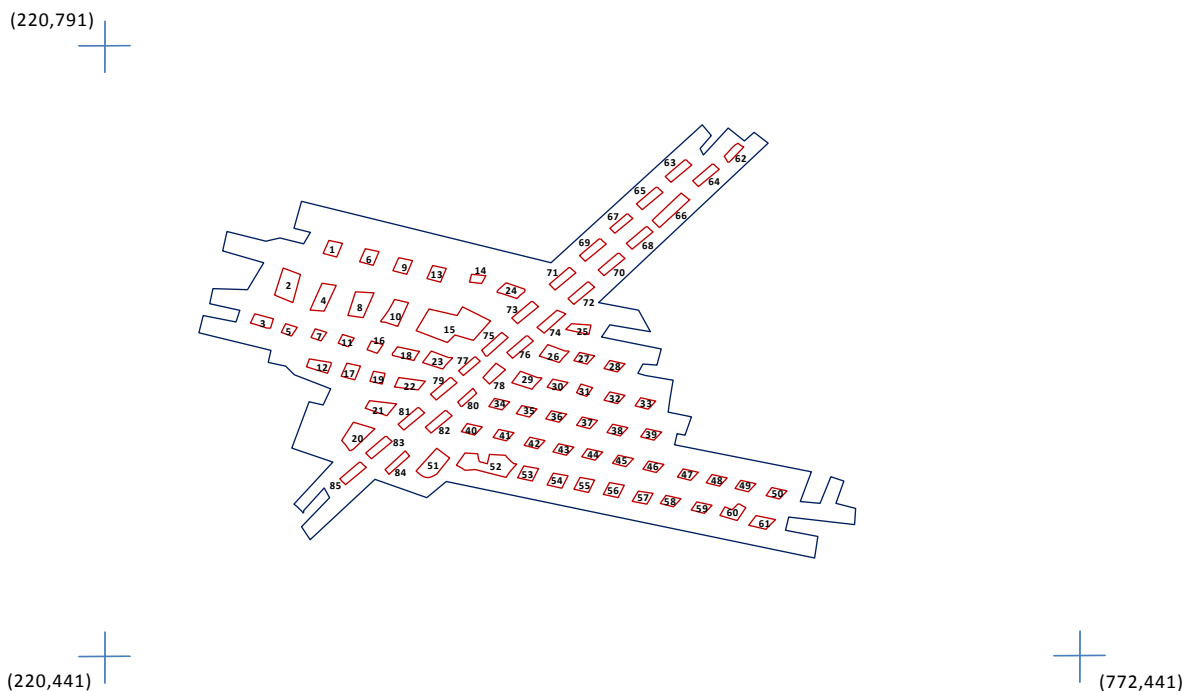
Figure 3-8: Extent of the newly established MG2 mining simulated in detail with TEXAN

The relative orientation of the two reefs and the pillar positions are shown in Figure 3-9.

Figure 3-9.Relative orientation of the pillars on the MG1 and MG2 reef horizons

Parameters used for the model

The parameters used for the model are given in Table 3-2. It is worth noting that although the density of some of the Bushveld rocks may be as high as 3400 kg/m^3, the average overburden density was estimated to be lower at 2900 kg/m^3 (Van den Heever, pers. comm.) owing to the proximity of the surface and the weathered zone. The applicability of this value needs to be verified for numerical modelling studies at specific sites.

Table 3-2: Modelling parameters

Parameter	Value
Young's Modulus	70 GPa
Poisson's ratio	0.25
k-ratio	1.5 (both dip and strike)
Overburden density	2900 kg/m^3
Equivalent stiffness	1320 MPa/m

Results from the simulations

The simulated APS values for selected MG1 pillars are given in Figure 3-10 and for the MG2 pillars in Figure 3-11. The pillar numbers are given in Figure 3-7 and 3-10. In Figure 3-10, two values of APS are shown; the first are values without the MG2 mining and the second is for the multi-reef scenario. Note that most of the MG1 pillar stresses *decrease* after mining of the MG2.

Figure 3-10: Simulated APS values for the pillars on the MG1 reef horizon

Note: The pillar numbers for Figure 3-10 are given in Figure 3-7. All these pillars are below the MG2 mining area.

The simulated pillar stresses on the MG2 reef horizon is shown in Figure 3-11. The pillar stresses are relatively low. Of interest is the stress on pillar P18 that is very low. This pillar is situated above a mined MG1 area (see Figure 3-8 and 3-11 for the position of this pillar) and can therefore not transmit much stress to the reef below.
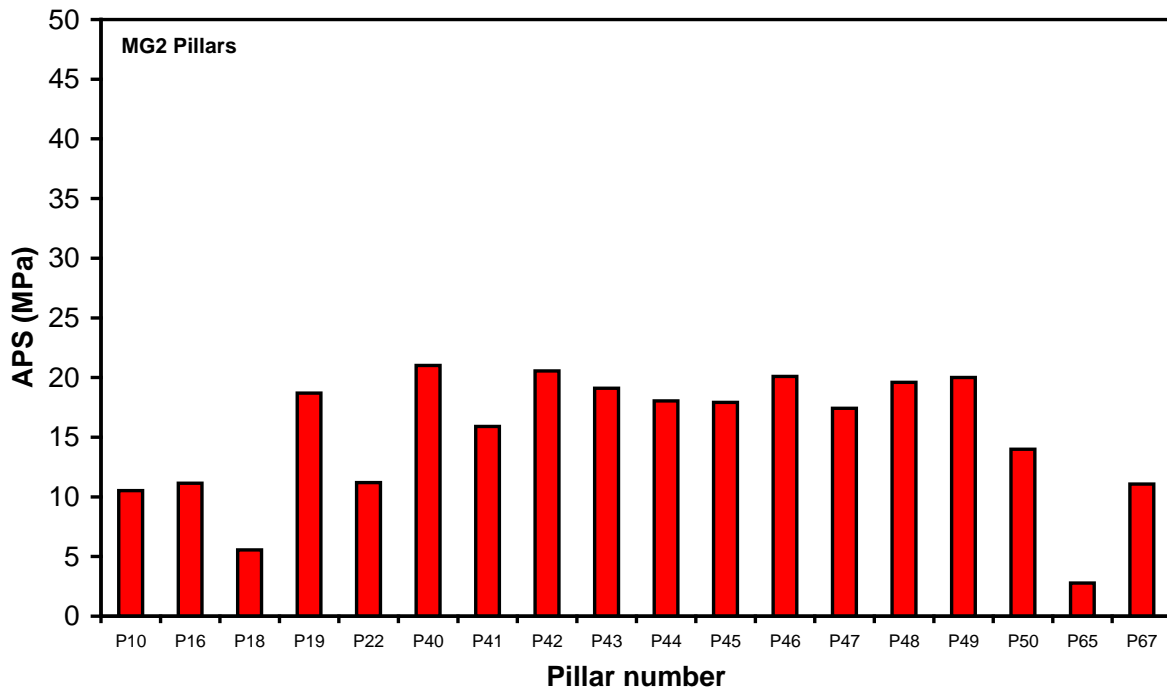
Figure 3-11: Simulated APS values for the pillars of interest on the MG2 reef horizon. The pillar numbers are given in Figure 3-8

As a simulated reduction in stress occurred on many MG1 pillars after mining of the MG2 reef (Figure 3-10), additional work was conducted to understand the stress transfer in this multi-reef scenario. All the pillars shown in Figure 3-10 were situated below the MG2 mining. Additional pillar stresses were therefore calculated for MG1 pillars located on the edges of (but not below) the MG2 mining. The simulated stresses are shown in Figure 3-12. In contrast to the pillars below the MG2 mining, for these pillars at the edges of the MG2 mining, the stress values *increase* after mining the MG2. It is hypothesised that (part of) the mechanism of stress redistribution in the multi-reef scenario is probably as follows: If MG1 and MG2 pillars are superimposed, some stress is still transferred through both pillars, and some shear stress may be induced in the pillars. If an MG2 pillar is positioned above an open MG1 stope far from MG1 pillars, very little stresses are transferred through this MG2 pillar. As less stress can now be easily transferred through the overstoped MG1 area, the additional stress is transferred to the edges of the MG2 mining and the stresses on the MG1 pillars at these positions increase accordingly. As the spans of the modelled MG2 mining is still small and the factor of safety on the pillars

is relatively high, the overstoped areas and the pillars are probably still stable. Of concern, however, is when the spans of the MG2 had increased substantially. It might become increasingly difficult to transfer the stress to the edges of the MG2 mining, and the stresses might be thrown back on the few pillars that are superimposed in the back areas. Pillar and beam failure may then occur. It is therefore critical that large MG2 regional pillars are superimposed on the regional MG1 pillars to assist with this stress transfer. The final stress field will be further complicated by the shear stress induced in these superimposed pillars.

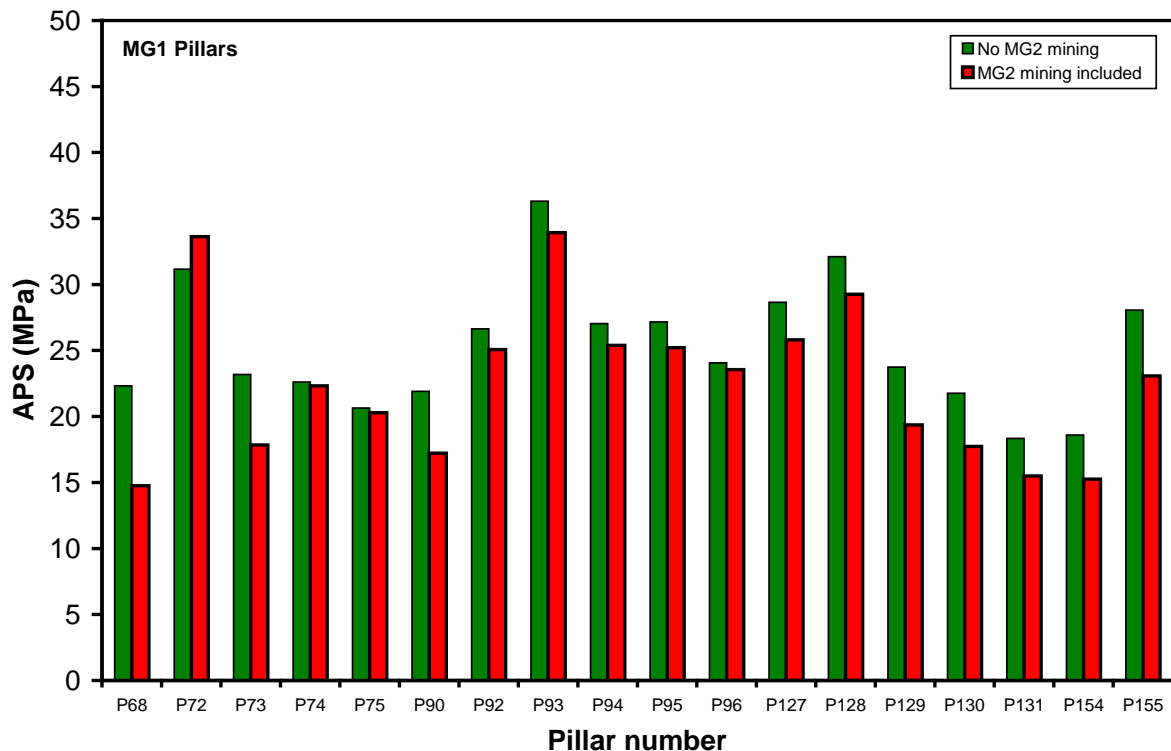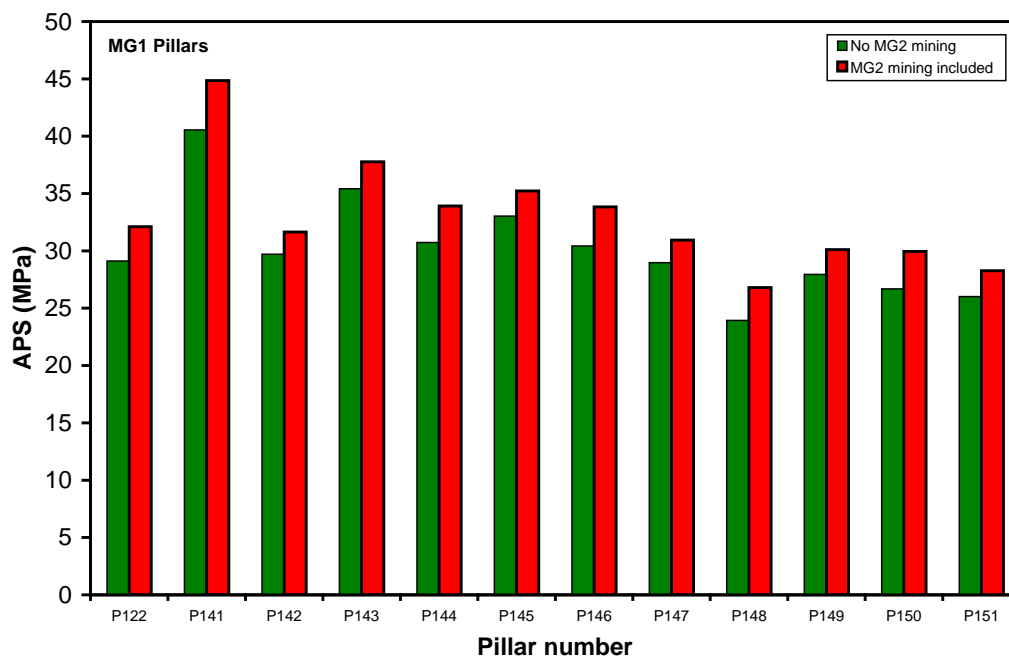**Figure 3-12: Simulated APS values for additional pillars on the MG1 reef horizon**

The pillar numbers for Figure 3-12 are given in Figure 3-7. These pillars are not below the MG2 mining area, but in front of one of the MG2 abutments.

The FoS values for the pillars shown in Figure 3-12 were calculated by means of the modelled stress on each and by assuming the Hedley and Grant formula for strength calculations. These values are given in Table 3-3. Note the reduction in FoS values as the stresses increase on these pillars. In comparison, for most of the MG1 pillars below the MG2 mining, the FoS will initially increase (although the effect of the possible induced shear stress is not clear).

Table 3-3: Simulated pillar stresses and estimated FoS for MG1 pillars close to, but in front of, the MG2 abutment

Pillar	Area (m²)	Circumference (m)	Mining height (m)	Equivalent width (m)	Strength (MPa) (Hedley and Grant: K=53 MPa)	APS (MPa) No MG2 mining	FOS No MG2 mining	APS (MPa) MG2 mining	FOS MG2 mining
P122	53.7	32.8	2	6.5	80.6	29.1	2.8	32.1	2.5
P141	15.4	15.8	2	3.9	62.1	40.5	1.5	44.9	1.4
P142	56.9	34.4	2	6.6	81.0	29.7	2.7	31.6	2.6
P143	22.5	19.2	2	4.7	68.2	35.4	1.9	37.8	1.8
P144	34.1	24.4	2	5.6	74.5	30.7	2.4	33.9	2.2
P145	29.6	23.5	2	5.0	70.7	33.0	2.1	35.2	2.0
P146	32.8	23.3	2	5.6	74.8	30.4	2.5	33.8	2.2
P147	32.8	23.5	2	5.6	74.5	29.0	2.6	30.9	2.4
P148	54.6	30.5	2	7.2	84.3	23.9	3.5	26.8	3.1
P149	34.1	24.1	2	5.7	75.0	27.9	2.7	30.1	2.5
P150	44.1	26.3	2	6.7	81.6	26.7	3.1	30.0	2.7
P151	47.2	28.8	2	6.6	80.7	26.0	3.1	28.3	2.9

Stability of the middling

To investigate the stability of the middling, reef-parallel benchmark sheets were calculated in the middling at positions 3 m and 6 m into the MG1 hangingwall. These benchmarks were calculated with and without the MG2 mining. The area over which the benchmarks were calculated is shown in Figure 3-13 to assist the reader to relate the stresses to the positions of the pillars.
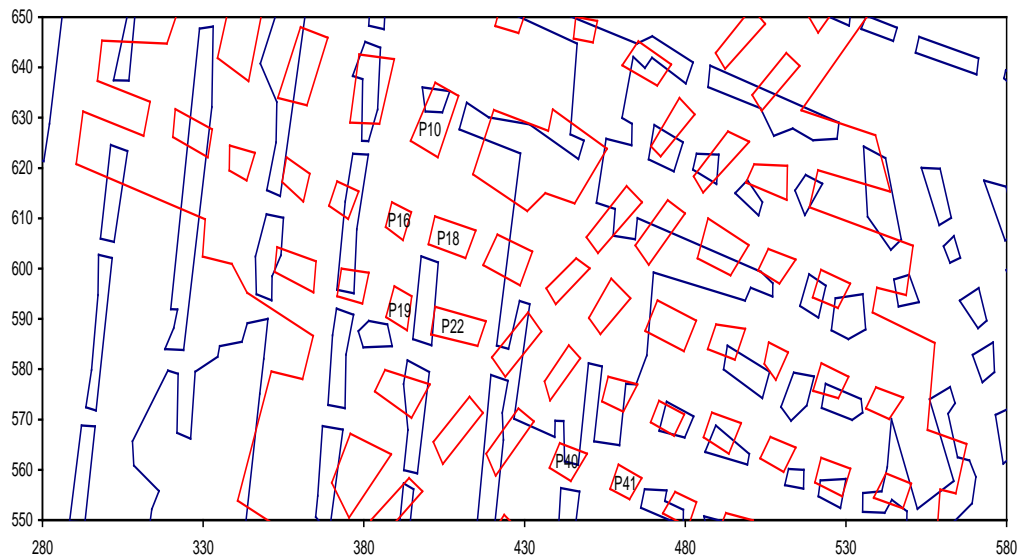
Figure 3-13: Area covered by the MG1 hangingwall benchmark sheets. (The blue outlines are the MG1 mining, and the red outlines are the MG2 mining). The pillar numbers refer to the MG2 pillar numbers

The vertical stress contours for no MG2 mining is shown in the plots in Figure 3-14. Note that 6 m into the hangingwall (Figure 3-14), no tensile vertical stresses (negative signs) are induced. For 3 m into the hangingwall, tensile stresses are seen in the middle of the large mining spans.

51
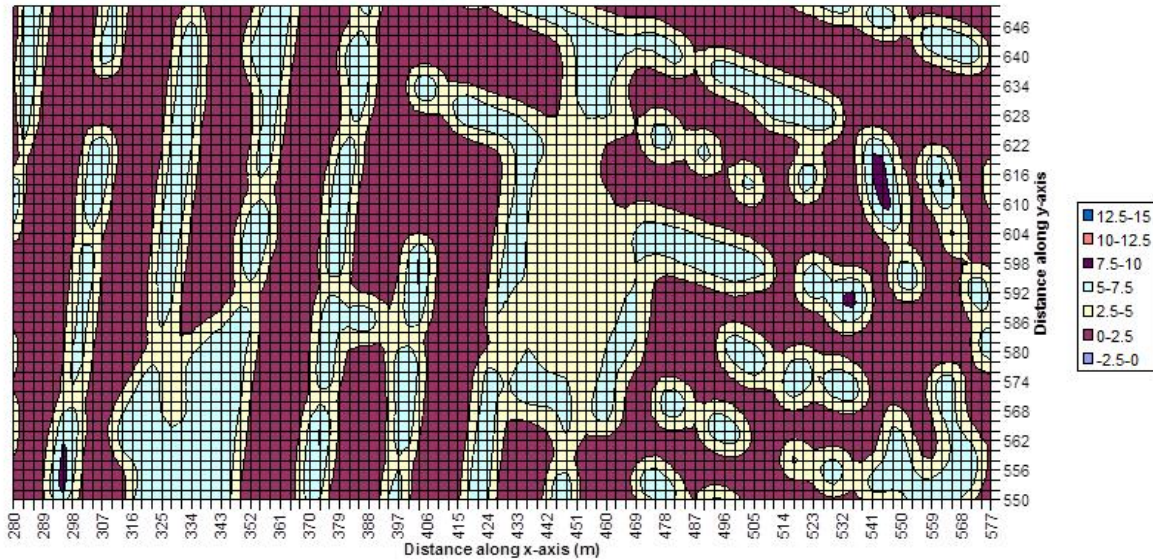
Figure 3-14: Contours of vertical stress at a height of 6 m into the MG1 hangingwall. No MG2 mining was included in this simulation
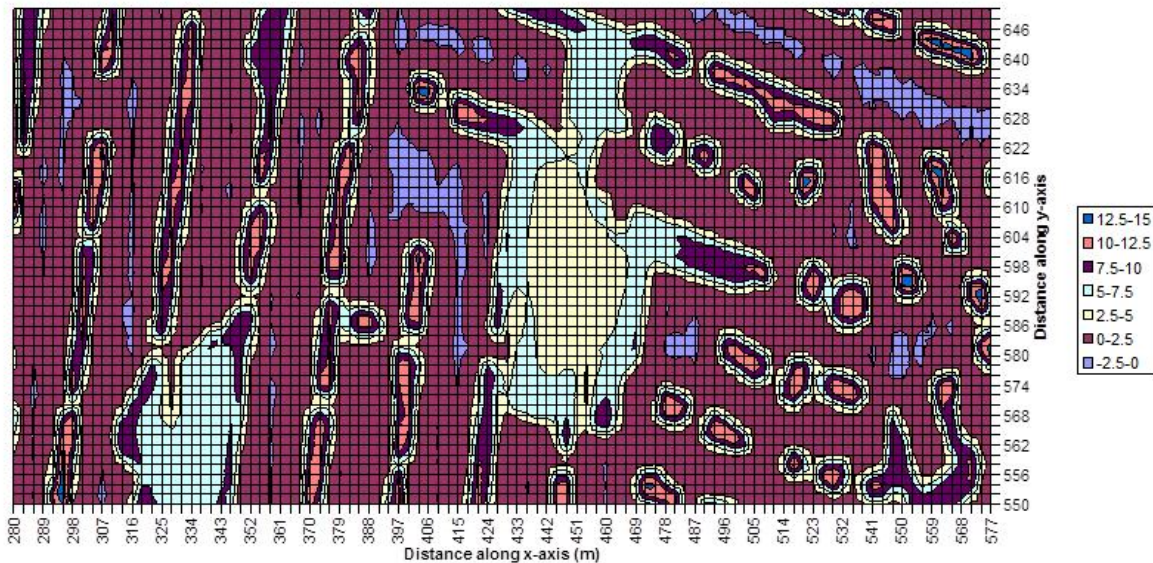
Figure 3-15: Contours of vertical stress at a height of 3 m into the MG1 hangingwall. No MG2 mining was included in this simulation

In comparison, the vertical stresses after mining the MG2 is shown in Figure 3-16. Note that zones of tensile vertical stress can now be seen even at a height of 6 m into the hangingwall. This is the approximate position of a chromitite stringer in this area, so mobilisation of this parting may induce instability of the middling.
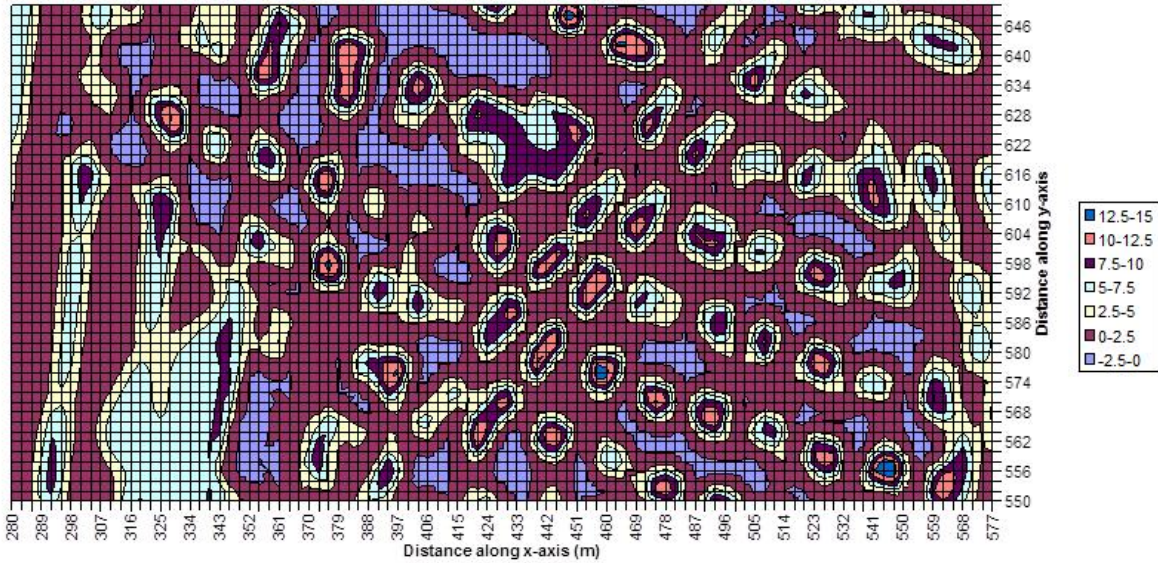
Figure 3-16: Contours of vertical stress at a height of 6 m into the MG1 hangingwall after mining the MG2
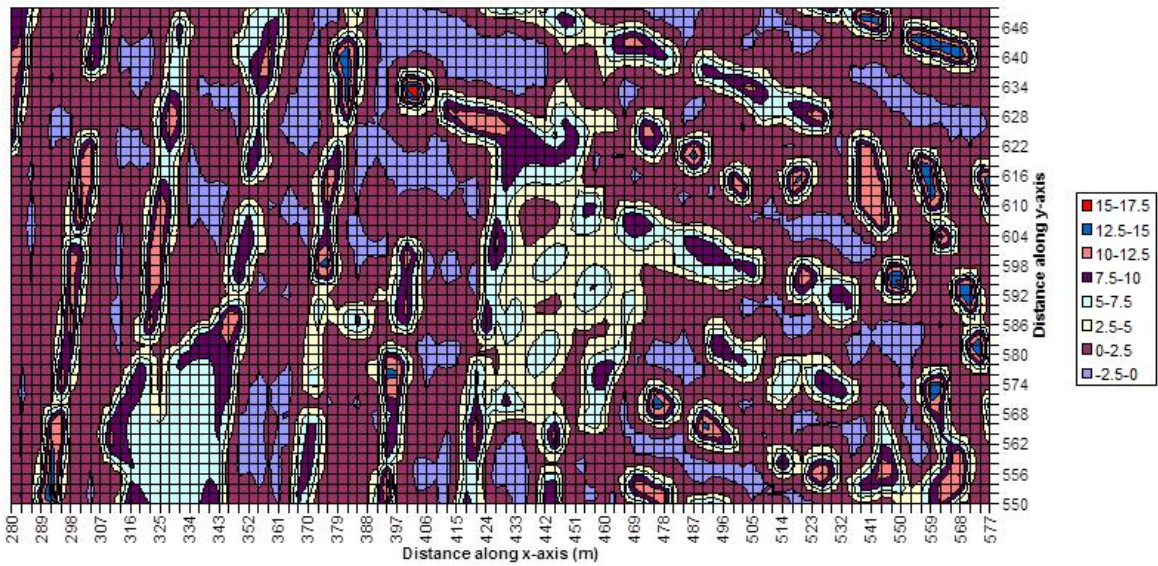
Figure 3-17: Contours of vertical stress at a height of 3 m into the MG1 hangingwall after mining the MG2

Concern is occasionally expressed that MG2 pillars positioned over mined stopes far away from MG1 pillars may punch into the middling beam. This appears not to be the case as illustrated by the modelling results. As an example, examine the positions of pillars P16 and P18 in Figure 3-13. By examining Figure 3-17, it can be noted that the vertical stresses in this region below the pillars are small, and very

little stress is transferred by them. This is confirmed by Figure 3-11 which illustrates that the APS of these pillars is relatively low compared to the other MG2 pillars.

3.1.2 Superimposed pillar conclusion

This study illustrates the complex stress interactions for multi-reef pillar layouts in areas where the middling between the reefs is small. The TEXAN boundary element code is well suited to simulate these layouts for mining problems containing large numbers of pillars. An important finding of this study is that shear stresses are induced in the pillars when identical pillar layouts are perfectly superimposed in a multi-reef layout. The shear stresses result in a reduction of the normal stresses on the pillars when compared to a single reef layout. This finding is counterintuitive and may lead to the incorrect conclusion that enhanced pillar stability may be obtained for this idealistic multi-reef scenario. The effect of the shear stress on pillar stability is not quantified, however, and it requires further study. The TEXAN code was also used to simulate an actual multi-reef chrome mine layout in the Eastern Bushveld. This illustrated the extremely complex stress interactions when pillars of irregular shapes are not superimposed. The simple coal mine rules of superimposing of pillars should therefore be treated with caution. Routine numerical modelling and underground monitoring of pillars and middling stability are considered vital to ensure that safe mining conditions are maintained for these layouts.

3.2 Numerical analysis on the existence of shear stress

In order to determine and prove the existence of the possible shear component on the pillars for an RP layout, numerical simulations were done using the Tabular Excavation Analysis (TEXAN) code. The parameter to be evaluated would be the shear stress component induced on the pillars (primary and secondary reef pillars) based on the scenario modelled.

3.2.1 Use of the TEXAN code to simulate tabular mining environments

Simulating mining environments have been part of Rock Engineering practice and mine design for decades and can be traced back to the days when digital computers became generally available some 50 years ago (Napier and Malan, 2007). The TEXAN code is able to solve both 2D and 3D complex problems. In TEXAN,

solutions are possible for a set of multiple interacting reef planes and geological contact planes or fault (Du Plessis, Malan and Napier, 2011). Details of the TEXAN code are discussed in Napier and Malan (2007).

"*The element planes are tessellated with displacement discontinuity elements to represent stope ride and elastic convergence movements or to model slip movements on fault planes. Elements can be in an 'infinite' space or in a 'semi-infinite' space with a flat, stress-free surface. The medium is assumed to be elastic and isotropic. Analytical kernel expressions are used to compute half-space influence functions in 3D. Elements can be 2D line segments, 3D triangles or 3D convex quadrilaterals. (In particular, square elements can be used if required). Both in-plane and anti-plane components are allowed in 2D analyses.*" – Maritz and Malan (2012: 3)

The element could have more than one collocation point (1, 10 or 15 for triangular elements) given constant, cubic (third order) or quartic (fourth order) discontinuity variations. Although this increases the number of calculations needed to solve any given problem, the accuracy is improved for irregular shaped outlines.

The code also allows for mixed attributes to be assigned to specific elements, for example, inclusion of backfill into mined areas or activating element tessellations to simulate fault slip (Maritz, Malan and Piper, 2012).

3.2.2 The TEXAN numerical modelling code

To simulate the shear stresses on the pillars, the TEXAN numerical modelling code (Napier and Malan, 2007) was used. It utilises the displacement discontinuity boundary element method (DDM). The mine layouts are approximated as planar "slits" where the 'width' of the slit – corresponding to the excavation height – is assumed to be negligible compared to the in-plane, lateral dimensions of the excavation. The TEXAN code utilises triangular or quadrilateral element shapes in conjunction with higher order variations of the displacement discontinuity shape functions. This facilitates an accurate evaluation of detailed stress and displacement components close to excavation surfaces and allows for the assessment of tabular layouts which include a large number of pillars.

3.2.3 Shear stress on in-stope pillar – Room and Pillar

In the South African hard rock mines in the Bushveld Complex, a weak parting forming the contact between the pillar and the hangingwall is frequently encountered. As the reefs typically dip at approximately 9°, some concern has been expressed that the shear stress acting on these pillars will cause a mobilisation of these partings. This may cause pillar failures at loads less than the expected failure load or even cause regional failure as the hangingwall "rides" over the pillars. This possible effect has not been quantified yet. The measure that will be used to investigate this effect in the modelling below is the excess shear stress (ESS). The equation for calculating the ESS on the hangingwall/pillar parting plane is:

$$ESS = \tau_{max} - \mu\sigma_n$$
[3-1]

where τ_{max} is the simulated shear stress acting on the pillar, $\mu = \tan\phi$ (ϕ is the friction angle of the pillar hangingwall parting) and σ_n is the normal "clamping" stress acting on the pillar.

ESS is commonly used to estimate stability on geological discontinuities; however, in this case, it will be used as a guide for determining stability in a rock mass. Results where the ESS value is positive, the shear failure on the parting will be possible since the driving force is greater than the opposing and resisting force governing stability.

3.2.4 Benchmark numerical model

In this section, the benchmark model is referred to as the base model. A number of TEXAN runs were conducted to determine the effect of the dip of the reef plane as well as the depth below surface on the ESS on the pillar partings. A number of different scenarios were simulated, and all of these were compared against the base model simulation results.

The base model is a room-and-pillar layout at 400 m depth, and the reef plane has a dip of 0°. The mining layout comprises a layout with 75 per cent extraction and 8.0 m x 8.0 m wide pillars. Square displacement discontinuity elements were used in the model with a size of 1.0 m. The size of the geometry simulated was approximately 49 000 m^2.

56

A portion of the base layout is presented in Figure 3-18. The stresses of the pillars highlighted in red are presented in the graphs that follow.
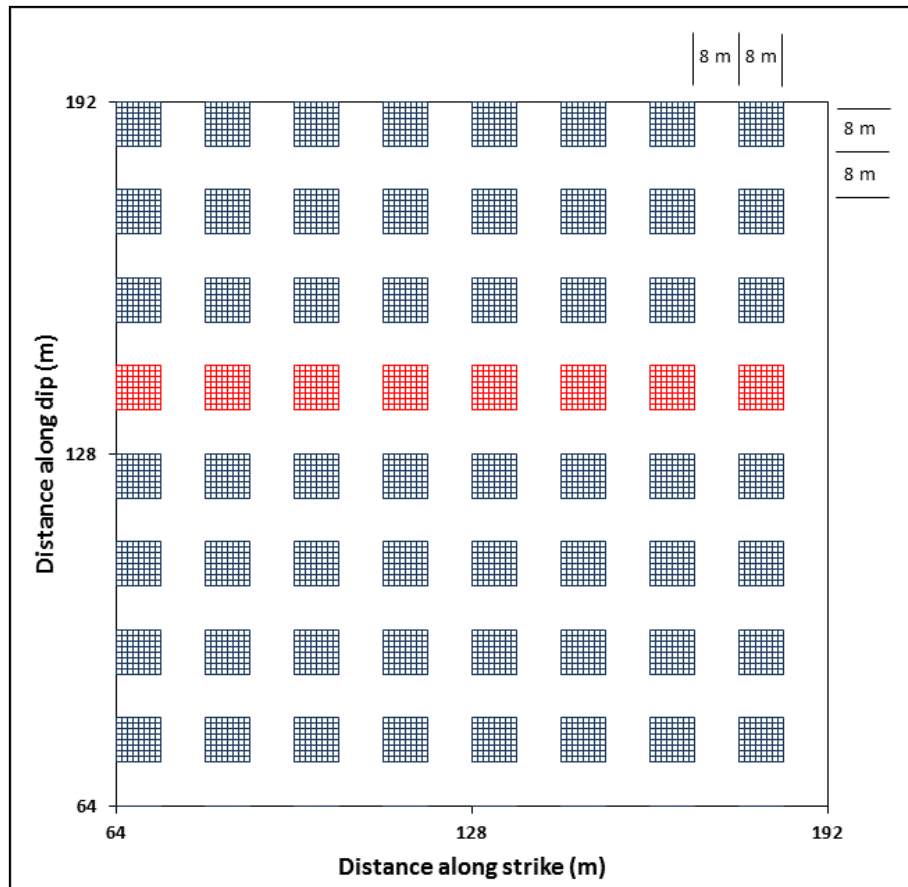
Figure 3-18: A portion of the pillar geometry simulated

The following input parameters were used in all the models.

Table 3-4: List of TEXAN input parameters.

Parameter	Unit value
Density	3000 kg/m^3
Depth below surface	400 m
Dip	0°
Gravitational constant g	9.81 m/s^2
k-ratio (x and y direction)	0.5 (x) 1.0 (y)
Vertical stress gradient	0.028 MPa/m
Poisson's ratio	0.25
Young's Modulus	70 GPa

Parameter	Unit value
Pillar dimension	8 m x 8 m
Board and split dimension	8 m
Element size (modelling grid)	1 m x 1 m
Friction angle (benchmark)	20°
Cohesion	0 MPa

The modelling results were used to calculate the ESS values according to equation 3-1. The results for the row of pillars highlighted in red are shown in Figure 3-19. It is noted that the ESS values on the pillar edges are slightly higher. This is caused by the change in stresses that is caused by the proximity to the abutments assumed by the modelling code.

Figure 3-19: ESS values for the base model simulation

No shear stresses are present on the pillars for the 0° dip model, and τ_{max} is therefore zero in this case.

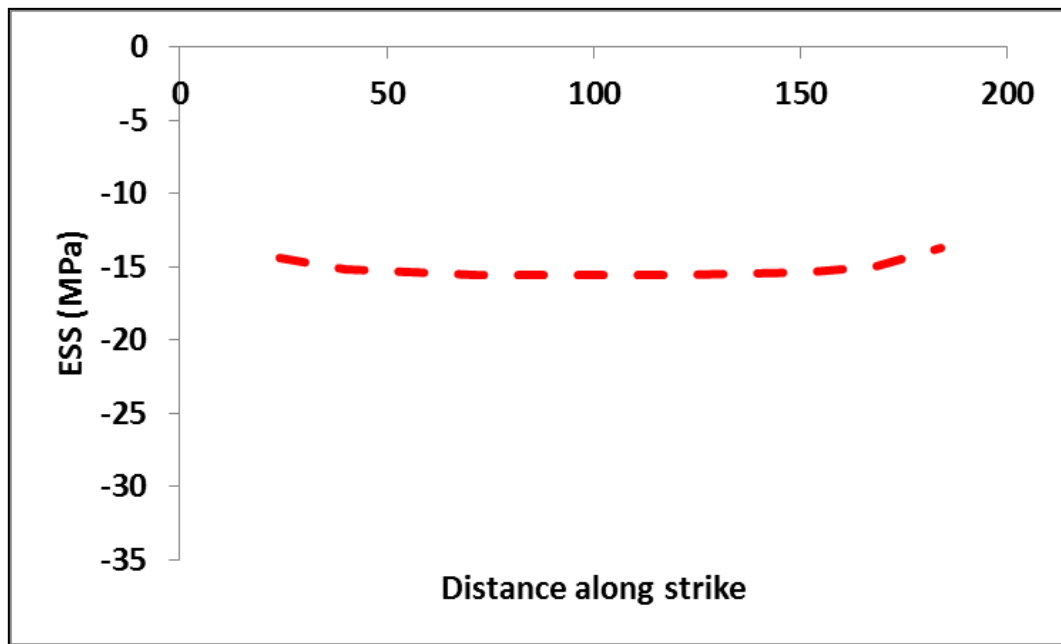At 400 m depth below surface, the simulated average pillar stress (APS) on the pillars highlighted in red is presented in Figure 3-20.
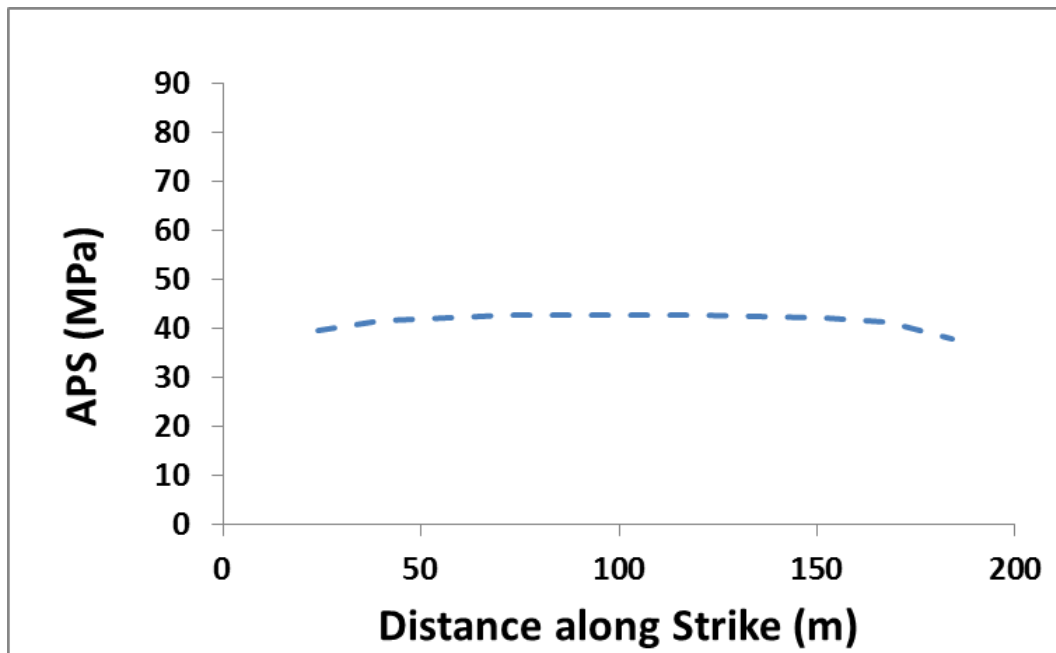
Figure 3-20: Base model average pillar stress in the strike direction

3.2.5 Simulating the effect of dip and depth

The magnitude of shear stress acting on the pillars was determined with a set of models simulated at various dip angles. The effect of depth below surface was also investigated. The models were simulated at depths varying from 400 m to 800 m below surface, and the dip of the reef varied in increments of 30 degrees, from 0° to 60°. It should be noted that a room-and-pillar layout will never be mined at a dip of 60°, and these values were included for academic interest only.

Table 3-5: List of models simulated with the associated parameters

Model Number	Dip of reef plane (°)	Depth below surface (m)
Base (BM)	0	400
C1	0	600
C2	0	800
C3	30	400
C4	30	600
C5	30	800
C6	60	400
C7	60	600
C8	60	800

As expected, the ESS values for a layout with no dip assume a larger negative value at greater depth owing to the increase in the clamping stresses (σ_n). This is illustrated in Figure 3-21. As this ESS has such a large negative value, the pillar parting will be clamped, and no shear slip is expected.
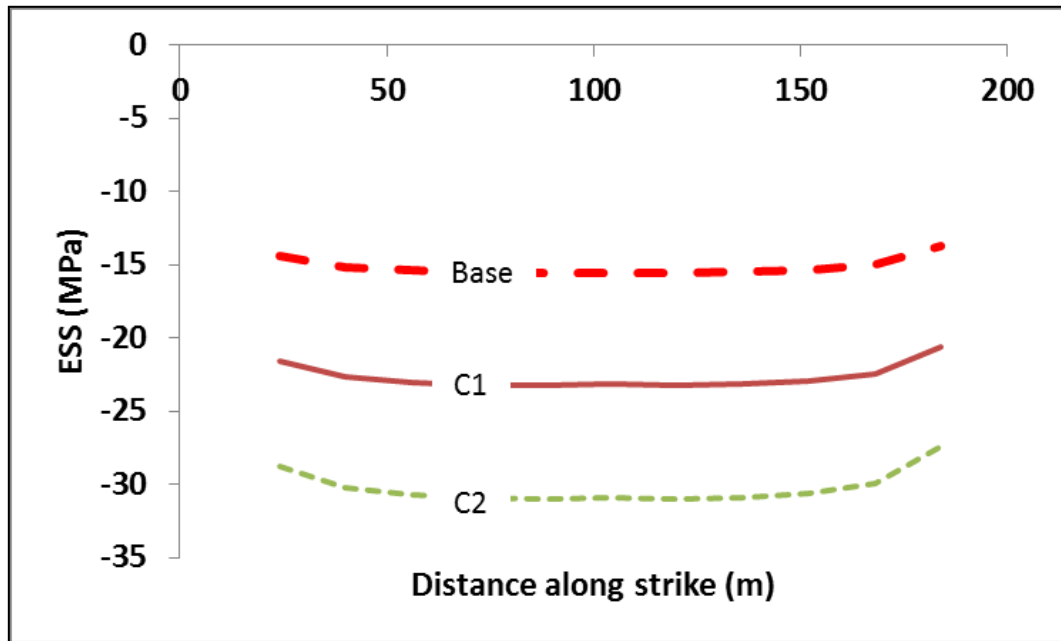
Figure 3-21: ESS values on the pillars for a model with no dip as a function of depth (friction angle of 20° on the pillar parting)

In the subsequent comparative simulations, the dip of the reef was increased. As a result, the ESS will attain a smaller negative value. This is caused by a combination of the shear stresses increasing and a decrease in the clamping stresses. Note that for a dip of 60° at a depth of 400 m, the ESS value is almost positive and slip on the parting may be imminent.
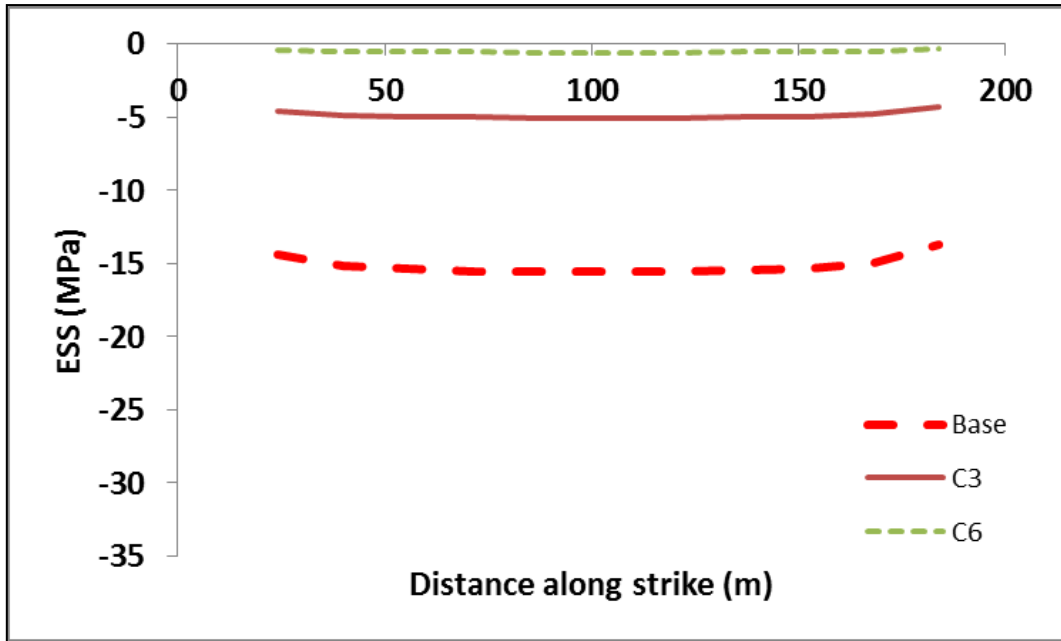
Figure 3-22: ESS values on a plane at constant 400 m depth as a function of dip with a friction angle of 20°

3.2.6 Multi-reef scenarios

An additional set of models where produced for evaluating the existence of shear stresses and a change in normal stresses on a single pillar in a room-and-pillar layout with 8 m square pillars and 8 m rooms when a multi-reef condition is assumed. Again, this has an extraction ratio of 75 per cent. The three benchmark models where Base A (mining only Reef A), Base B (mining of Reef B only) and Base M (multi-reefing both Reefs A and B). The other input design parameters are given in the Table 3-6.

Table 3-6: TEXAN input parameters

Parameter	Unit value
Vertical stress gradient	3000 MPa/m
Depth below surface	400 m
Gravitational constant *g*	9.81 m/s^2
k-ratio (x and y direction)	1.5
Model size Strike (x dir)	240 m
Dip (y dir)	240 m

Parameter	Unit value
Poisson's ratio	0.25
Young's Modulus	65 GPa
Pillar dimension	8 m x 8 m
Board and split dimension	8 m
Element size (modelling grid)	2 m x 2 m
Benchmark depth below reef	2 m
Single reef – Base A	Reef A Only
Single reef – Base B	Reef B Only
Multi-reef – Base M	Reefs A and B
Multi-reef middling	10 m

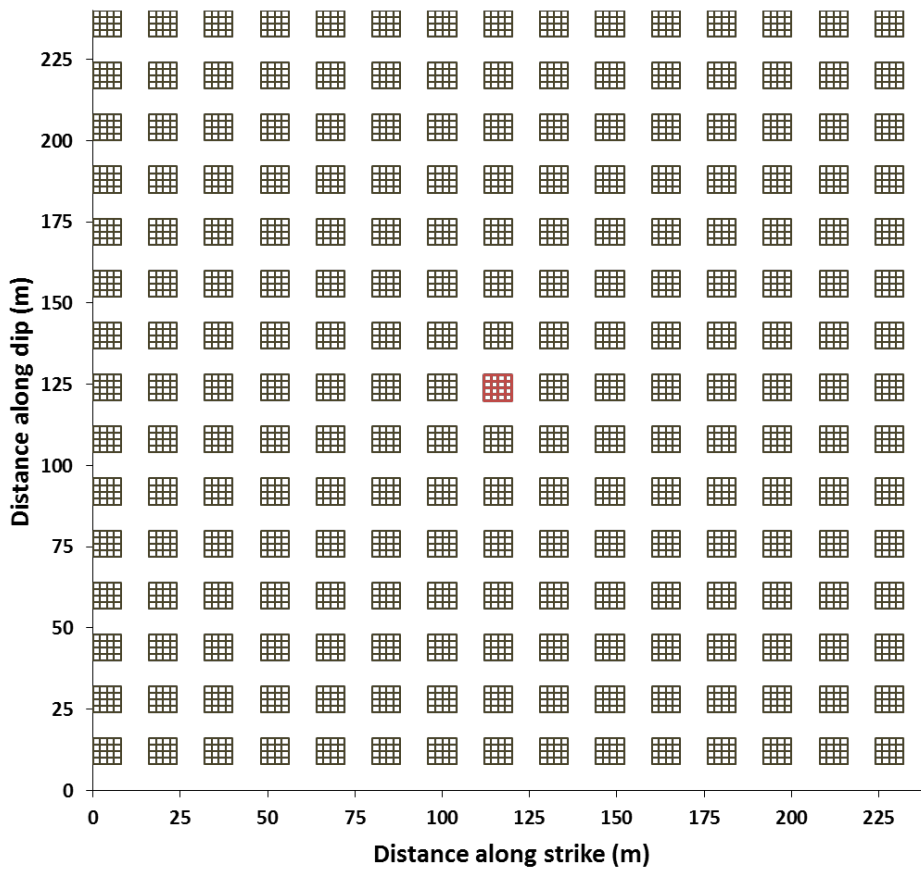The base layout as modelled in TEXAN can be viewed in the figure that follows.

Figure 3-23: Simulated layout for scenario modelled (red pillar indicating pillar under investigation)

A number of scenarios where modelled, of which the results are presented below. For each scenario, the set-up was first based on a single reef being mined (either Reef A or Reef B) and then additional runs were done on an identical and superimposed second reef scenario.

The models change with regard to the dip of the reef horizon modelled. The dip ranged from 0°- 40° with 10 degree intervals.

Results from elastic modelling

The results obtained from the numerical modelling are presented in the figures in Table 3-7. A total of 15 scenarios had been solved, each reporting first on the vertical stress (τ_{zz}) acting on the centre pillar (this would be the normal stress on the pillar in dipping horizons) and, secondly, on the shear stress (τ_{xy}) on the centre pillar (if present). Finally, based on these values and by applying the ESS formula (equation 3-1), the values are compared and plotted.

Table 3-7: Numerical modelling results

| Number of reef horizons	Dip angle	Reef A				Reef B			
		τ_{xz}	τ_{yz}	τ_{zz}	ESS	τ_{xz}	τ_{yz}	τ_{zz}	ESS
Single reef	0	-	-	45.68	-9.71	-	-	46.82	-9.95
	10	0.00	-3.98	46.39	-5.89	0.00	-4.07	47.55	-6.03
	20	0.00	-7.27	48.29	-3.00	0.00	-7.45	49.50	-3.07
	30	0.00	-9.89	51.41	-1.04	0.00	-9.92	52.19	-1.17
	40	0.00	-11.22	55.11	-0.49	0.00	-11.51	56.48	-0.50
Multi-reef	0	0.10	0.03	43.72	-9.32	-0.10	-0.02	44.88	-9.52
	10	0.10	-3.72	44.39	-5.72	-0.10	-3.83	45.53	-5.84
	20	0.10	-5.61	45.83	-4.13	-0.11	-6.05	47.24	-3.99
	30	0.12	-10.62	49.88	0.02	-0.13	-11.23	51.13	0.36
	40	0.13	-11.55	53.41	0.20	-0.15	-12.18	54.39	0.62
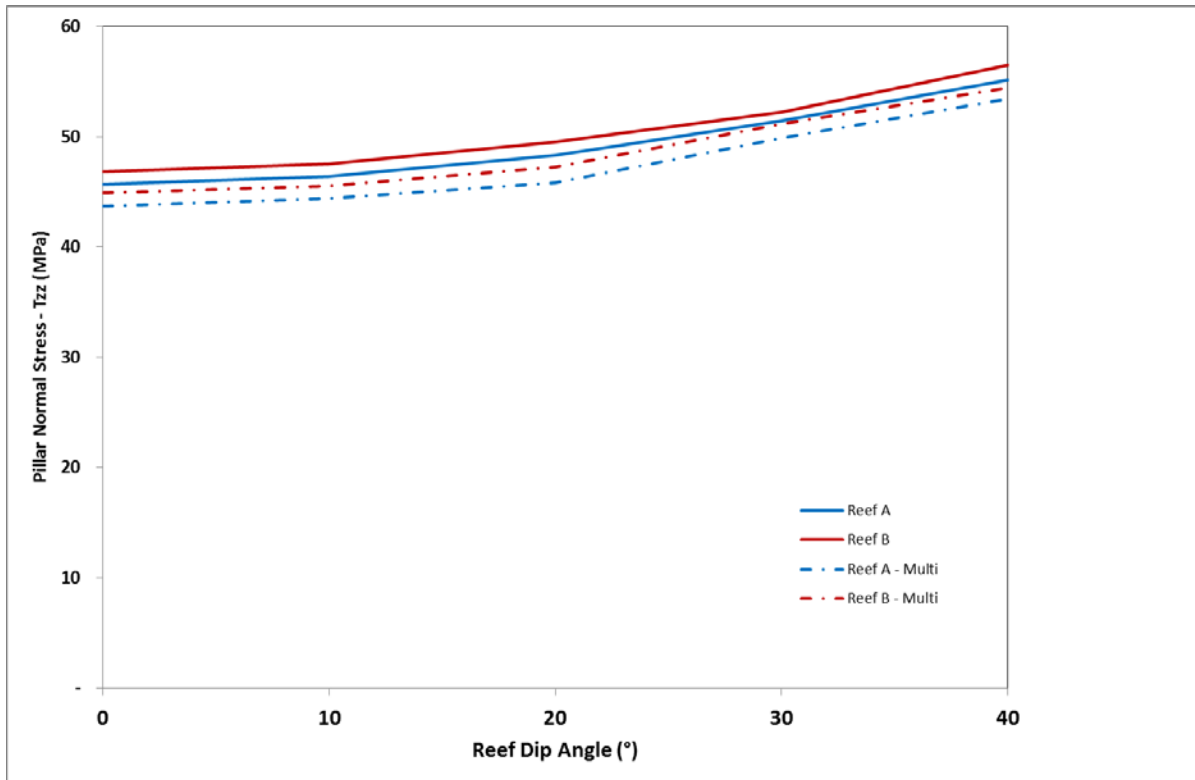
Figure 3-24: Pillar normal stress at varying dip angles

The results from the modelling are interpreted and prove that as the dip of the reef horizon increases, so does the normal stress on the pillar. As the depth of the pillar is being kept constant, the increase of the stress can best be described by the dip changes; the normal to the pillar are being influenced more by the higher horizontal stress (k-ratio equal to 1.5). When the stress levels on each reef horizon are compared between single and multi-reef mining, the modelling results indicate that the multi-reef stresses are in the order of 2 to 5 per cent less than that of the single reef values. This might give rise to a better FoS since a lower load is used in the calculation for the same strength, yet the complete stress regime has changed. As can be seen in Figures 3-25 and 3-26, a change of up to 20 per cent in the shear stress levels can possibly occur.
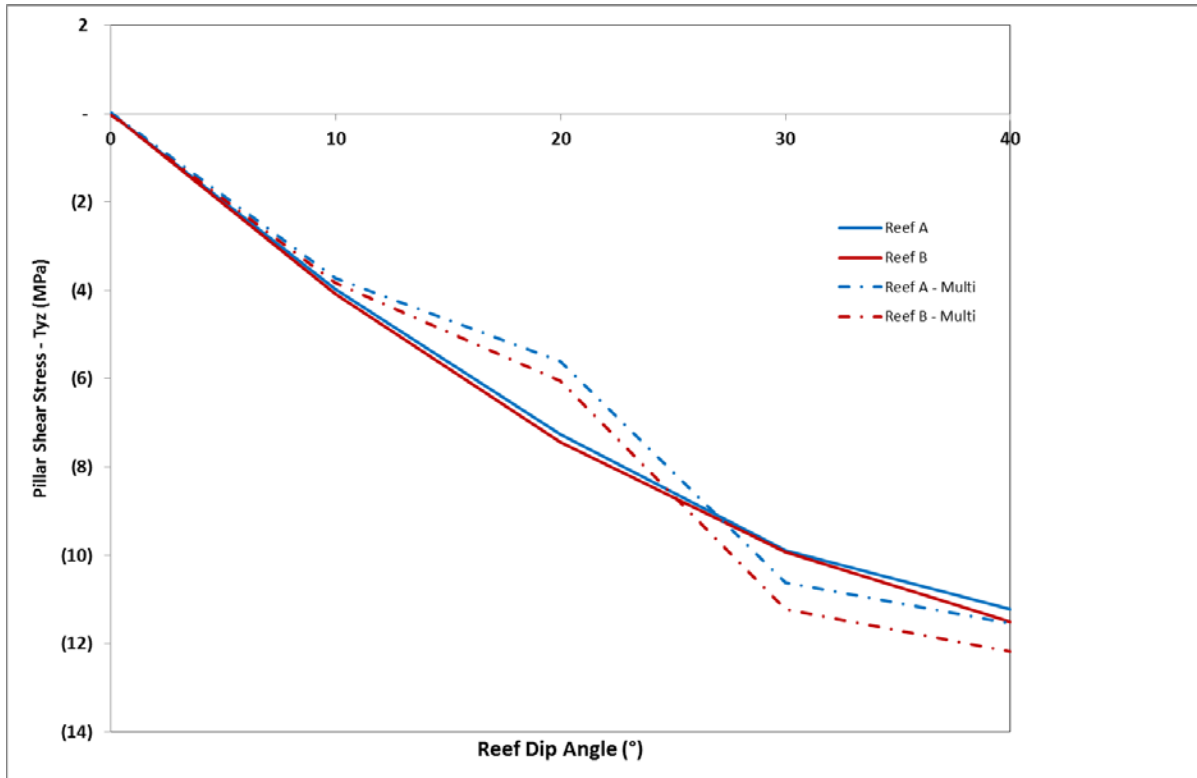
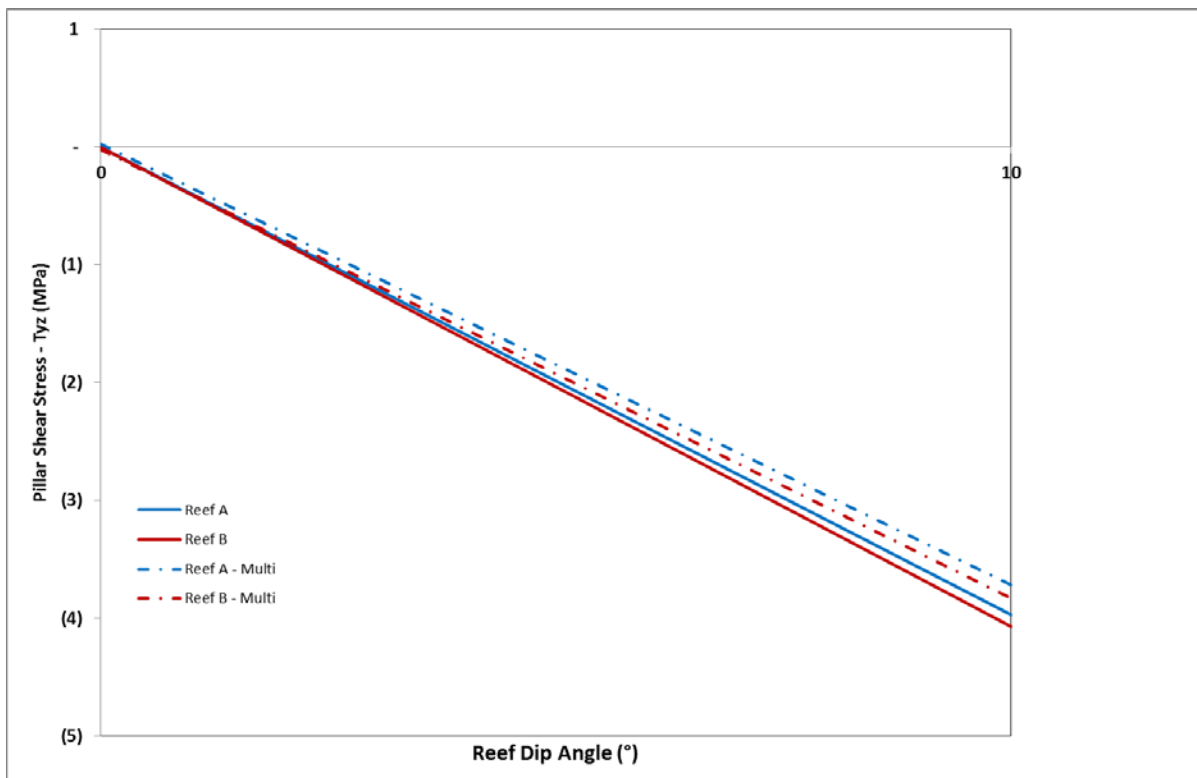**Figure 3-25: Pillar shear stress at changing dip angles**

Figure 3-26: Pillar shear stress at changing dip angles (Dip range 0° to 10°)

From Figure 3-25, an area of concern has been highlighted. For the given layout (75 per cent extraction with 8 m square pillars), at 20° dip angle, the stress shadows of the pillar reduce the shear stresses experienced by the pillar on the subsequent horizon.

As the ESS values are calculated as a function of the normal and shear stresses acting on the pillar, the ESS plot (Figure 3-27) indicate similar trends as for the shear stress.

Figure 3-27: Pillar ESS levels at varying dip angles
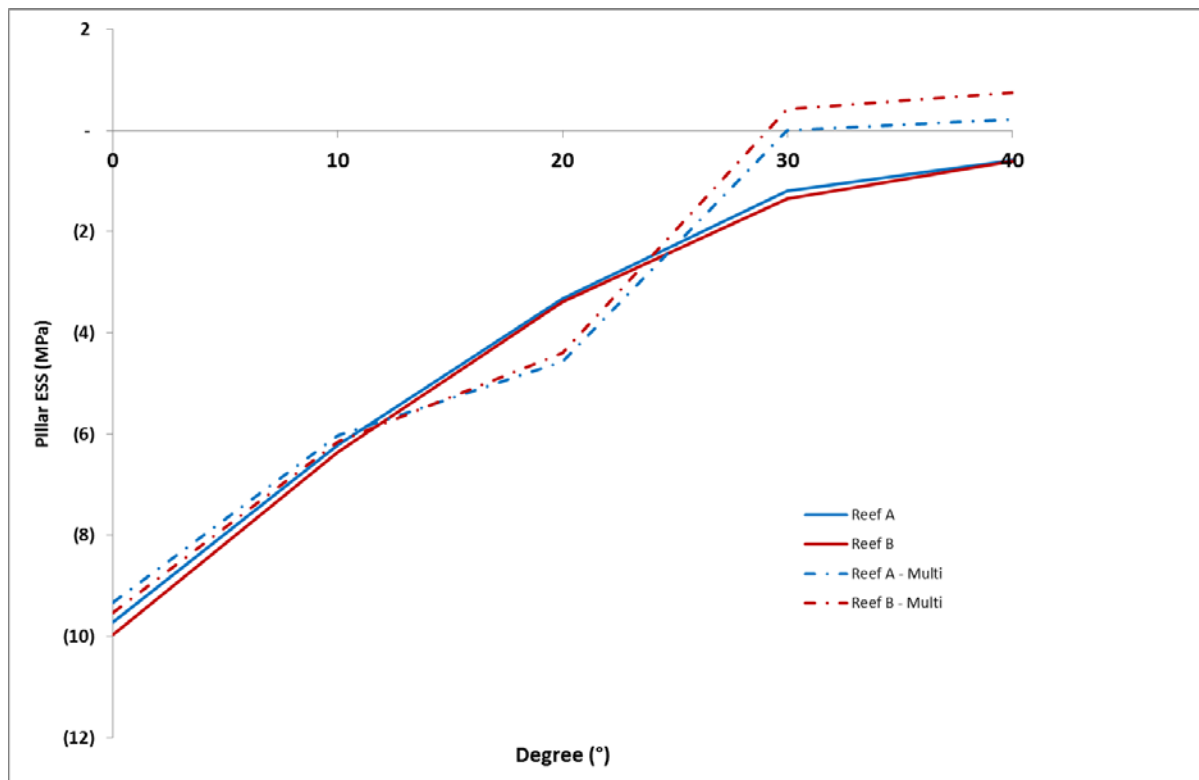
The results indicate that ESS levels could become positive at a specific combination of parameters; however, the significant changes are only observed at relatively steep dip angles.

The FoS as discussed in the previous sections can be calculated based on the traditional formulae or the formula proposed by Swart et. al. (2000). The values are presented in Figure 3-28.
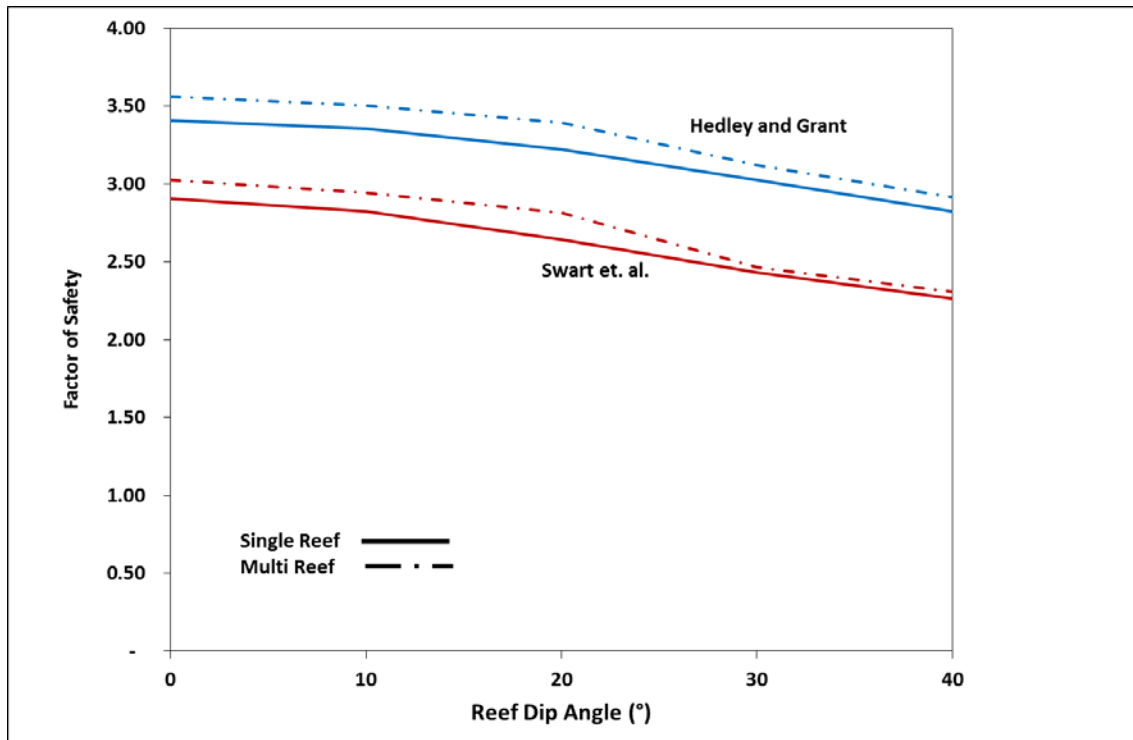
Figure 3-28: Factor of Safety (Hedley and Grant (1972) and Swart et al. (2000)). Single and Multi-reef

Findings from the study depict that as the load and orientation change, the FoS changes. It can be noted that the FoS calculated using the equation proposed by Swart et. al. (2000) is approximately 13 per cent less than the calculated FoS when using the traditional formula. Still, both formulae indicate that as the multi-reef scenario results in lower normal and or shear stresses due to the interaction that occurs, the FoS calculated is higher than that of the single reef scenario.

3.3 Shear stress on stability pillars

Since the mid-1960s, deep South African mining operations employed the methodology of designing unmined blocks of ground to act as stabilising structures for supporting and ensuring regional stability. This has been done to great success, yet not without teething problems and significant problems arising in practice. Stabilising pillar, often also referred to as barrier pillars, exploits the fact that efficient regional support should be obtained whilst still extracting the maximum from the mineralised zone in order to obtain the financial potential. For example, the energy release rate, or ERR, is a function of the mining span which relates to an increased span; it will result in an increased ERR value, hence better ground conditions, since

ERR levels correspond well to general mining conditions. Jager and Ryder (1999) stated that ESS levels are also greatly influenced by these stability pillars:

"The use of stabilising pillars not only decrease face ERR levels with corresponding expected improvements in general mining conditions, but also results in a diminution of seismic-inducing ESS lobes which sweep through the rock in front of the advancing mining faces." (Jager and Ryder (1999: 62)

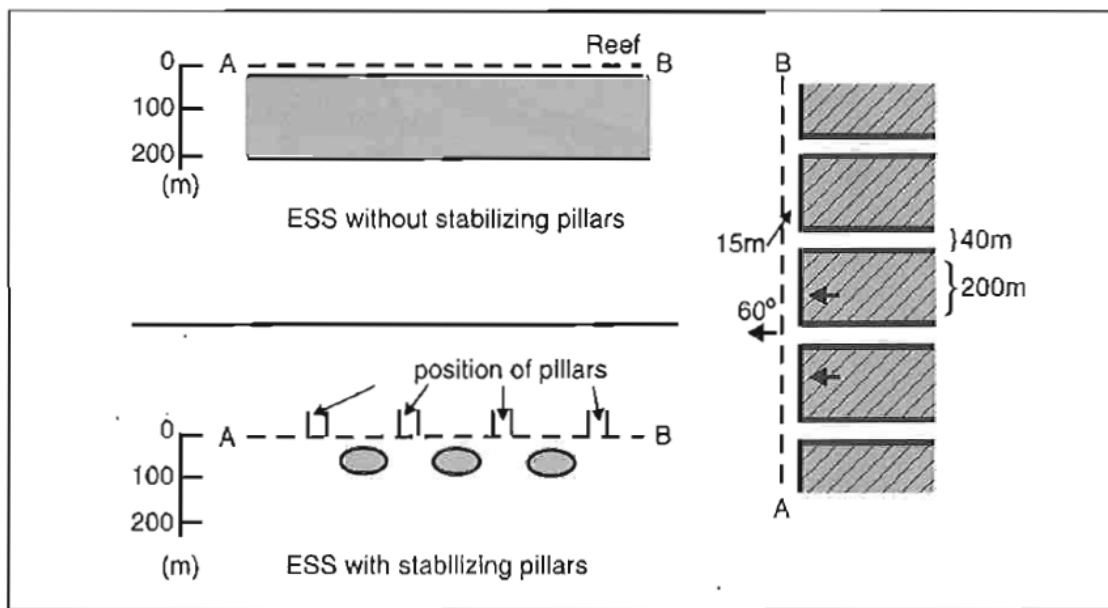The effect stabilising pillars have on these ESS lobes is depicted in Figure 3-29.

Figure 3-29: Effect of stabilising pillars on ESS in front of stope faces (after Jager and Ryder (1999))

During the design phase, the guideline at which these pillars are placed is such that the APS on the pillar should not exceed 2.5 times the value of the UCS of the weakest rock (hangingwall, footwall or actual pillar).

Such a layout has been simulated to ascertain the influence orientation (strike of dip orientated) has on the level of stress acting on the pillar and what effect will superimposed pillars have in this regard.

The TEXAN numerical model was set up with the parameters as presented in Table 3-8.

Table 3-8: Stability pillar – TEXAN input parameters

Parameter	Unit value		
Vertical stress gradient	3000 MPa/m		
Depth below surface	1500 m		
Gravitational constant *g*	9.81 m/s^2		
k-ratio (x and y direction)	1.5		
Reef dip	30°		
Model size Strike (x dir) Dip (y dir)	250 m 240 m		
Poisson's ratio	0.25		
Young's Modulus	65 GPa		
Pillar dimension	*Dip Dimension*	*Strike Dimension*	
Dip Stability	40 m	16 m	
Strike Stability	16 m	40 m	
Holings	10 m		
Element size (modelling grid)	2 m x 2 m		
Multi-reef middling	20 m		

The schematic of the layout in both the strike stability and dip stability orientation is given in Figure 3-30. In the case of the multi-reef scenario, the identical layout has been superimposed with a 20 m middling. The area around the pillars has been modelled as being mined so as to ensure that there is no influence from the "unmined" boundaries of the model.
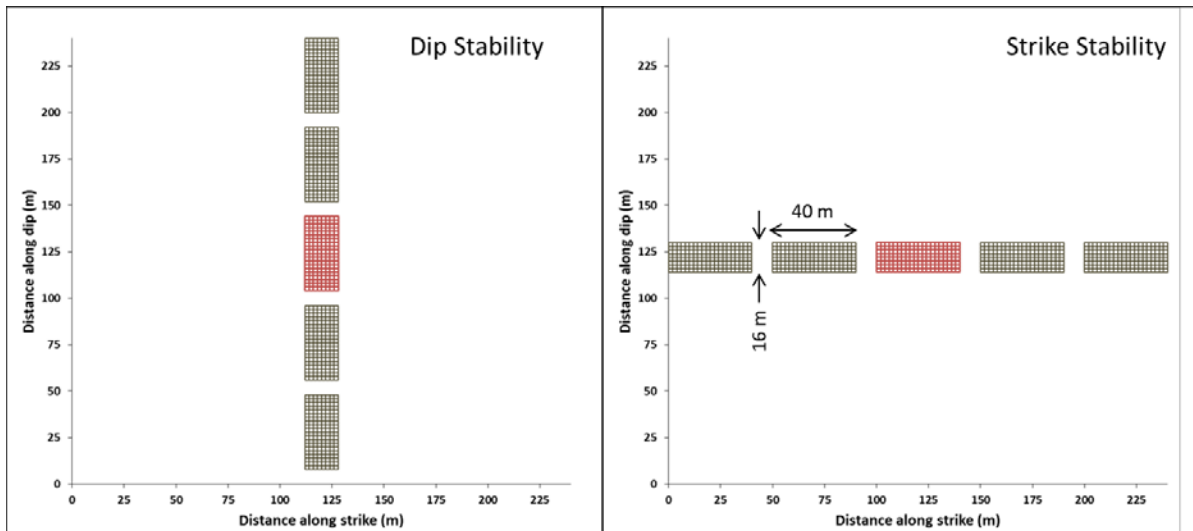
Figure 3-30: Schematic of modelled stability pillar layouts (red pillar indicating the pillar analysed)

3.3.1 Dip stability

The analysis on the stress acting on the pillar yielded the following results:

Table 3-9: Dip stability stress results

		Normal	Shear
Maximum	MPa	670	122
Minimum	MPa	189	34
Average	MPa	302	54

For the given scenario, the calculated vertical virgin stress amounts to 44.2 MPa. The pillar corners experience the highest levels of stress with the average stress calculated as 302 MPa.

When plotting the stresses levels, nothing less is presented. Higher stress levels, in this case, normal (Figure 3-31) and shear (Figure 3-32) stresses, can be seen on the pillar corners with lower levels towards the centre of the pillar. The contours of these stress levels are plotted in Figure 3-31.
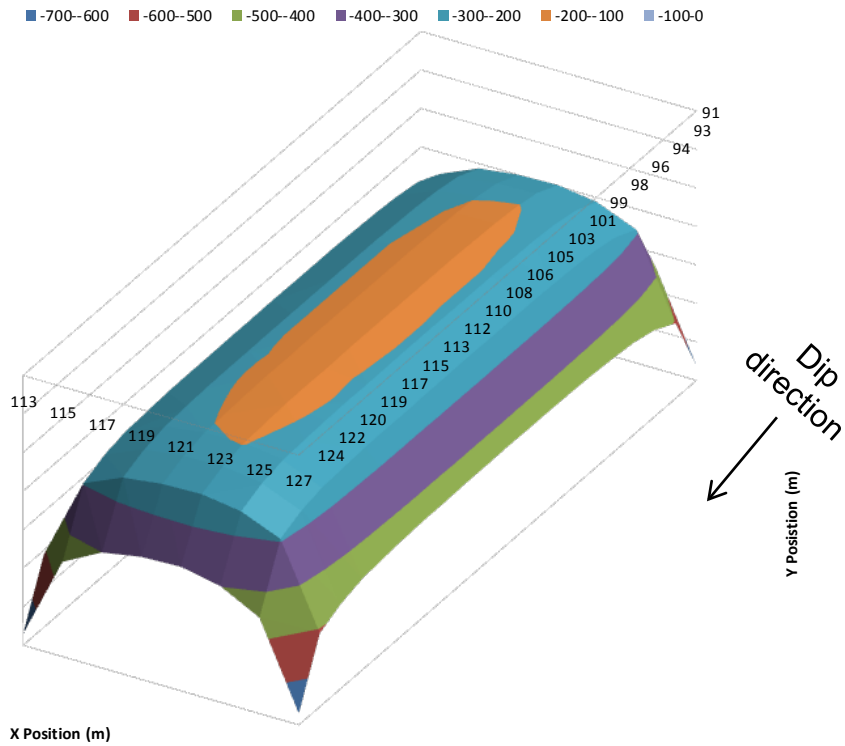
70

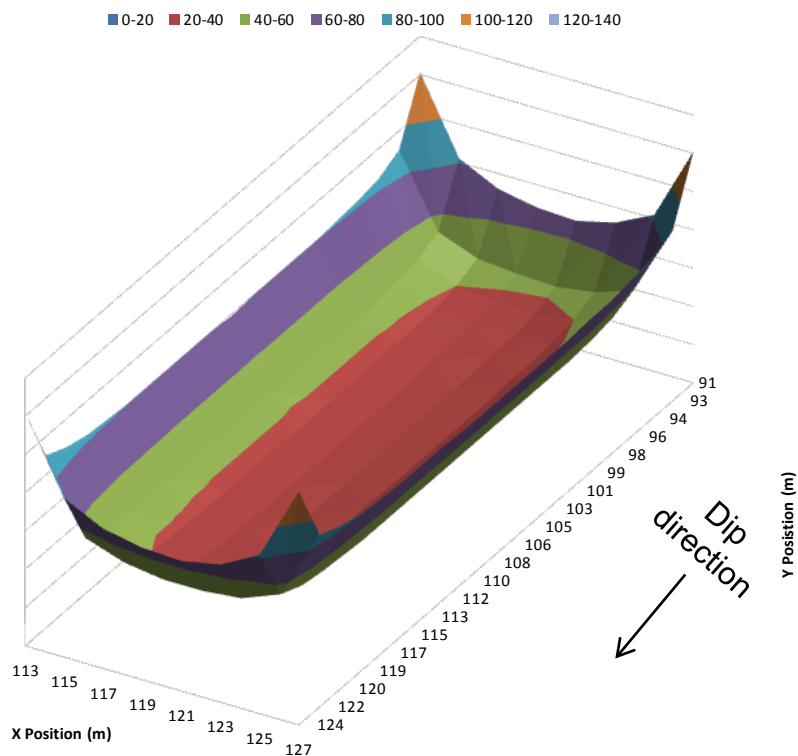**Figure 3-31: Pillar normal stress – Dip stability pillar**

Figure 3-32: Pillar shear stress – Dip stability pillar

In contrast with the findings in section 3.1.1 where the shear stress levels are both positive and negative (acting in both directions) for a pillar on a flat horizon, the dip pillar on dip does not display any signs of stress direction change.

When these are plotted in an ESS relation (with $\phi = 12°$) where increased normal stress increase the resisting levels, the contours can be seen in Figure 3-33.
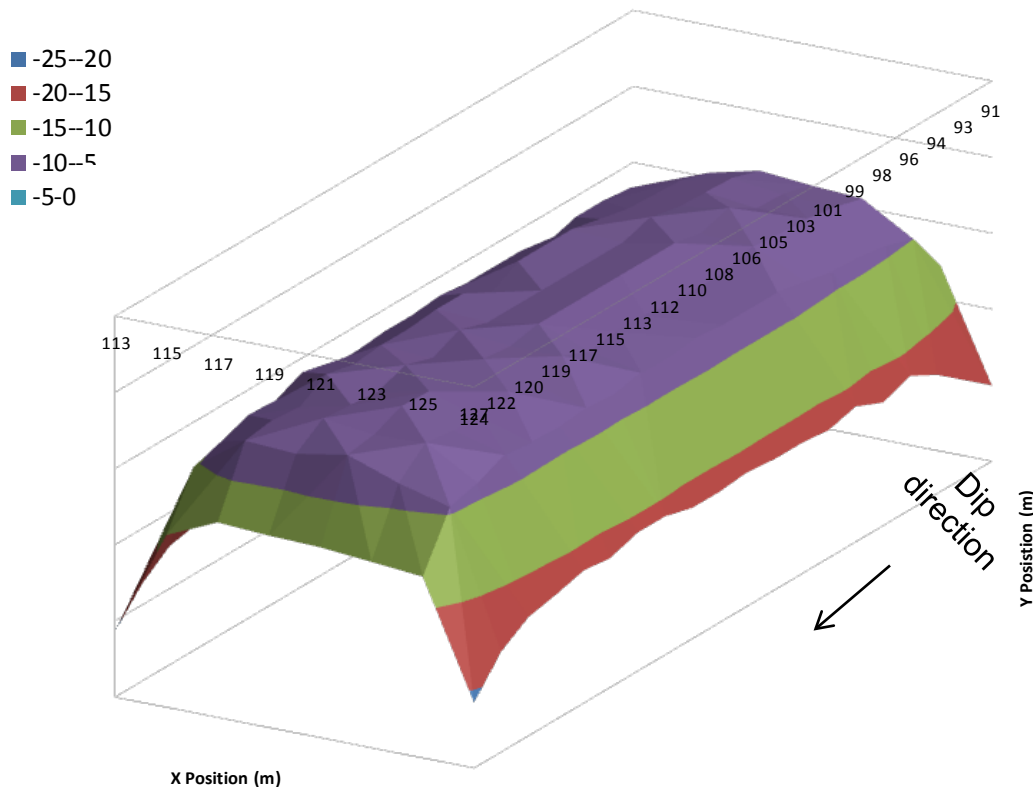

Figure 3-33: ESS contours – Dip stability

Instability is expected where ESS values are positive. The values calculated range between -20.7 MPa and -6.1 MPa, with an average of -10.3 MPa, hence in all aspects related to the modelling conditions – a stable pillar.

3.3.2 Strike stability

On changing the orientation of the stability pillar (as in the case for longwall mining) to strike stability pillar, it is suggested that the smaller dimension along dip might affect the stress levels even at the same depth as for a dip stability pillar in the previous section. The analysis on the shear stress acting on the pillar yielded the results that follow.

Table 3-10: Strike stability stress results

		Normal	Shear
Maximum	MPa	724	145
Minimum	MPa	191	39
Average	MPa	313	64

The contours of these stress levels are plotted in the figures that follow (*Note the increased stress levels again at the corners of the pillars*):
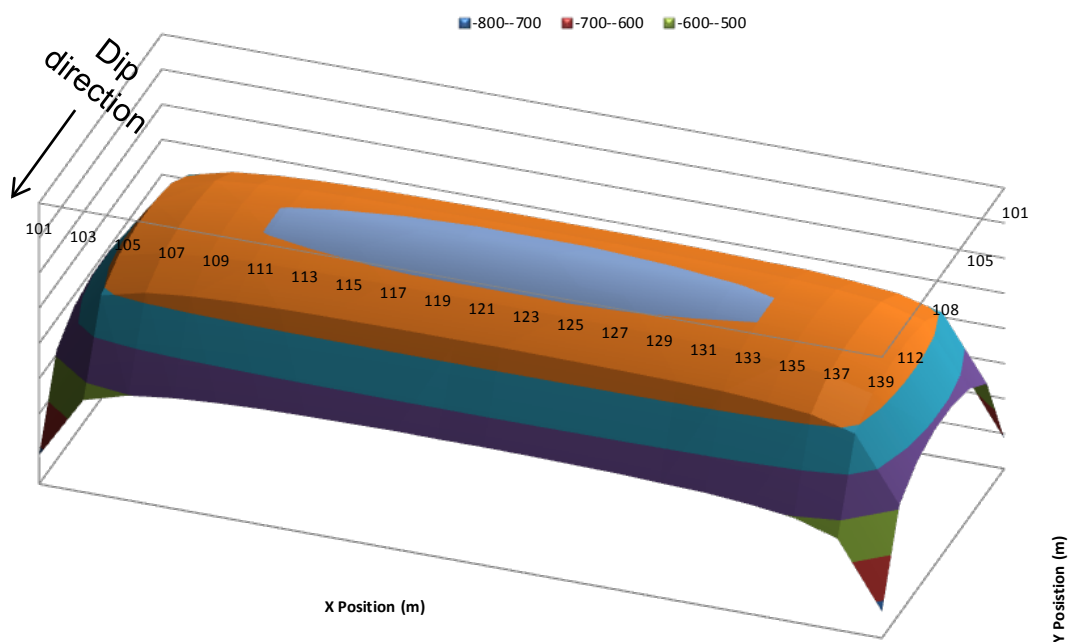

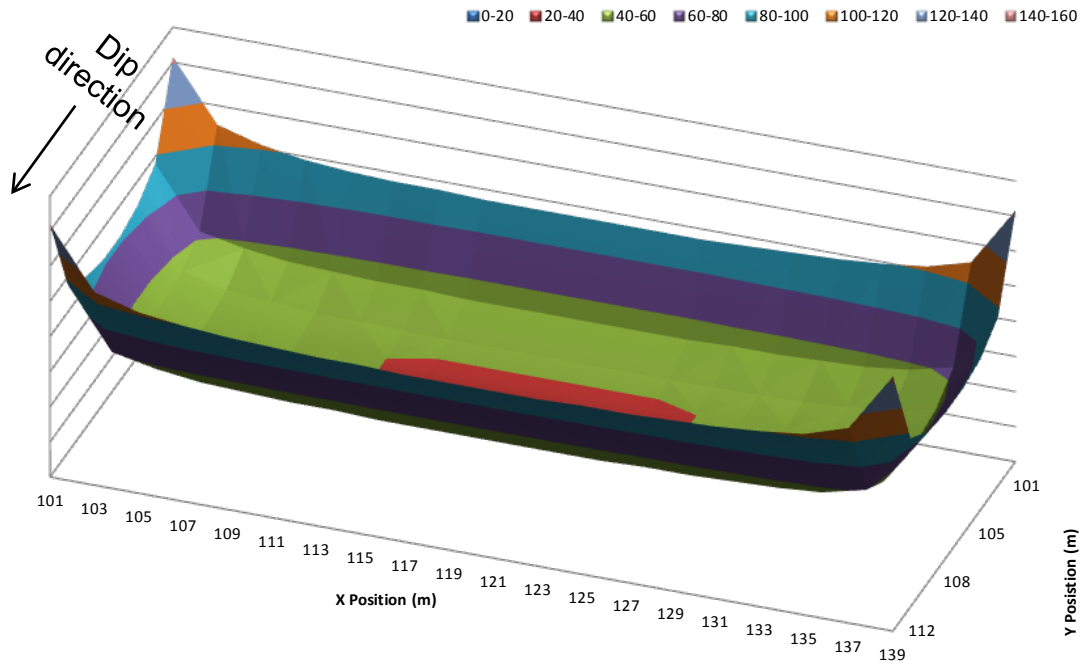**Figure 3-34: Pillar normal stress – Strike stability pillar**

Figure 3-35: Pillar shear stress – Strike stability pillar
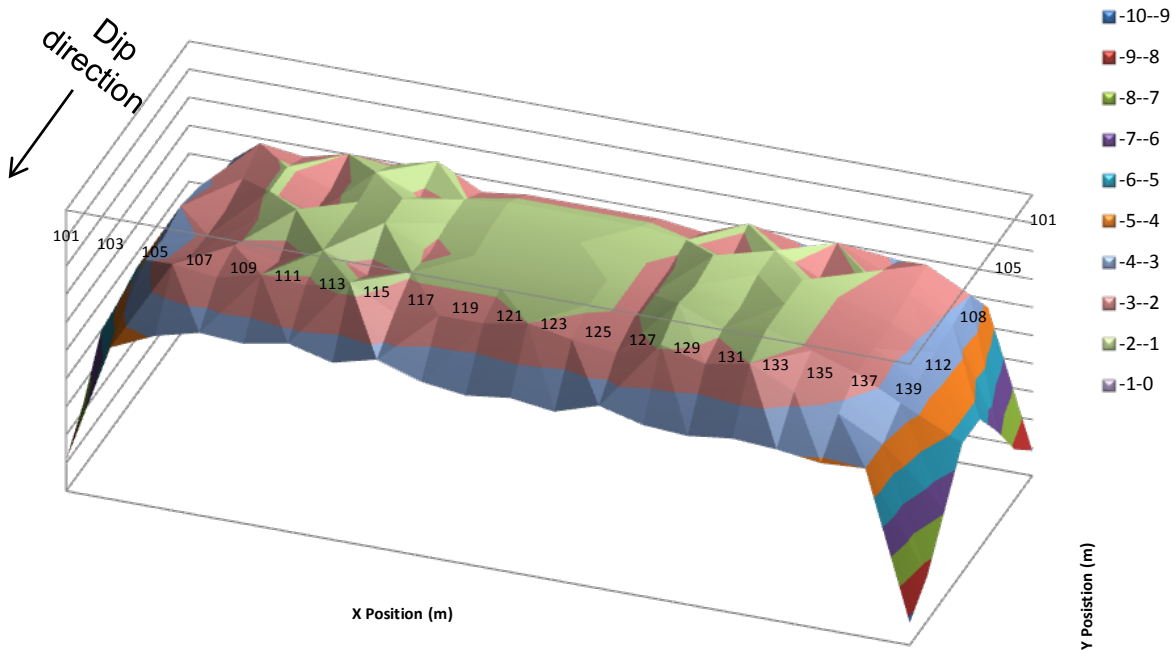

Figure 3-36: ESS contours – Strike stability

Compared to the dip stability pillar under section 3.3.1, the plot seems much different. The ESS values calculated range between -9.2 MPa and -1.3 MPa, with an average level of -3.0 MPa. As all of these values are also negative, the pillar should be stable according to definition, yet the levels do indicate that areas of concern

develop when orientated along strike versus the dip orientation of the previous section. The normal stresses do not experience that big a change as the orientation changes (3.6 per cent increase); however, the shear stresses undergo a drastic change when orientated on strike rather than dip (18.5 per cent increase). A summary is depicted in Table 3-11.

Table 3-11: Stress levels for dip versus strike stability pillars

Orientation		Single Normal (MPa)	Shear (MPa)
Dip	Maximum	670	122
	Minimum	189	34
	Average	302	54
Strike	Maximum	724	145
	Minimum	191	39
	Average	313	64

3.3.3 Multi-reef scenario

When stability pillars are superimposed (dip and strike orientations) where a small middling is expected, interaction is eminent. The results from the simulation are presented in

Table 3-12. The values presented reflect the values on the pillar with respect to the same horizon as that analysed in sections 3.3.1 and 3.3.2.

A schematic is given so as to illustrate the position of the two reef horizons relative to each other.
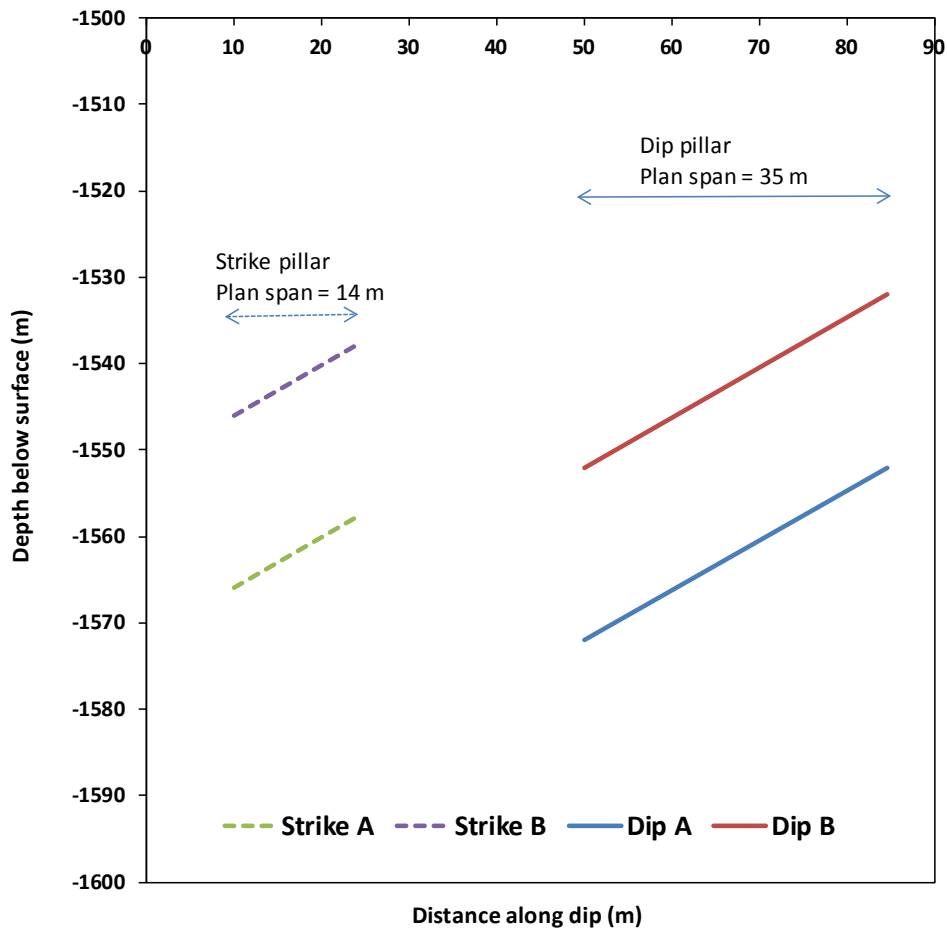

Figure 3-37: Schematic of pillar position relative to multi-reef pillar position

Noticeable when plotted in relation to each other is the span of each set-up on plan. As explained earlier in this section, the stress shadow will influence the stress interaction of the pillar in relation to the span and middling distance.

Table 3-12: Comparison of average stress levels – Single pillar, Single vs. Multi-reef

		Orientation	Single Normal	Shear		Multi Normal	Shear
Maximum	MPa	Dip	670	122		565	140
Minimum			189	34		176	30
Average			302	54		**267**	**57**
Maximum	MPa	Strike	724	145		795	69
Minimum			191	39		88	-11
Average			313	64		**221**	**10**

The analysis show that the normal stresses (on average) are reduced in both cases (11.6 per cent on dip and 29.4 per cent on strike). Still, the shear stresses on the reef horizon for a strike pillar see a dramatic reduction (84.4 per cent) with a minute change to the shear on a dip-orientated pillar (5.5 per cent).

A schematic of the ESS levels is shown in Figure 3-38. The positive ESS levels on the dip orientation are much more significant as they are for the strike pillar.
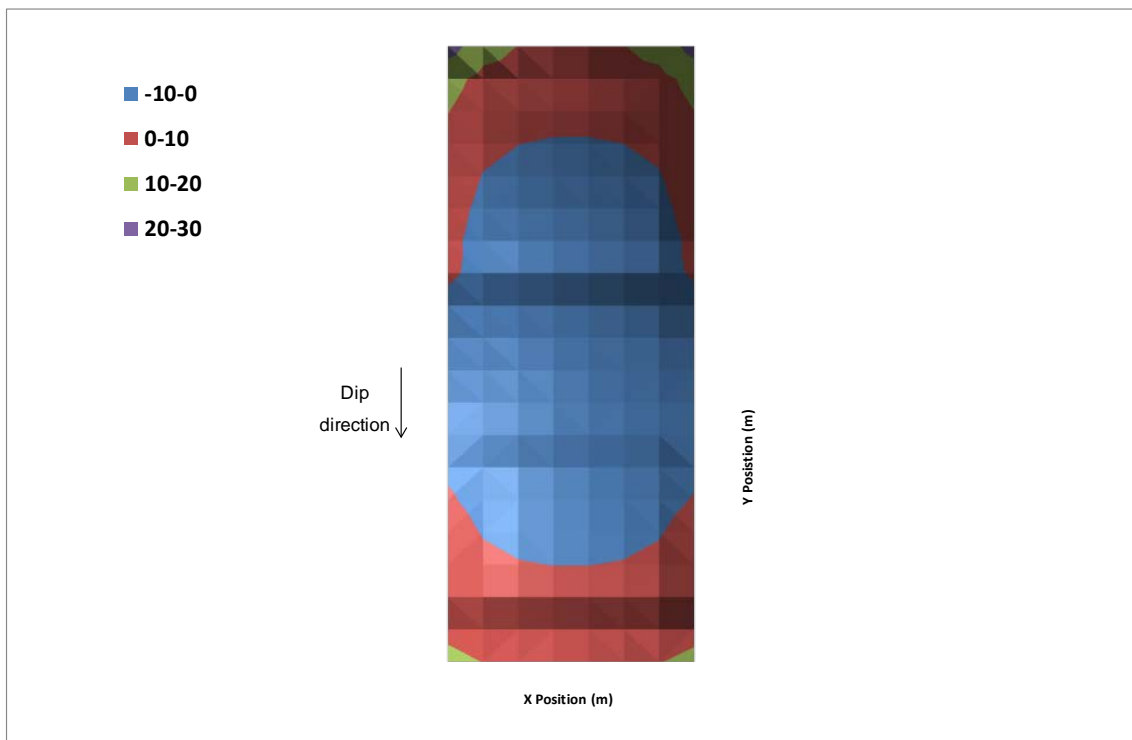

Figure 3-38: ESS contours on dip stability pillar – Multi-reef condition

On the dip pillar plot in Figure 3-38, the red, green and purple contours highlight areas with positive ESS values. The plot indicates that only the pillar core is predicted to be in a stable state.
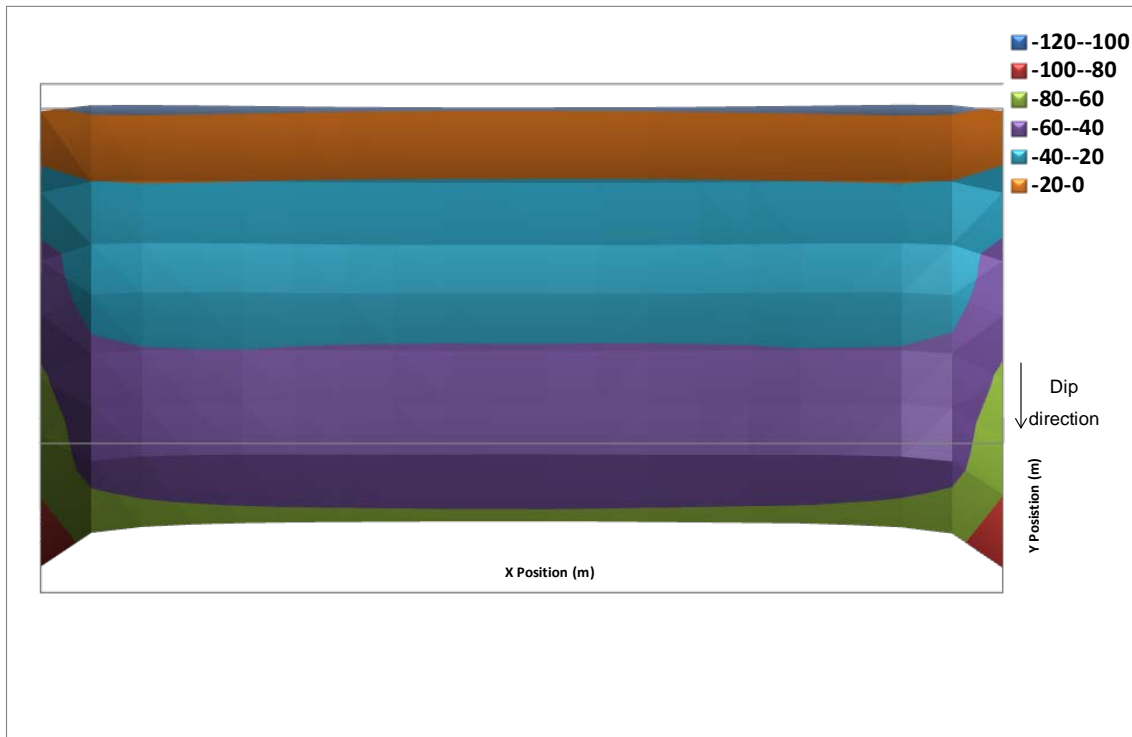

Figure 3-39: ESS contours on strike stability pillar – Multi-reef condition

With the strike stability pillar, the ESS values decline as the depth increases. It shows that at the top position of the pillar, the pillar is in the stress shadow of the alternate pillar, which, in turn, reduces the normal stress on the position, resulting in the ESS levels being closer to zero (or unstable positive values).

3.4 Summary

This chapter illustrates the complex stress interactions for multi-reef pillar layouts in areas where the middling between the reefs is small. It is also proved that the pillar orientation and positioning greatly affect the loading conditions.

The TEXAN boundary element code is well suited to simulate these layouts for mining problems containing large numbers of pillars. An important finding of this study is that shear stresses are induced in the pillars when identical pillar layouts are perfectly superimposed in a multi-reef layout. The shear stresses result in a reduction of the normal stresses on the pillars when compared to a single reef layout.

This finding is counterintuitive and may lead to the incorrect conclusion that enhanced pillar stability may be obtained for this idealistic multi-reef scenario. The effect of the shear stress on pillar stability is not quantified, however, and it requires further study. The TEXAN code was also used to simulate an actual multi-reef chrome mine layout in the Eastern Bushveld. This illustrated the extremely complex stress interactions when pillars of irregular shapes are not superimposed.

The simple coal mine rules of superimposing of pillars should therefore be treated with caution. Routine numerical modelling and underground monitoring of pillars and middling stability are considered vital to ensure that safe mining conditions are maintained for these layouts.

Orientation of stability pillars appears to be crucial in the sense that stress conditions, particularly shear stresses, are greatly affected by the direction of dip. First indications showed that dip stability pillars are "stressed" less in both normal and shear orientations.

3.5 References

Du Plessis, M.; Malan, D.F.; Napier, J.A.L. (2011, December). Evaluation of a limit equilibrium model to simulate crush pillar behaviour. The Journal of The Southern African Institute of Mining and Metallurgy, Vol 111, pp 875-885.

Hedley, D.G.F. and Grant, F. (1972). Stope-and-pillar design for Elliot Lake Uranium Mines. Bull. Can. Inst. Min. Metal., pp. 37-44.

Jager, A.J and Ryder, J.A. (1999). A handbook on rock engineering pratice for tabular hard rock mines. Johannesburg: The Safety in Mines Research Advisory Committee.

Maritz, J.A.; Malan, D.F. (2011). The influence of shear stress and weak contacts on pillar behaviour. 12th ISRM International Congress on Rock Mechanics. Beijing.

Maritz, J.A.; Malan, D.F.; Piper, P.S. (2012). Estimating pillar stresses in complex multi-reef layouts. Southern Hemisphere International Rock Engineering Symposium, (pp. 125-143). Sun City, South Africa.

Napier, J.A.L.; Malan, D.F. (2007, November). The computational analysis of shallow depth tabular mining problems. The Journal of The Southern African Institute of Mining and Metallurgy, Vol 107, pp 725-742.

Salamon, M.D.; Oravecz, K.I. (1976). Rock Mechanics in Coal Mining. P.R.D. Series No 198.

Swart, A., Keyter, G., Wesseloo, J., Stacey, T., & Joughin, W. (2000). Influence of surface topography on the loading of pillar workings in near surface and shallow mines – OTH 501. SIMRAC.

Van der Merwe, J.N.; Madden, B.J. (2002). Rock Engineering for underground coal mining. Johannesburg: The South African Institute of Mining and Metallurgy.

4 SHEAR STRESS EFFECT ON PILLAR STRENGTH

The elastic modelling presented in the previous chapter highlighted the concern with regards to the presence and possible influence of shear stresses on the loading of a pillar system. To further investigate this effect, and especially on the traditionally used Factor of Safety method of pillar design, an inelastic numerical model was constructed using the UDEC modelling code by ITASCA. The numerical model was run to simulate the effect of reef dip on single reef and interaction in multi-reef scenarios with a small middling (10 m). This chapter describes the finding of the assessment.

4.1 Geotechnical data

The geotechnical input parameters for the models have been sourced from previous laboratory tests carried out on hard rock samples so as to simulate a realistic rock mass. A summary of the rock mass strength parameters assigned in the models is presented in Table 4-1.

Table 4-1: Summary of the rock mass strength parameters

	Material Type	Soft Overburden	Reef 1	Reef 2	Host rock
Density	Density (kg/m^3)		3000	4000	2800
Moduli	Bulk Modulus (GPa)	0.1	3.9	1	10
	Shear Modulus (GPa)	1.40	3.7	1	8
Rock mass strength	Cohesion (MPa)	0.01	10	10	6
	Friction angle (°)	20	40	50	35
	Tensile strength (MPa)	0.01	1	0.75	1

4.2 Model setup

For the numerical modelling, the ITASCA code, UDEC, was selected. UDEC, a two-dimensional code, is capable of simulating the response of a rock mass to either static or dynamic loading. The mining height was assumed to be 1.8 m and the pillar width 8 m.

The models were initially run applying an elastic constitutive model (prior to mining). The Mohr-Coulomb constitutive model was then applied to determine potential tensile and shear fracturing zones. The failure envelope for this model corresponds to a Mohr-Coulomb criterion (shear yield function) with tension cut-off (tensile yield function). A strain-softening model was also adopted, the details of which are discussed in the sections below.

Reef dip angles ranging from 0° to 40° were simulated with intervals of 10°. The reefs were assumed to be separated by a middling of 10 m (vertical distance) at a depth of 400 m below surface. The pillars are superimposed.

Both vertical edges of the model were simulated as lines of symmetry; the upper boundary simulated the ground surface (free surface); and the bottom of the models was simulated as a fixed boundary in the vertical direction.

The stress gradient was allowed to develop in the model based on the densities assigned to each rock material layer. The gravitational acceleration was assumed to be 9.81 m/s² in the vertical direction and zero in the horizontal direction, with a k-ratio of 1.5 applied in the models.

An example of the UDEC code input file is presented in APPENDIX A.

4.3   UDEC modelling results

The results are presented as two steps. First, the single-reef environment, being 400 m below surface at various reef dip angles and secondly, as a multi-reef environment, being 400 m below surface, with the second reef being 10 m below the first.

For each model, the single-reef scenario was simulated and iterated until equilibrium delineating mining step number 1, after which the second reef was introduced and the stress redistribution simulated.

4.3.1 Reef dip angle of 0 degrees

Figure 4-1 depicts a schematic showing the principal stress components around the excavations on Reef 1 prior to mining the second reef, which is approximately 10 m below the first reef. A similar plot is presented in Figure 4-3, showing the principal stress components after extracting the second reef. As can be seen, the stress

components through the middle of the 8-m wide pillars remain vertical for both the single-reef extraction, as well as the multi-reef extraction.
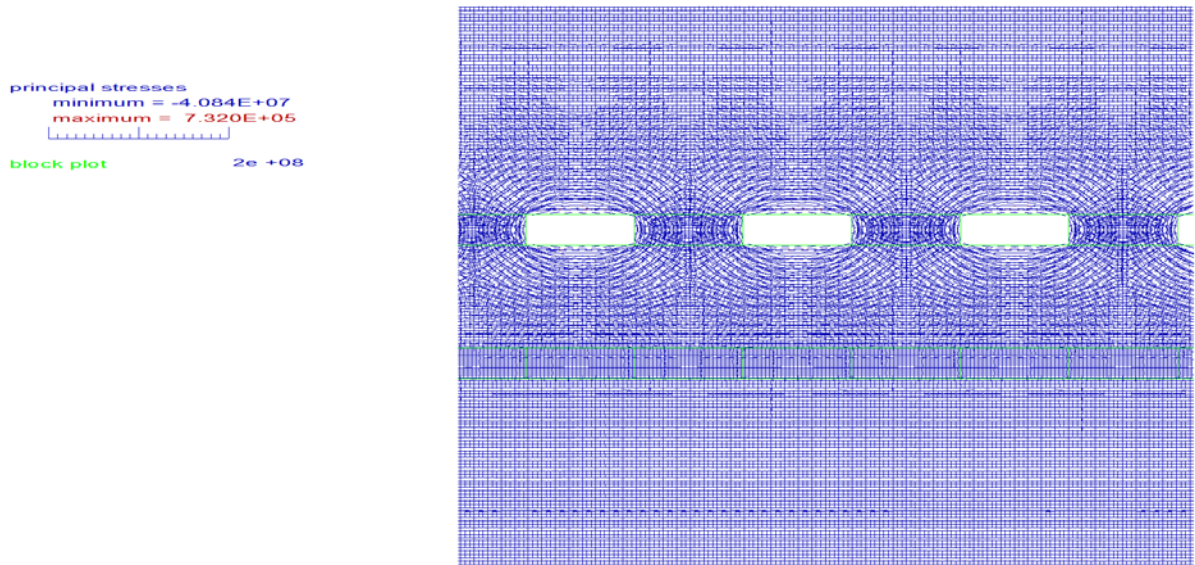

Figure 4-1: Single-reef extraction (simulated as mining step 1)
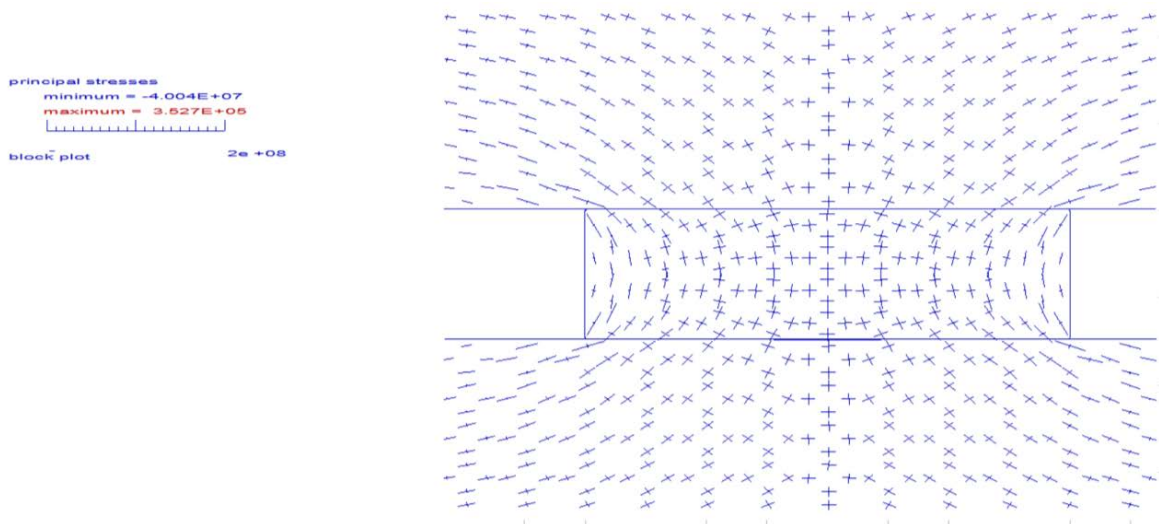

Figure 4-2: Zoomed in Single-reef extraction (simulated as mining step 1)

principal stresses
   minimum = -4.089E+07
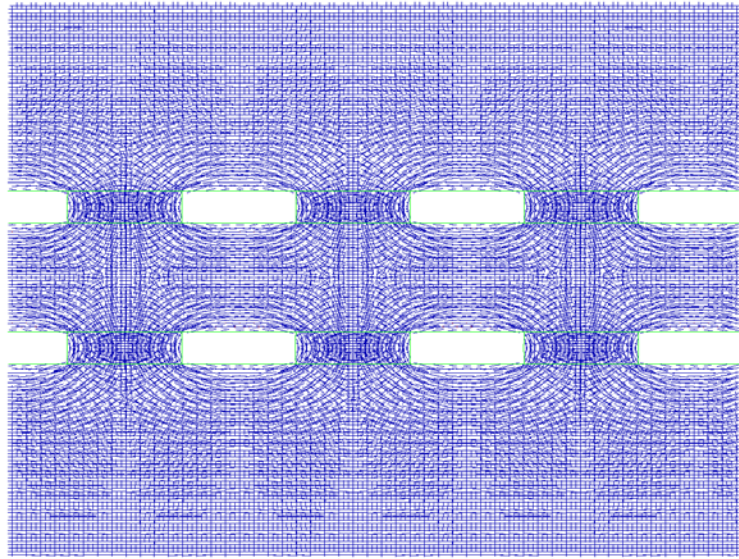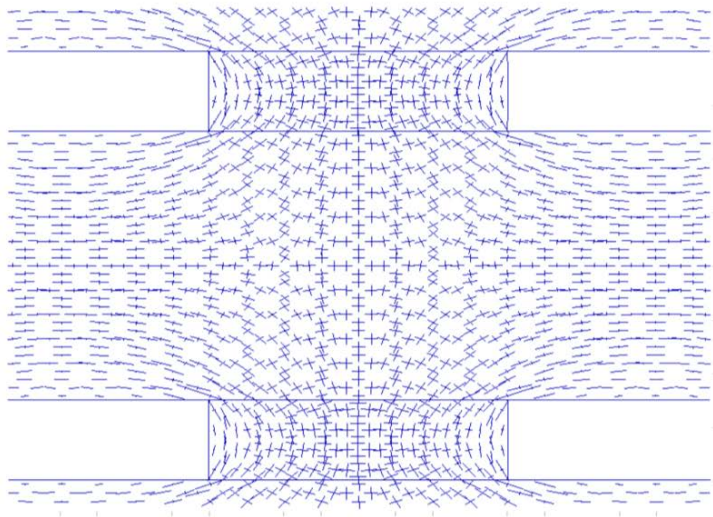   maximum = 8.041E+05

block plot   2e +08

Figure 4-3: Multi-reef extraction (simulated as mining step 2)

principal stresses
   minimum = -4.007E+07
   maximum = 7.446E+05

block plot   2e +08

x=   86.633 y=   -405.675
block=   782 zone= 2156168

Figure 4-4: Zoomed in Multi-reef extraction (simulated as mining step 2)

A plot showing the vertical stress contours around the two reefs for the case of multi-reef extraction is presented in Figure 4-5. The stress level within the pillars is predicted to reach approximately 22 MPa.
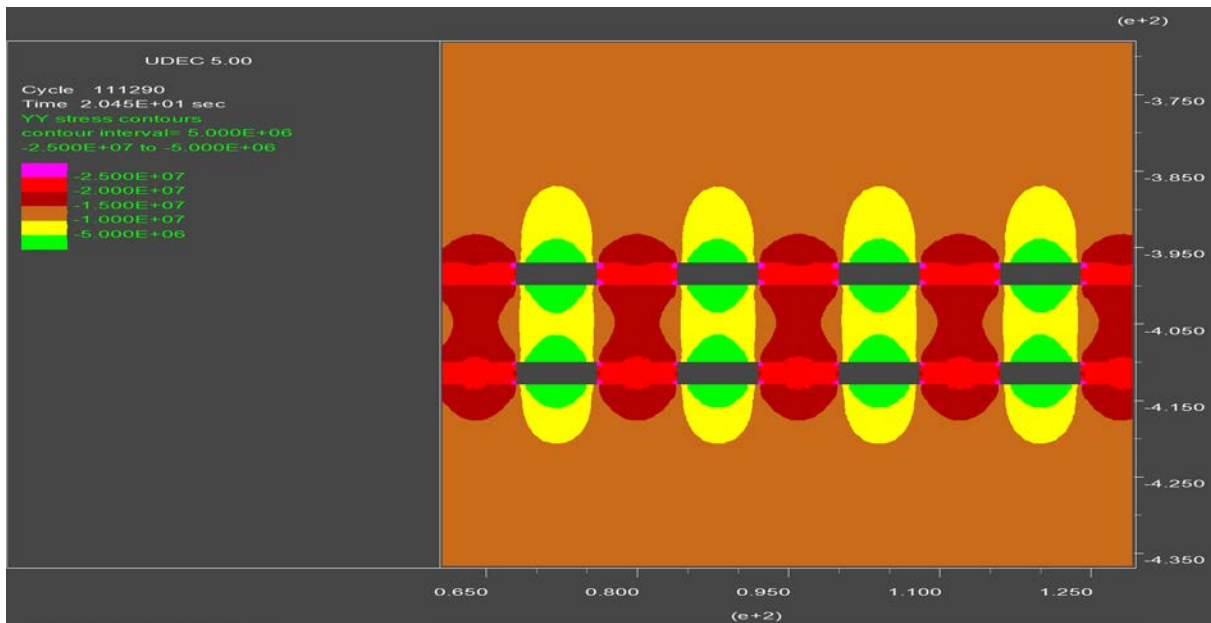
Figure 4-5: Vertical stresses around the two reefs

The shear on the pillars are limited to the boundary of the excavations and even more so on the corners as can be seen in Figure 4-6 and Figure 4-7.
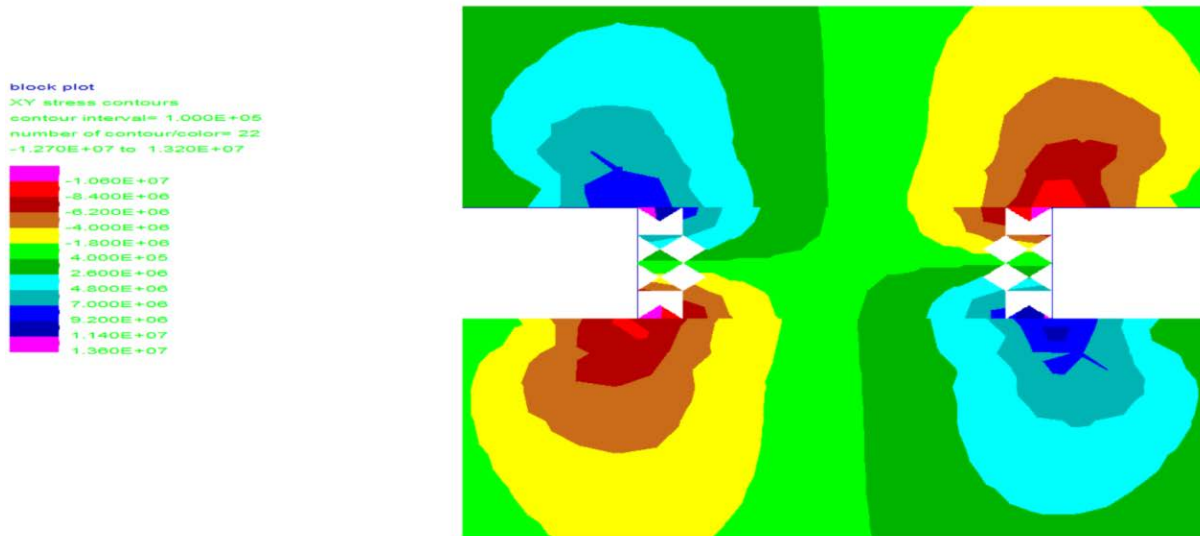

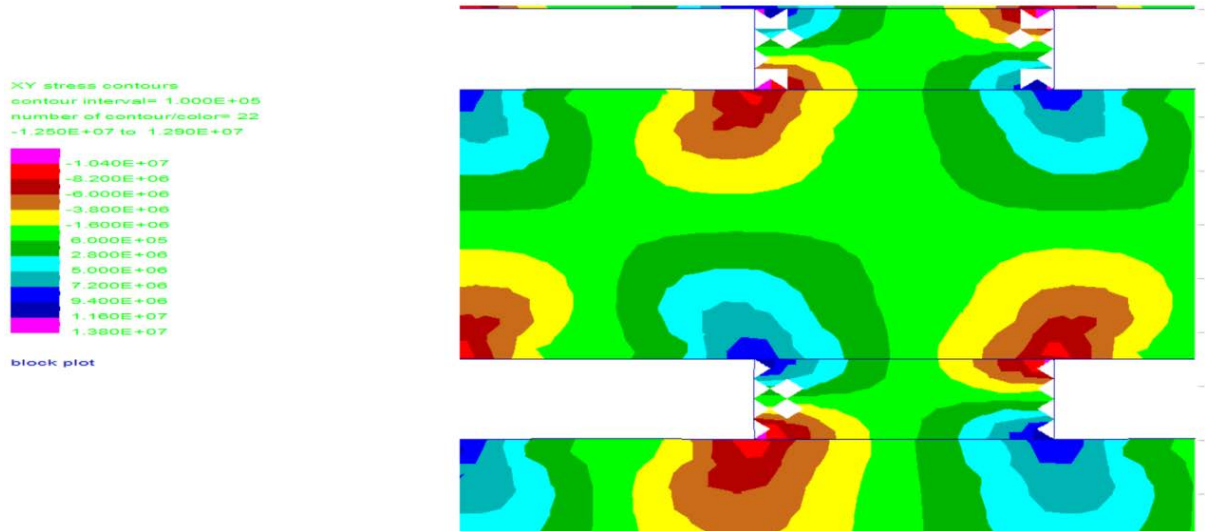**Figure 4-6: Shear stress contours around single reef pillars**

85

Figure 4-7: Shear stress contours around multi reef pillars

Figure 4-8 and Figure 4-9 present the vertical displacement contours around the two reefs. After excavation of the second reef, the general direction of displacement becomes downward, i.e. the floor of the excavation on Reef 1 also moves downwards, whereas if only a single reef is mined, the floor displaces upward into the excavation.
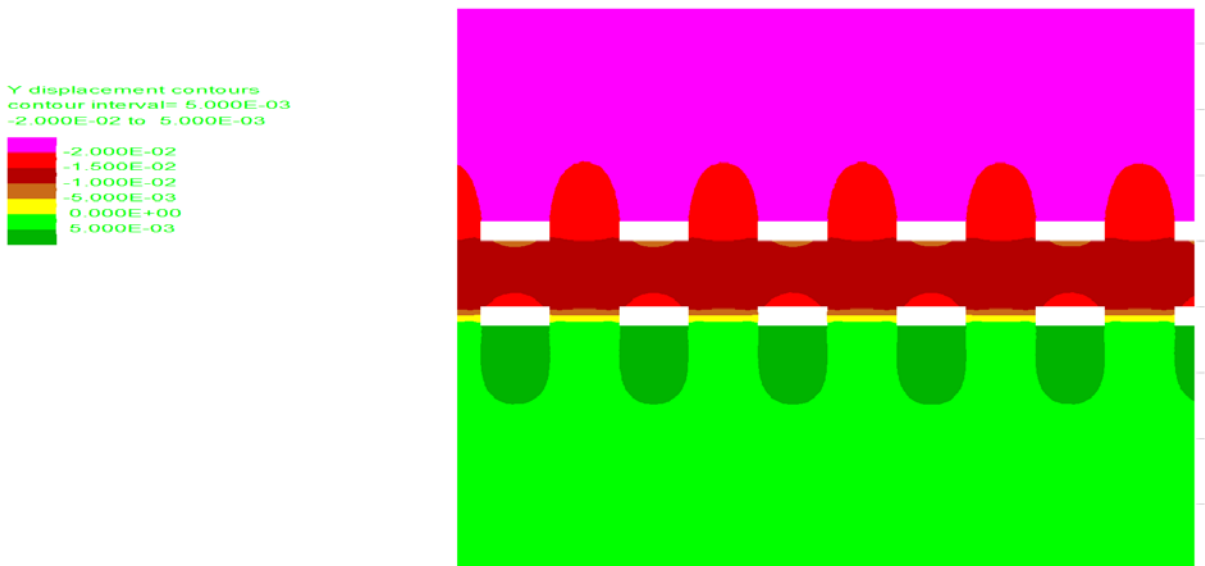

Figure 4-8: Vertical displacement around multi-reef excavations

Y displacement contours
contour interval= 2.000E-03
-2.400E-02 to -1.000E-02

-2.400E-02
-2.200E-02
-2.000E-02
-1.800E-02
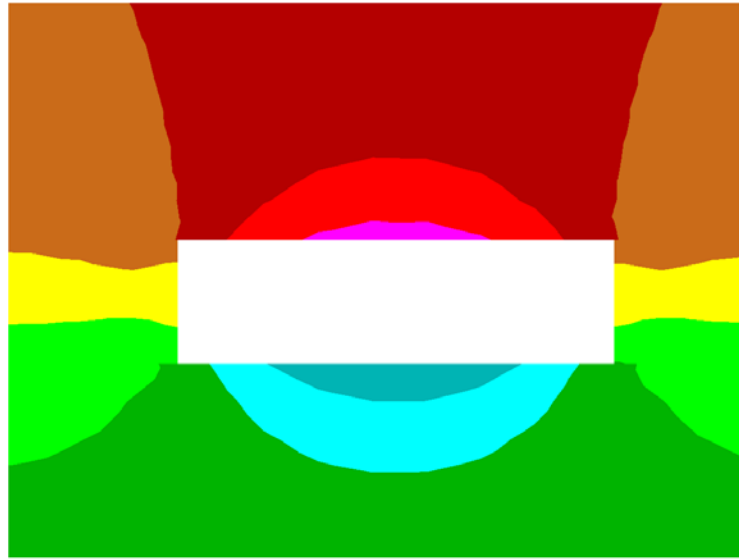-1.600E-02
-1.400E-02
-1.200E-02
-1.000E-02

Figure 4-9: Vertical displacement around one excavation on the top reef

The plots show the zones where shear yielding and tensile failure is predicted around the excavations for the single-reef extraction case (Figure 4-10) and the multi-reef extraction case (Figure 4-11). The results clearly indicate interaction between the two reefs with the shear yielding zones extending from the top reef to the bottom reef.

no. zones : total   12400
at yield surface (*)   0
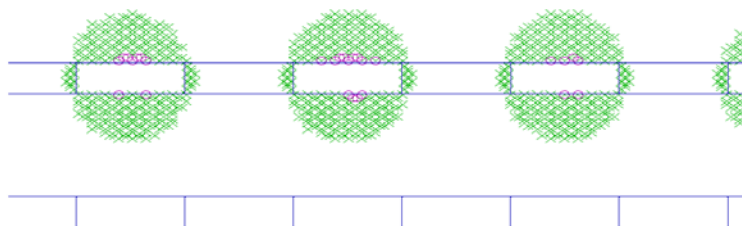yielded in past (X)   908
tensile failure (o)   28
block plot

Figure 4-10: Shear yield and tensile failure zones for the single-reef extraction case
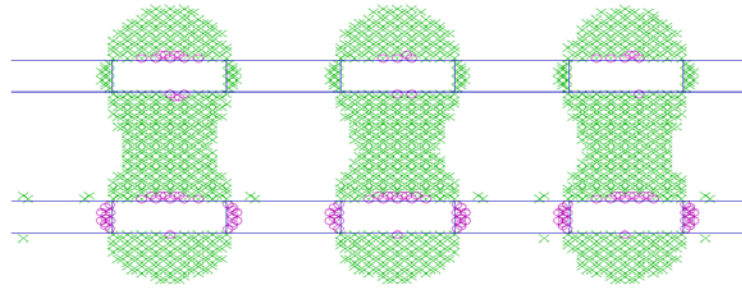
Figure 4-11: Shear yield and tensile failure zones for the multi-reef extraction case

Various investigation points were selected within pillars at various positions for both the top and bottom reef horizons. A screen shot indicating these positions is presented in Figure 4-11.
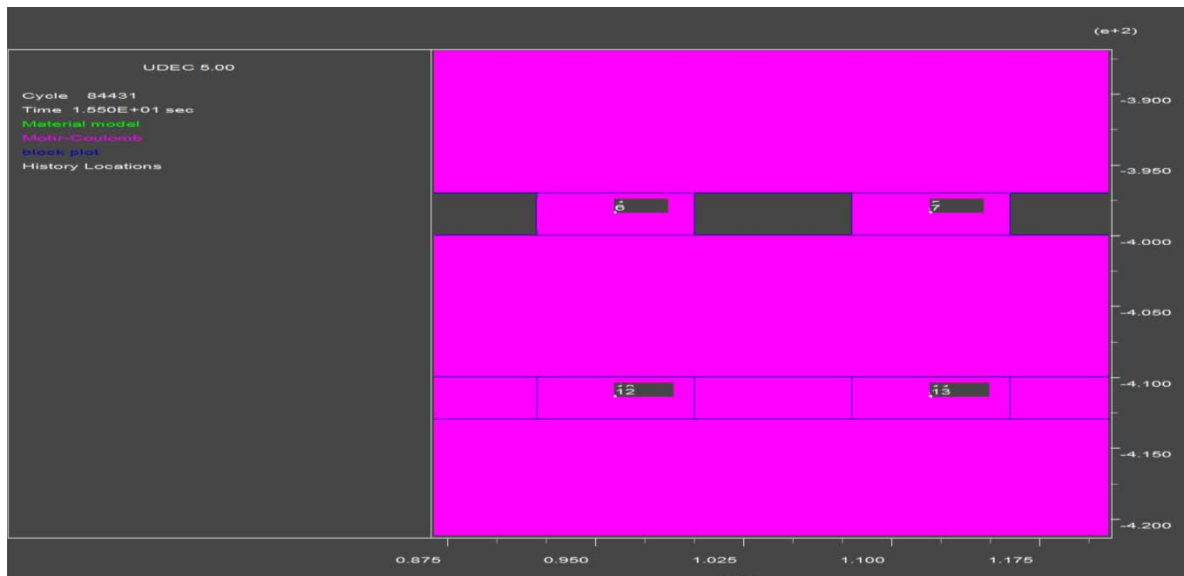

Figure 4-12: Benchmark points within model (showing the mining of the top reef completed)

The stress-strain behaviour of two separate pillars on the top reef is presented in Figure 4-13 and Figure 4-14. This shows that the pillars do not reach failure and will remain stable. The shear stress within these pillars was recorded to be approximately 3 kPa and 9 kPa as shown in Figure 4-15.
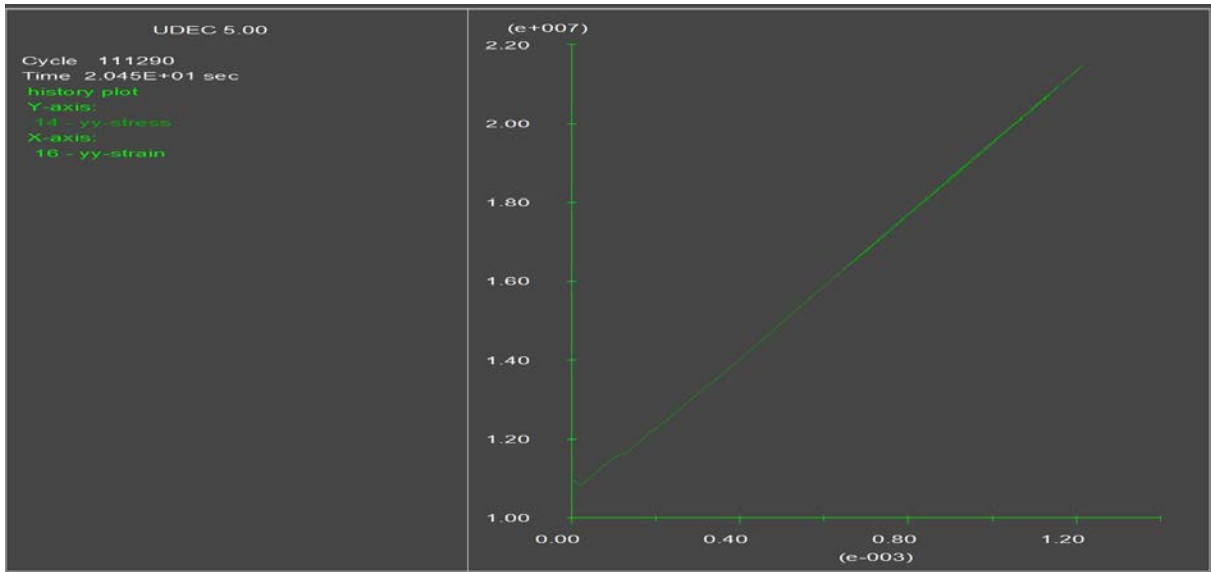
88

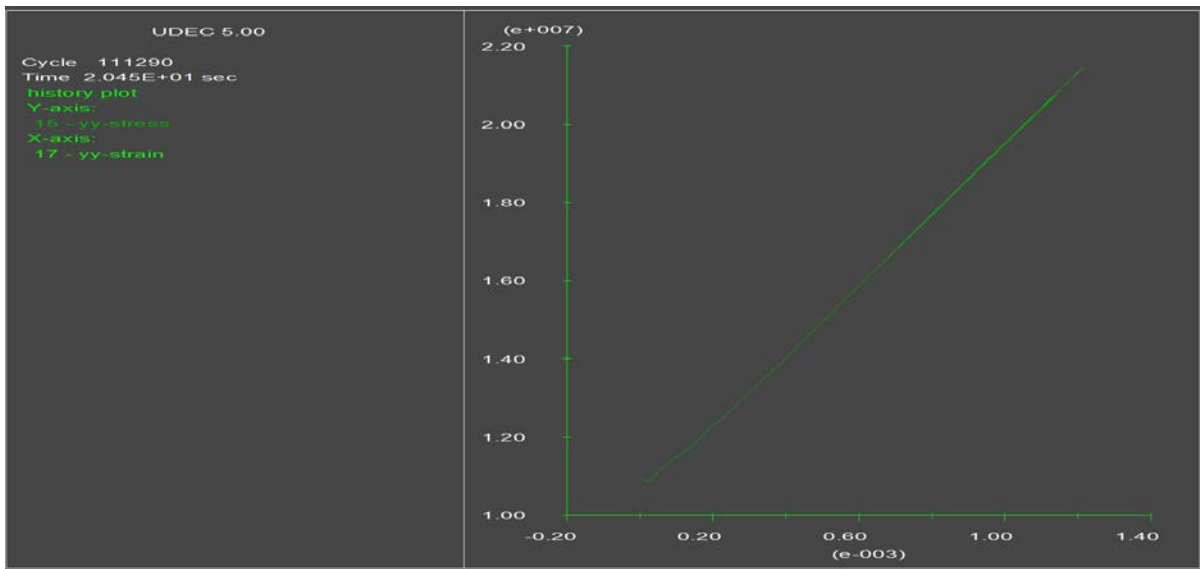**Figure 4-13: Stress-strain behaviour of a pillar on the top reef**

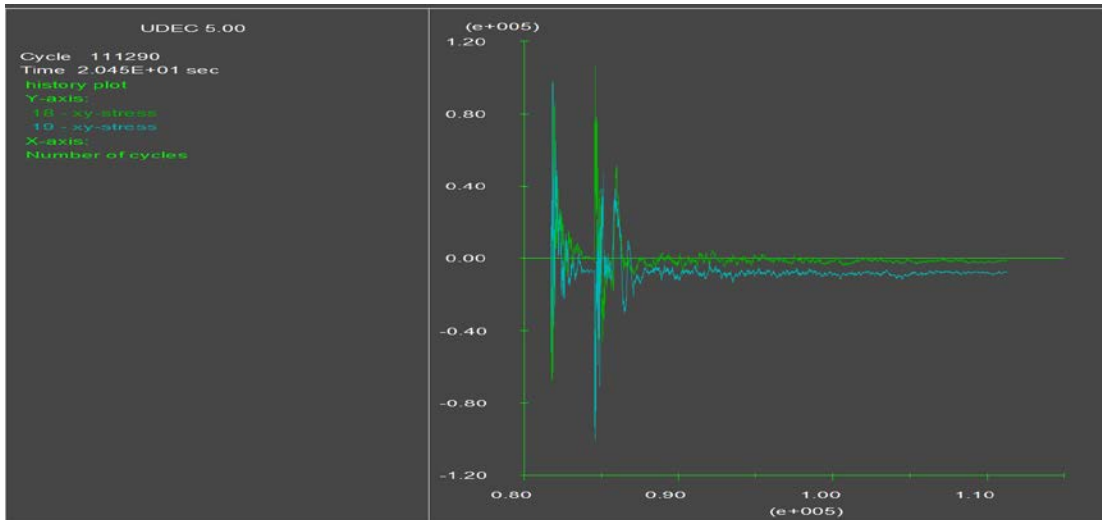**Figure 4-14: Stress-strain behaviour of another pillar on the top reef**

Figure 4-15: Shear yield and tensile failure zones for the multi-reef extraction case – Point 18 and 19.

At these shear stress levels, shear failure is unlikely to occur within the pillars.

4.3.2 Reef dip angle of 10 degrees

A plot showing the principal stress components around the excavations between the reefs after mining the second reef is presented in Figure 4-16. A similar plot is presented in Figure 4-17, zoomed into the area between the reefs. The stress components through the middle of the 8-m wide pillars deviate from the horizontal and vertical directions around the excavations. However, the stresses between the reefs, below and above the pillars appear to remain almost vertical, whereas the stresses between the excavations of the different reefs clearly run diagonally between the excavation corners.
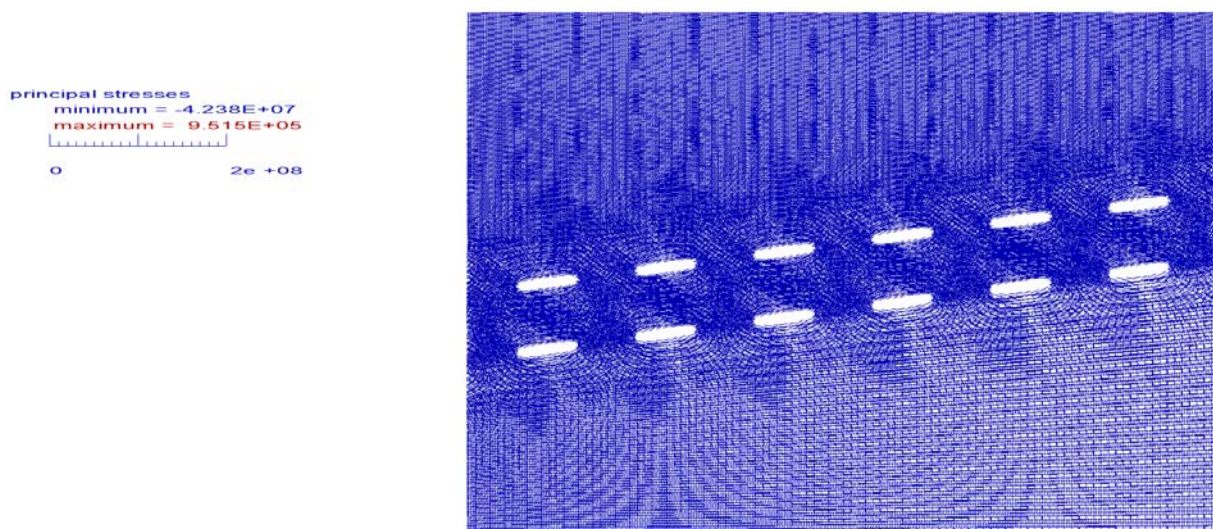
Figure 4-16: Principal stress components between 12 roads for the multi-reef extraction case at 10° dip

principal stresses
minimum = -4.040E+07
maximum = 8.935E+05
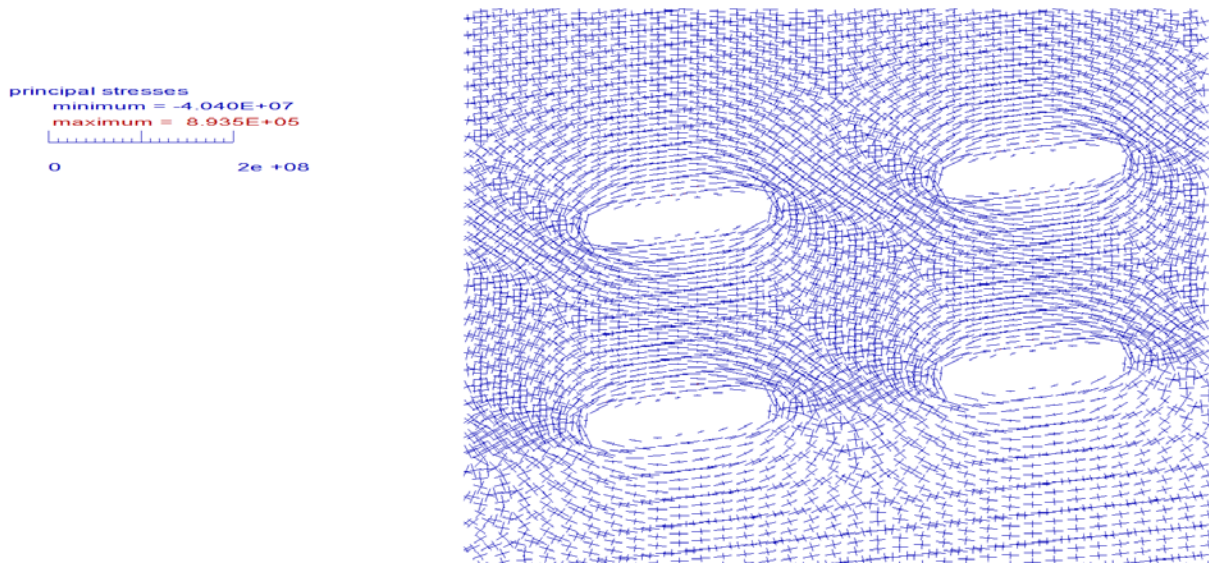
0   2e +08

Figure 4-17: Principal stress components between four excavations for the multi-reef extraction case at 10° dip

A plot showing the zones where shear yielding and tensile failure is predicted around the excavations for the multi-reef extraction case is presented in Figure 4-18 for single reef and Figure 4-19 for the multi-reef scenarios. The results indicate similar interaction between the two reefs as seen for the flat reefs, with the shear yielding zones extending from the top reef to the bottom reef around the excavations.

no. zones : total   8948
at yield surface (*)   0
yielded in past (X)   844
tensile failure (o)   40
boundary plot

Figure 4-18: Shear yield and tensile failure zones for the single-reef extraction case at 10° dip
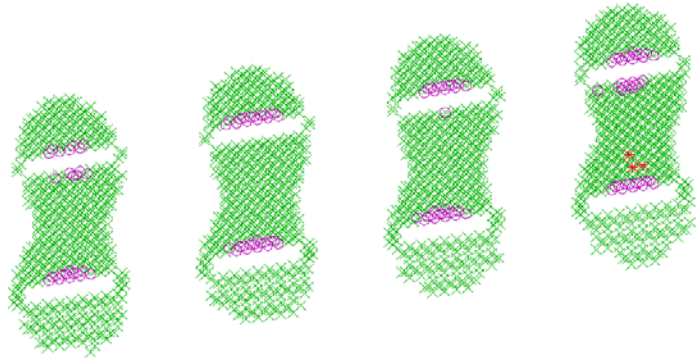
Figure 4-19: Shear yield and tensile failure zones for the multi-reef extraction case at 10° dip

A plot showing shear stress contours around the excavations for the multi-reef extraction case is presented in Figure 4-20. The shear stress remains relatively low between the pillars on the top and bottom reefs.
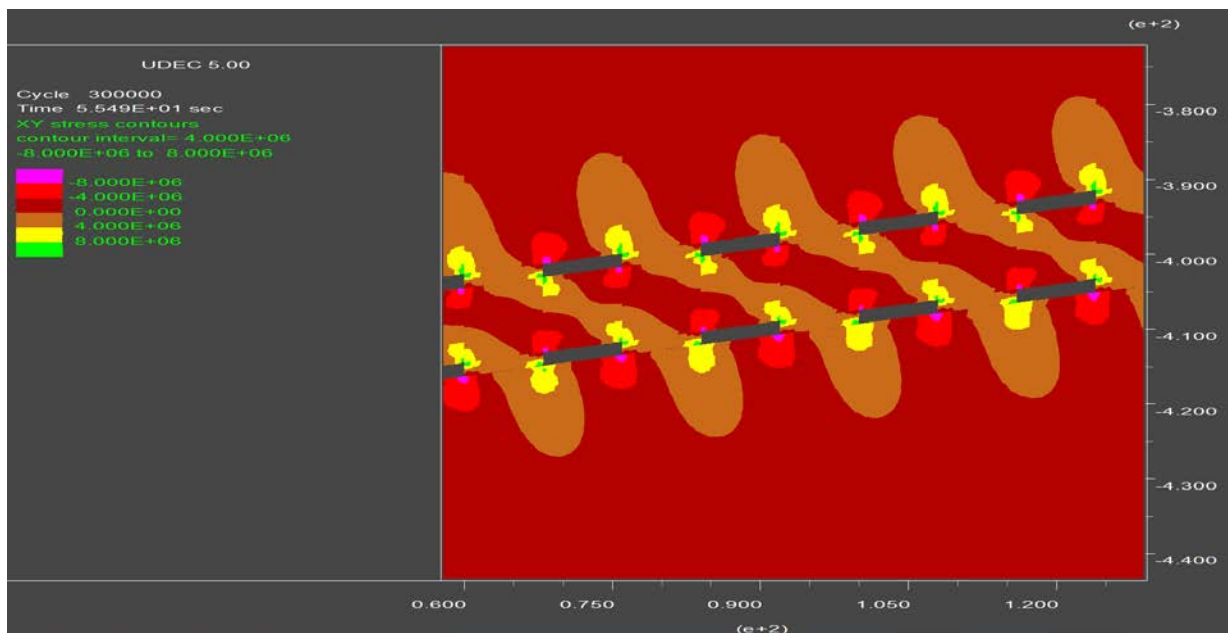

Figure 4-20: Shear stress for the multi-reef extraction case at 10° dip
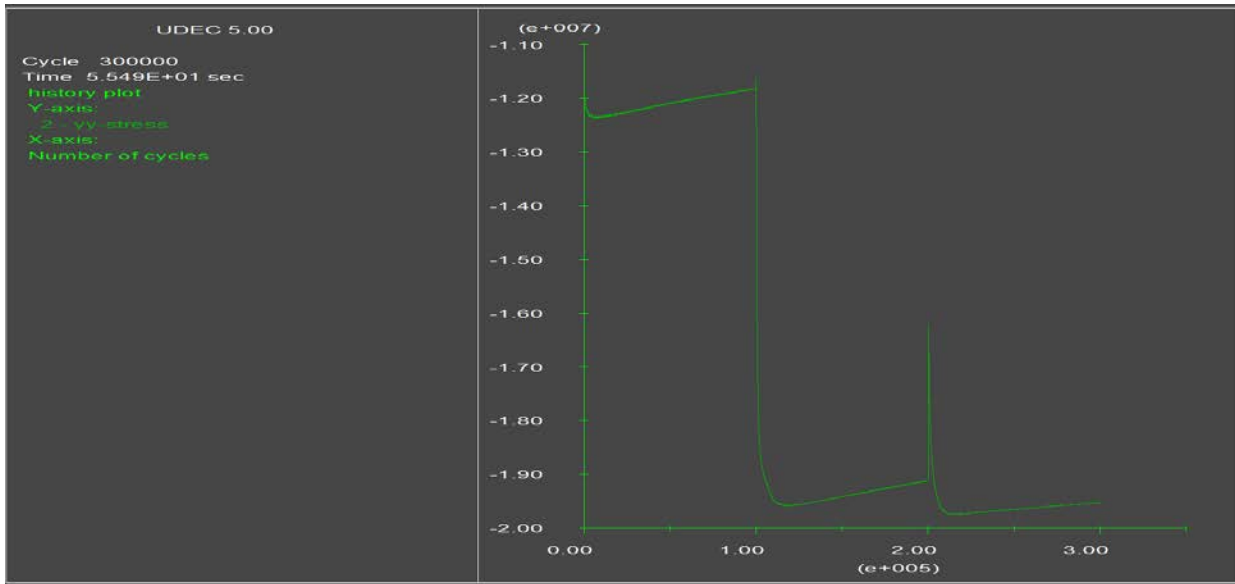
Figure 4-21: Vertical stress history for the multi-reef extraction case at 10° dip at 400 m below surface – Point 2 (top reef)

The figure above indicates the vertical stress increase after the first reef has been extracted and the second reef is mined. Mining of the second reef increase the vertical stress at this point within the pillar from approximately 12 MPa to 19.5 MPa.

4.3.3 Reef dip angle of 20 degrees

A plot showing the principal stress components around the excavations between the reefs after mining the second reef is presented below in Figure 4-22. Figure 4-23 depicts a similar plot that is zoomed into the area between the reefs. The stress orientations are virtually similar to that of the 10° reef dip.
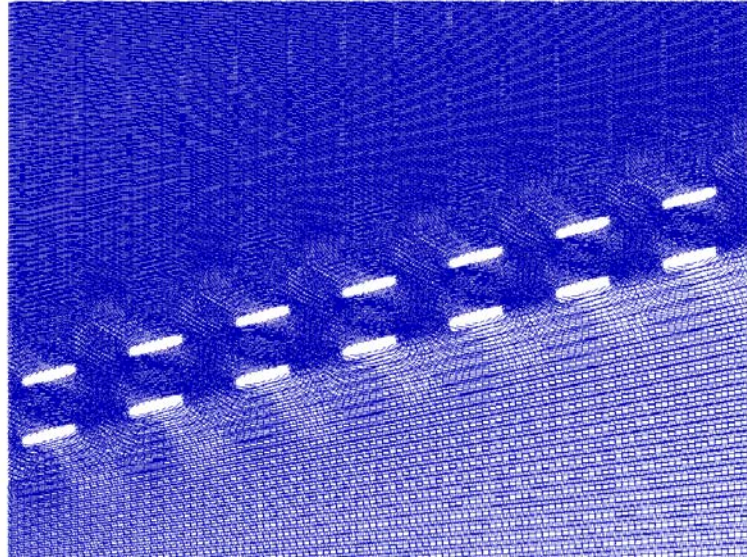
Figure 4-22: Principal stress components between 14 panels for the multi-reef extraction case at 20° dip
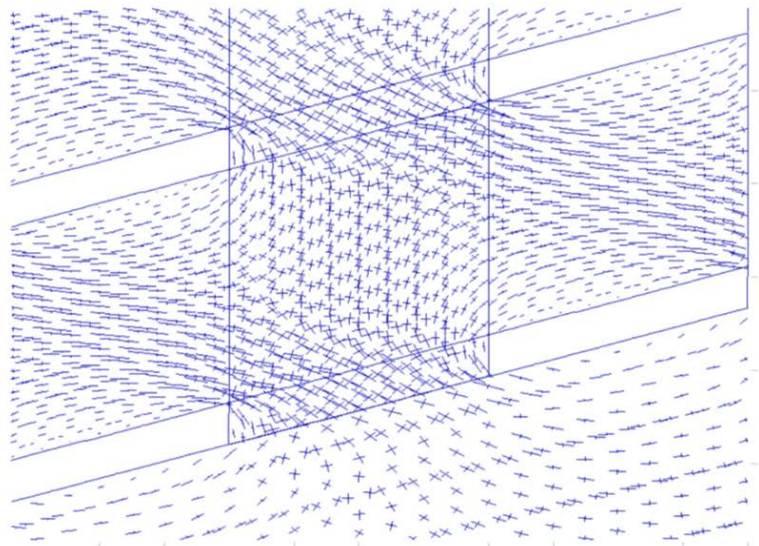
Figure 4-23: Principal stress components between 4 panels for the multi-reef extraction case at 20° dip

A plot showing the zones where shear yielding and tensile failure is predicted around the excavations for the single and multi-reef extraction cases are presented below (in Figure 4-24 and Figure 4-25). Again, the results indicate similar interaction between the two reefs as seen for the flat reefs and the 10° reef dip, with the shear yielding zones extending from the top reef to the bottom reef around the excavations.

94
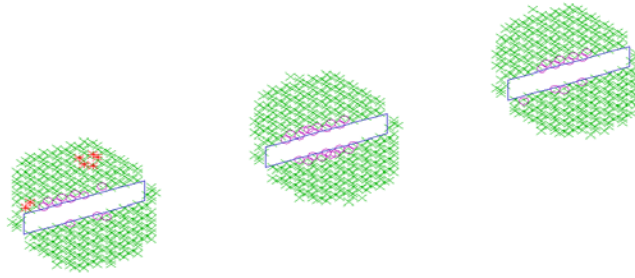
Figure 4-24: Shear yield and tensile failure zones for the single-reef extraction case at 20° dip showing shear and tensile failure

Figure 4-25 indicates the shear failure between the two pillars (middling failure) and tensile failure between the two excavations on the different reefs.
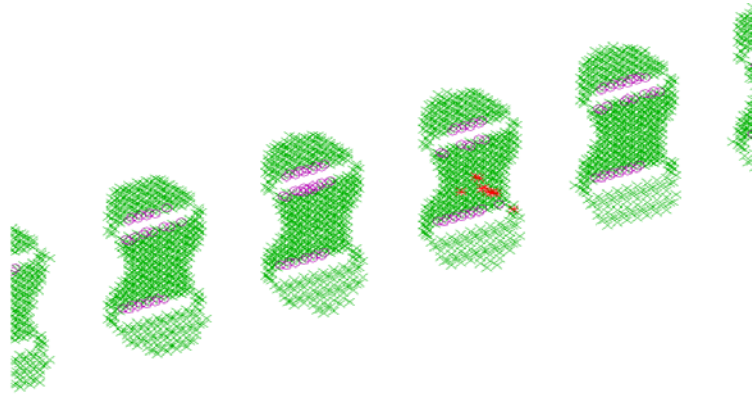
Figure 4-25: Shear yield and tensile failure zones for the multi-reef extraction case at 20° dip

Figure 4-26 that shows shear stress contours around the excavations for the multi-reef extraction case. The shear stress between the pillars on the top and bottom reefs is higher than for the 10° reef dip and the flat reef cases.
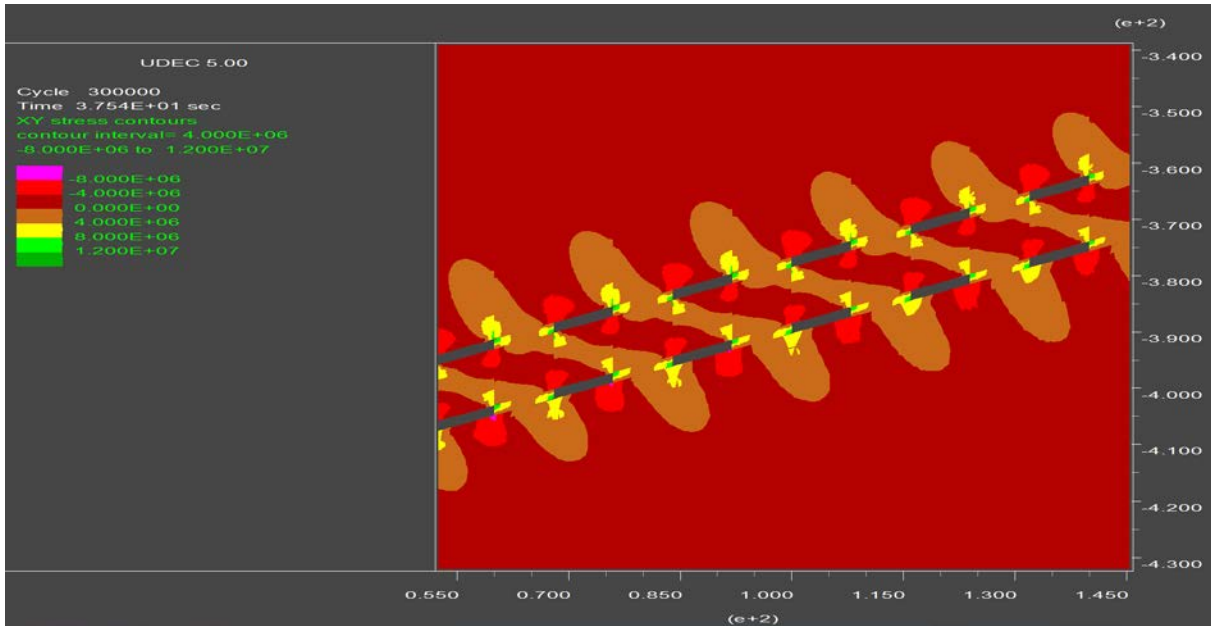
Figure 4-26: Shear stress contours between 14 excavations for the multi-reef extraction case at 20° dip

4.3.4 Reef dip angle of 30 degrees

The principal stress components are presented in Figure 4-27, with the failure zones for the single-reef case presented in Figure 4-28.
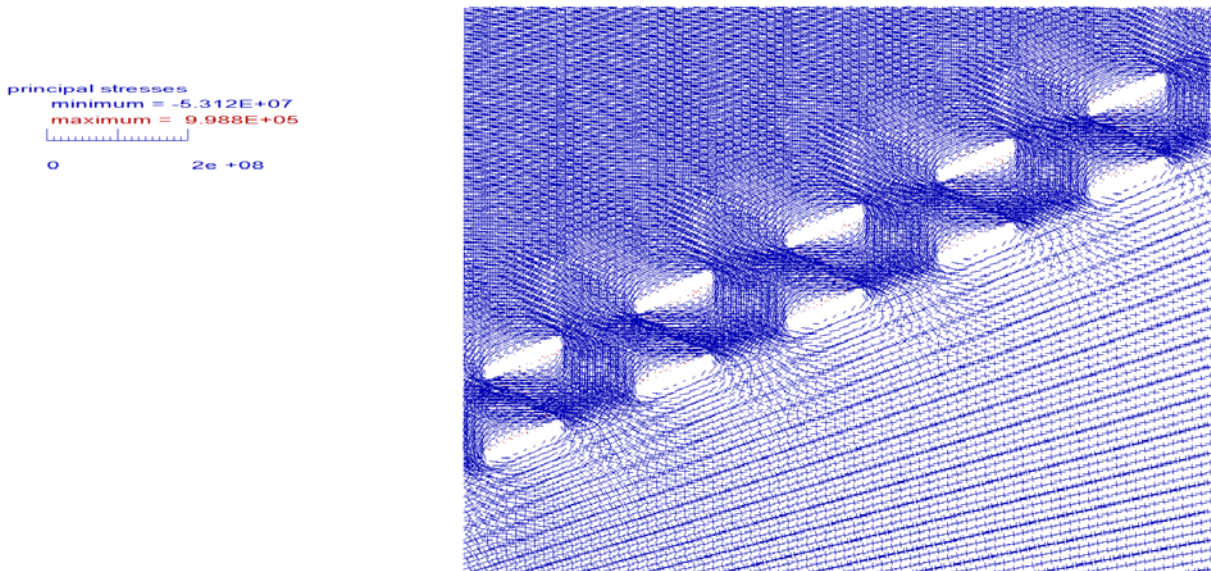
Figure 4-27: Principal stress components between 16 excavations for the multi-reef extraction case at 30° dip

no. zones : total   10000
at yield surface (*)   4
yielded in past (X)   1439
tensile failure (o)   60
boundary plot
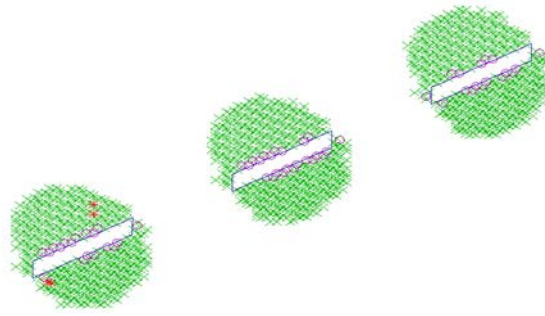
Figure 4-28: Shear and tensile failure zones for the single-reef extraction case at 30° dip

From Figure 4-29, it can be observed that shear fractures are forming between the pillars and tensile fractures between the excavations of a multi-reef scenario. The shear fractures between the pillars may lead to middling failure, and the tensile fractures between the excavations may lead to back-break collapse into the excavations on the bottom reef. This would be possible in the case where differential displacement along the fracture has occurred.

no. zones : total   19038
at yield surface (*)   42
yielded in past (X)   4265
tensile failure (o)   309
boundary plot
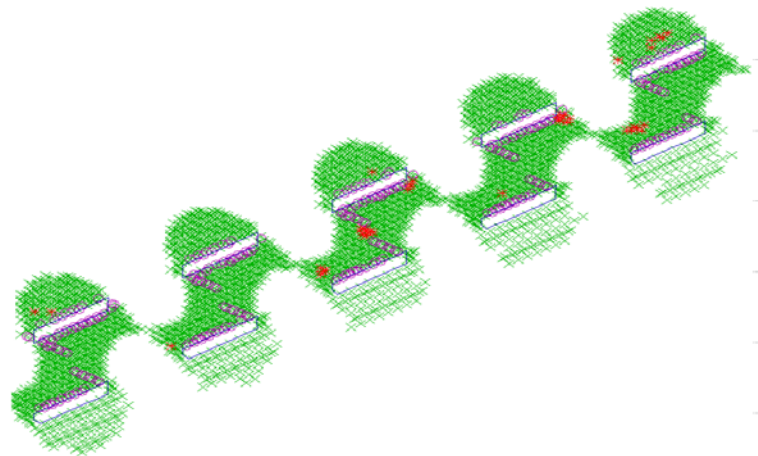
Figure 4-29: Shear yield and tensile failure zones for the multi-reef extraction case at 30° dip

Figure 4-30 presents the vertical displacement contours between the reefs.

97
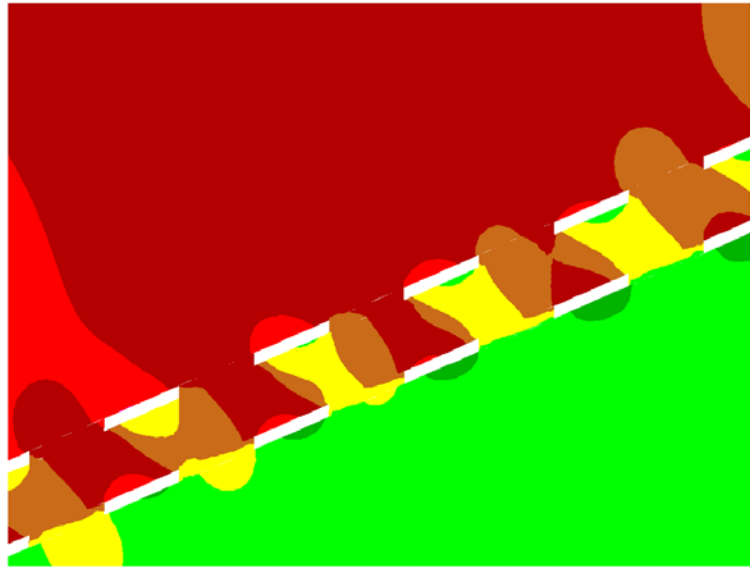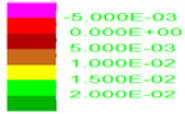
Figure 4-30: Vertical displacement contours between the multi-reef excavations at 30° dip

4.3.5 Reef dip angle of 40 degrees

A plot showing the principal stress components around the excavations between the reefs after mining the second reef, which is approximately 10 m below the first reef, is presented in Figure 4-31. As this scale might be difficult to interpret, a similar plot is presented in Figure 4-32, zoomed into the area between the reefs. The stress orientations between the pillars are no longer vertical but run diagonally between the corners of the pillars on the two reefs.
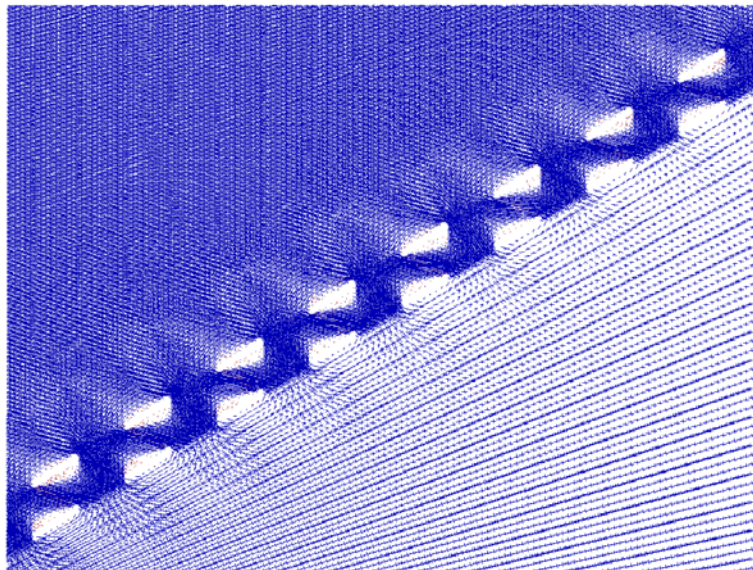
Figure 4-31: Principal stress components between 16 excavations for the multi-reef extraction case at 40° dip

principal stresses
minimum = -7.972E+07
maximum = 9.942E+05

0   5e +08
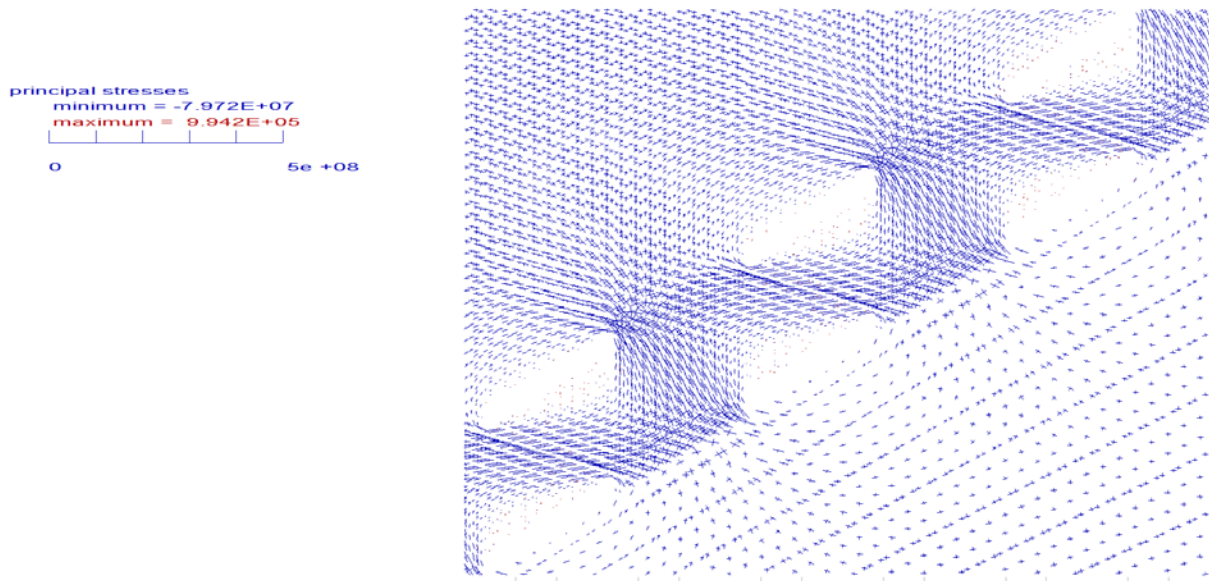
Figure 4-32: Principal stress components between six panels for the multi-reef extraction case at 40° dip

A plot showing the zones where shear yielding and tensile failure is predicted around the excavations for the multi-reef extraction case is presented in Figure 4-34. The onset of these failure zones are already visible with only a single reef simulated, as can be seen in Figure 4-33.

The results indicate similar interaction between the two reefs, as seen for the flat reefs and the 10° reef dip; however, the shear yielding zones extend not only between the excavations, but between the pillars as well. This is an indication of potential middling failure below the top reef pillars and above the bottom reef pillars.

no. zones : total   20650
at yield surface (*)   40
yielded in past (X)   3298
tensile failure (o)   170
boundary plot
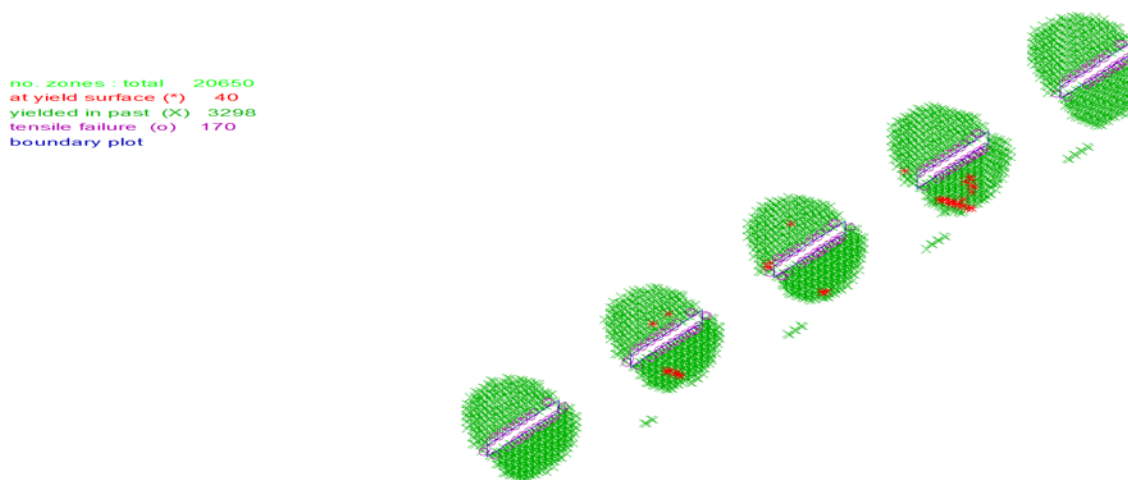
Figure 4-33: Shear and tensile failure for the single-reef extraction case at 40° dip

no. zones : total   6872
at yield surface (*)   69
yielded in past (X) 3252
tensile failure (o)   585
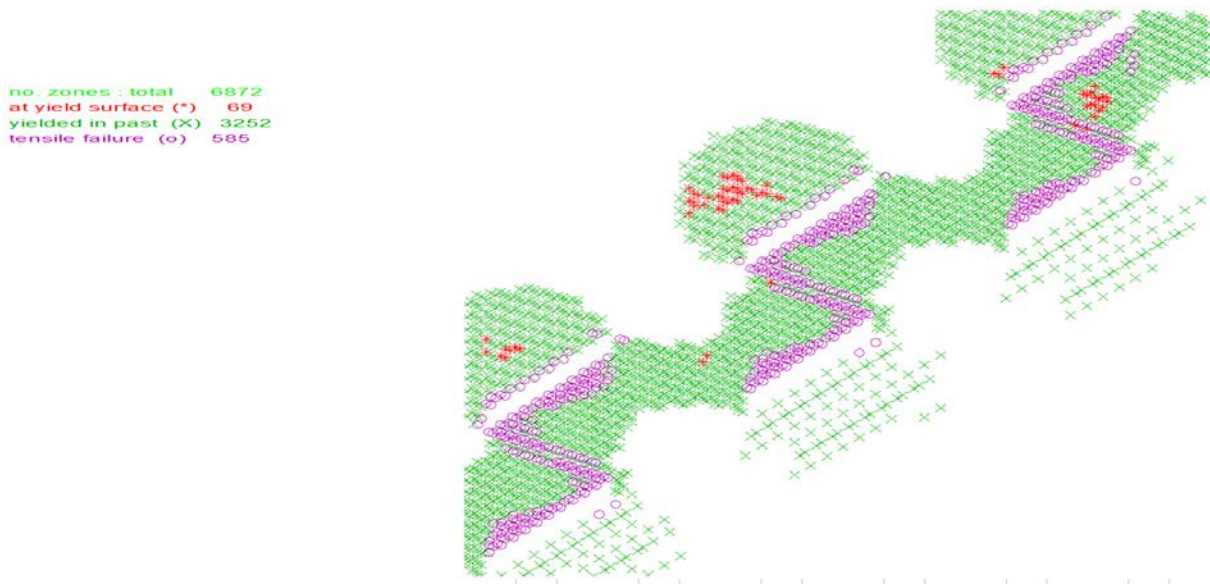
Figure 4-34: Shear yield and tensile failure zones for the multi-reef extraction case at 40° dip

A prominent tensile and shear fracture extends diagonally between the corners of the excavations on the different reefs. Potential opening along this prominent fracture is confirmed by the differential vertical and horizontal displacement contour plot (Figure 4-35 and Figure 4-36).

Thus, not only are the pillar foundations potentially unstable at a 40° reef dip, but the potential for a back-break collapse of the hangingwall above the bottom reef is also a possible.

Y displacement contours
contour interval= 5.000E-03
-1.000E-02 to 2.000E-02

-1.000E-02
-5.000E-03
0.000E+00
5.000E-03
1.000E-02
1.500E-02
2.000E-02
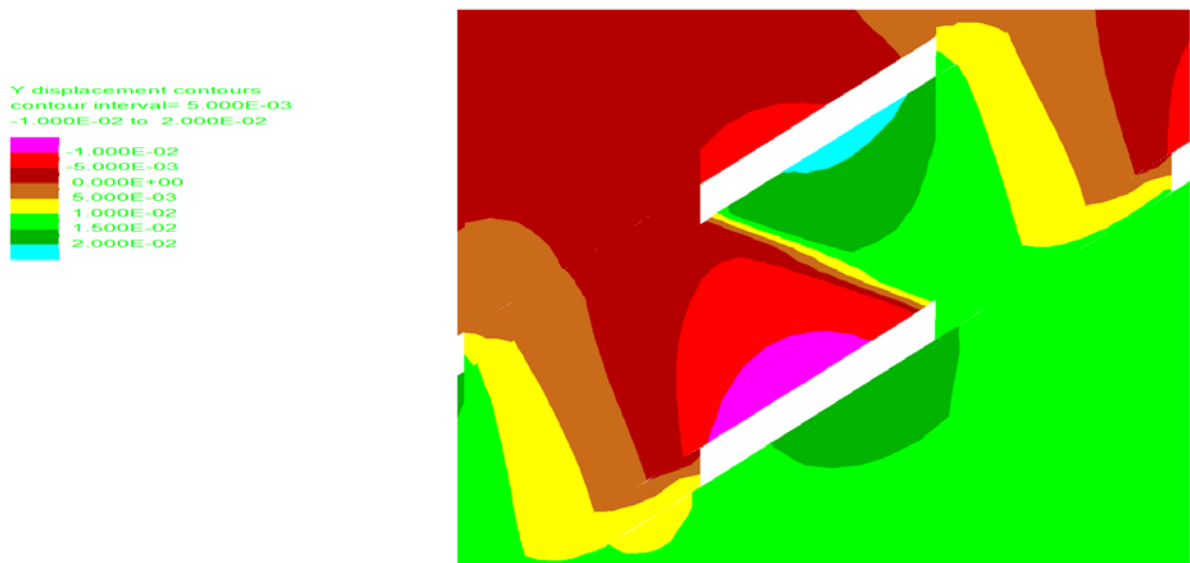
Figure 4-35: Vertical displacement contours between the multi-reef excavations at 40° dip

Figure 4-36: Horizontal displacement contours between the multi-reef excavations at 40° dip

A plot showing shear stress contours around the excavations for the multi-reef extraction case is presented in Figure 4-37. The shear stress between the pillars on the top and bottom reefs is higher than for the previous cases (0°, 10° and 20° reef dip).
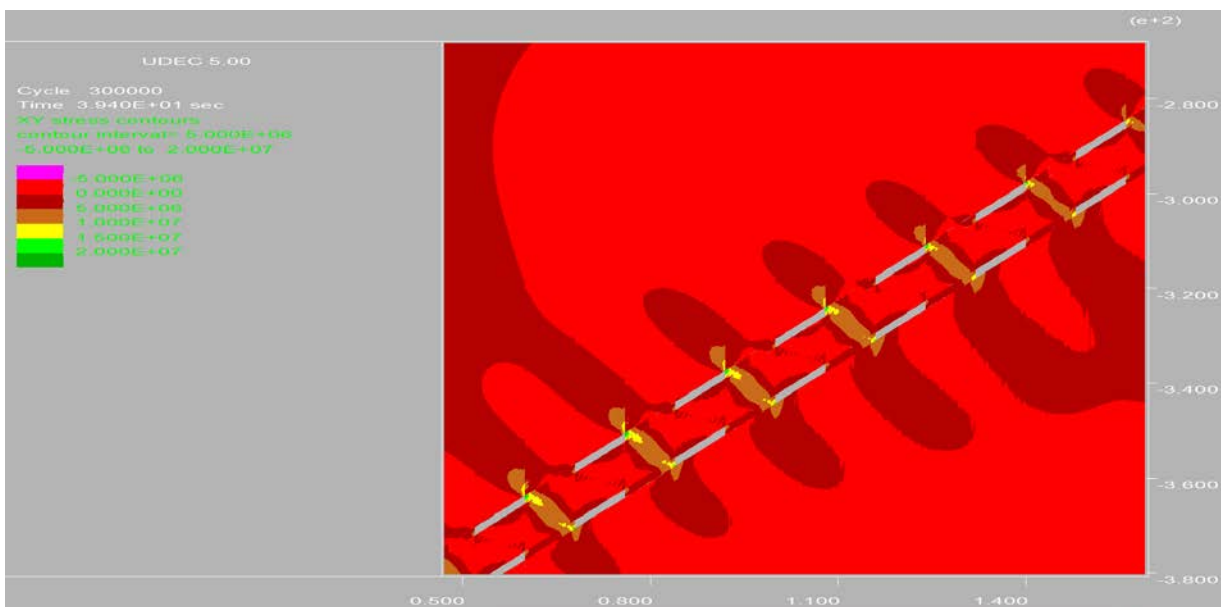
Figure 4-37: Shear stress contours between 14 excavations for the multi-reef extraction case at 40° dip

The benchmark points are shown below at which the stress history plots have been plotted.

101

Figure 4-38: Benchmark points

The shear stress between the excavations on the two reefs increases with an increase in reef dip angle as presented in Figure 4-39. Note the decrease in horizontal stress from approximately 22 MPa to approximately 17 MPa that occurs after the mining of the second reef.
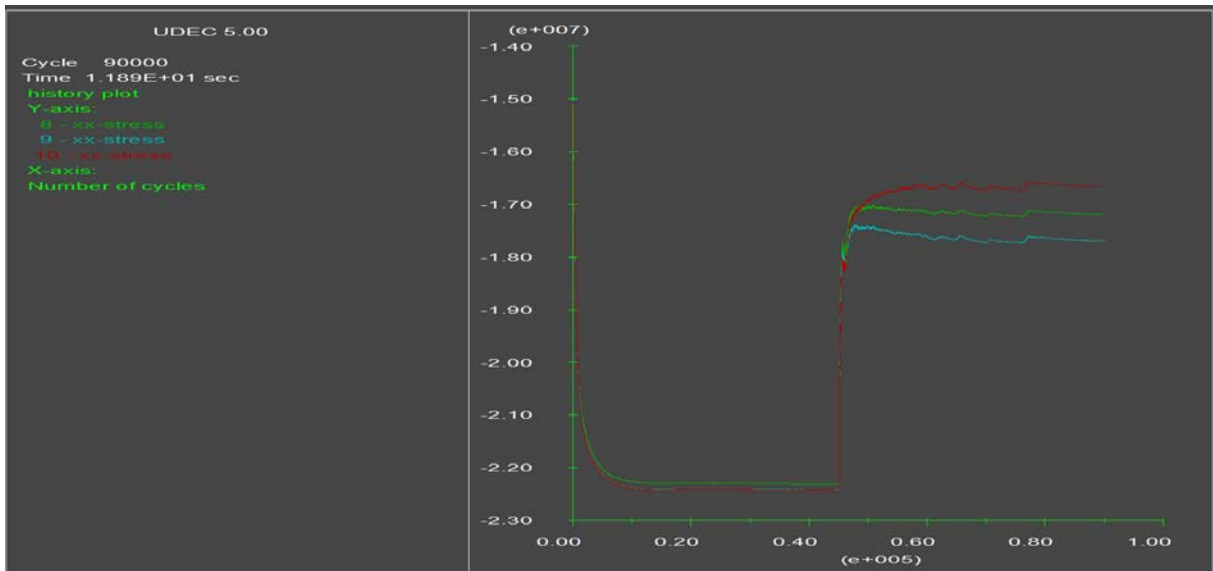
Figure 4-39: Horizontal stress history in pillar for the multi-reef extraction case at 40° dip at 400 m below surface

On the contrary, whereas the horizontal stress decreases in magnitude, the vertical stress increases from approximately 14 MPa to 18 MPa after mining of the second

reef. The decrease in horizontal stress, together with the increase in vertical stress magnitudes, causes the increase in shear stress within the pillar (Figure 4-40).
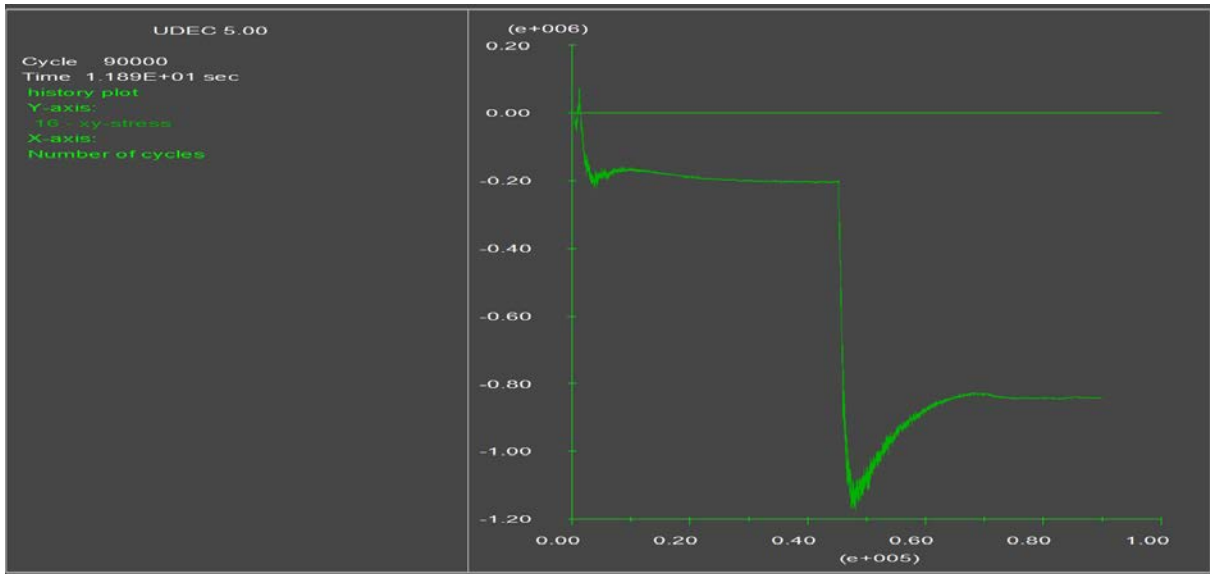
Figure 4-40: Shear stress history in pillar for the multi-reef extraction case at 40° dip at 400 m below surface – Point 16 (top reef)

4.3.6 Stress-strain behaviour of pillars for Strain Softening models

The same strength parameters were assigned for all waste rock as in the case of the Mohr-Coulomb models; however, the post-peak values for the cohesion friction and tensile strengths were reduced as a function of plastic strain for Reef 1 and Reef 2. A summary of the strain-softening parameters assigned to the models is presented in Table 4-2.

.

Table 4-2: Summary of the strain-softening parameters

Material Type	@ Strain (mm/m)	Reef 1	Reef 2
Friction angle (°)	1.2	40.0	50.0
	1.5	34.0	42.5
	1.8	30.5	38.5
	2.0	30.5	38.5
Cohesion (MPa)	1.2	10.0	10.0
	1.5	8.5	8.5
	1.8	7.0	7.0
	2.0	7.0	7.0
Tensile strength (MPa)	1.2	1.0	0.8
	1.5	0.9	0.7
	1.8	0.7	0.6
	2.0	0.7	0.6

Graphs presenting the recorded stress-strain behaviour of the pillars when applying the strain-softening constitutive models are presented in this section for each of the dip angles of 0°, 20° and 40°.
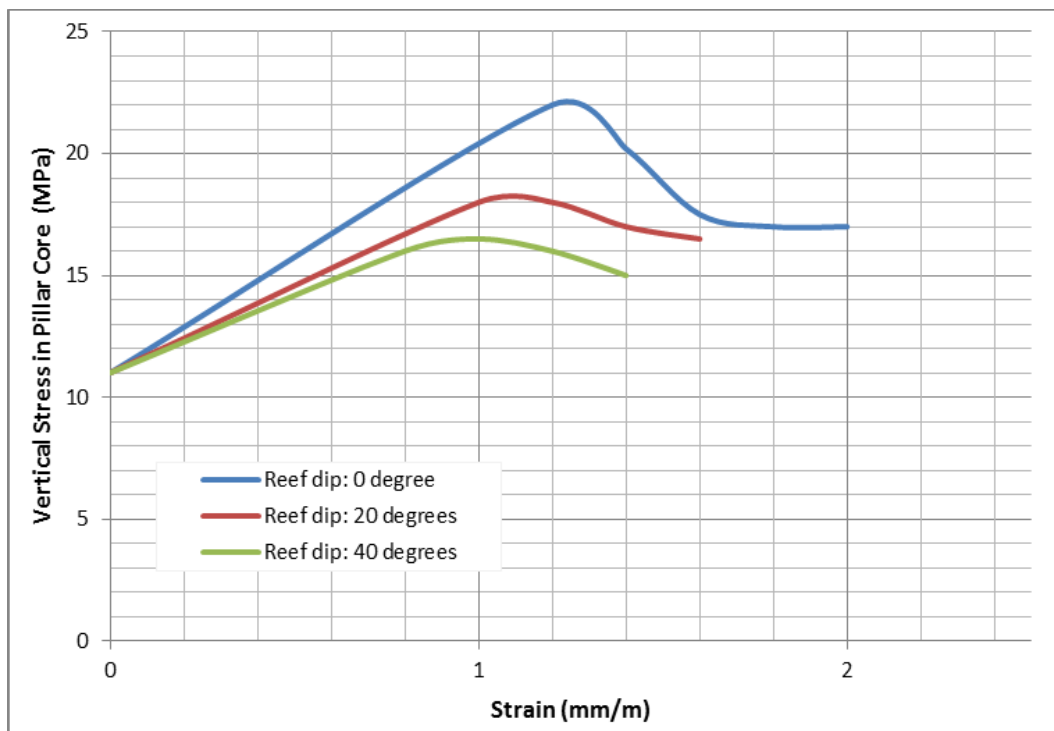
Figure 4-41: Stress-strain graphs in pillar for the multi-reef extraction case at 0°, 20° and 40° dip at 400 m below surface

4.4   Summary of modelling results

The following conclusions have been drawn based on the UDEC analysis:

i.   The maximum vertical pillar stresses are predicted to reach approximately 22 MPa for the flat reefs option. This value is taken as the base for the evaluation with the subsequent models compared against this value. It is found that as the dip of the reef increases, the vertical stress which is predicted in the core of the pillars at 400 m below surface decreases as shown in Figure 4-42. The relationship between shear stress and reef dip angle is also presented in Figure 4-42. The shear stress line indicat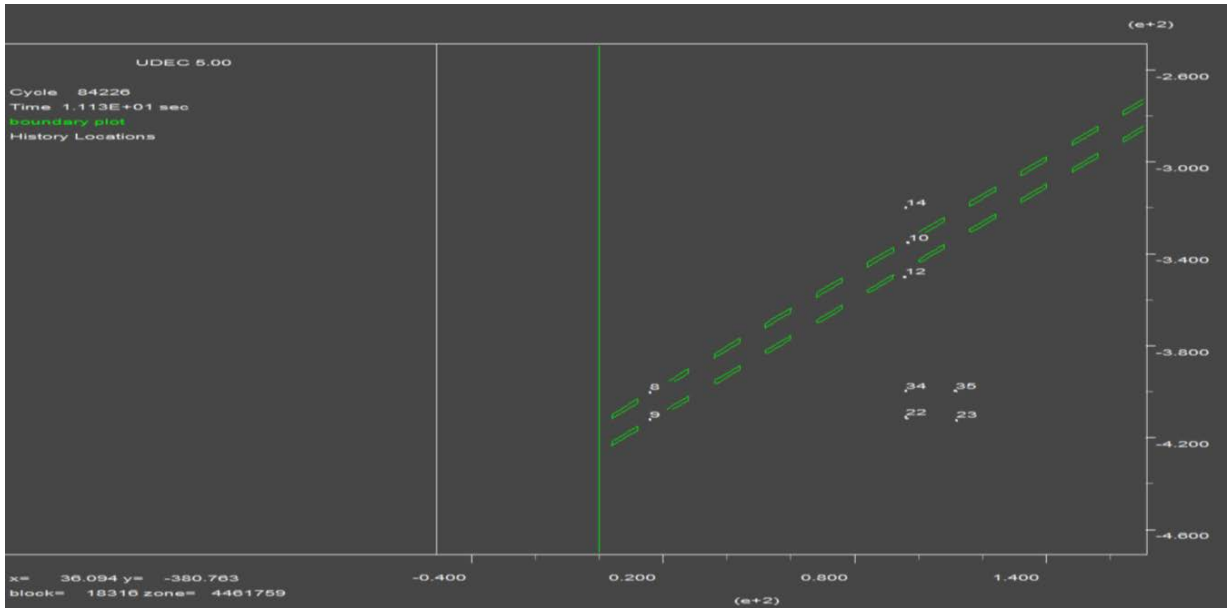es that the shear stress between the excavations on the two reefs increases with an increase in reef dip angle, specifically after mining of the second reef.

Figure 4-42: Maximum modelled vertical stress in pillar core and increased shear stress between reefs as a function of dip angle

105

ii.   Tensile failure is predicted to occur along the edges of the excavations, but it would be limited to within 0.5 m into the rock mass for the shallow reef dip cases.

iii. For the steeper reef dip of 40°, prominent tensile cracks are predicted to form diagonally between the corners of the excavations on the different reefs. The formation of these cracks will cause opening to occur, as confirmed by the differential vertical and horizontal displacement contour plots.

iv.   For the steeper reef dip of 40°, prominent tensile cracks are predicted to form diagonally between the corners of the excavations on the different reefs. The formation of these cracks will cause an opening to occur as confirmed by the differential vertical and horizontal displacement contour plots.

v.   The potential for hangingwall back-break failure into the bottom reef excavation at steep dips of greater than 30° is a concern when pillars and excavations are vertically superimposed.

vi.   Shear failure within the pillars at 0° reef dip are unlikely, as the shear stress levels vary between approximately 3 kPa and 9 kPa, which is significantly less than the shear strength of the reef pillars.
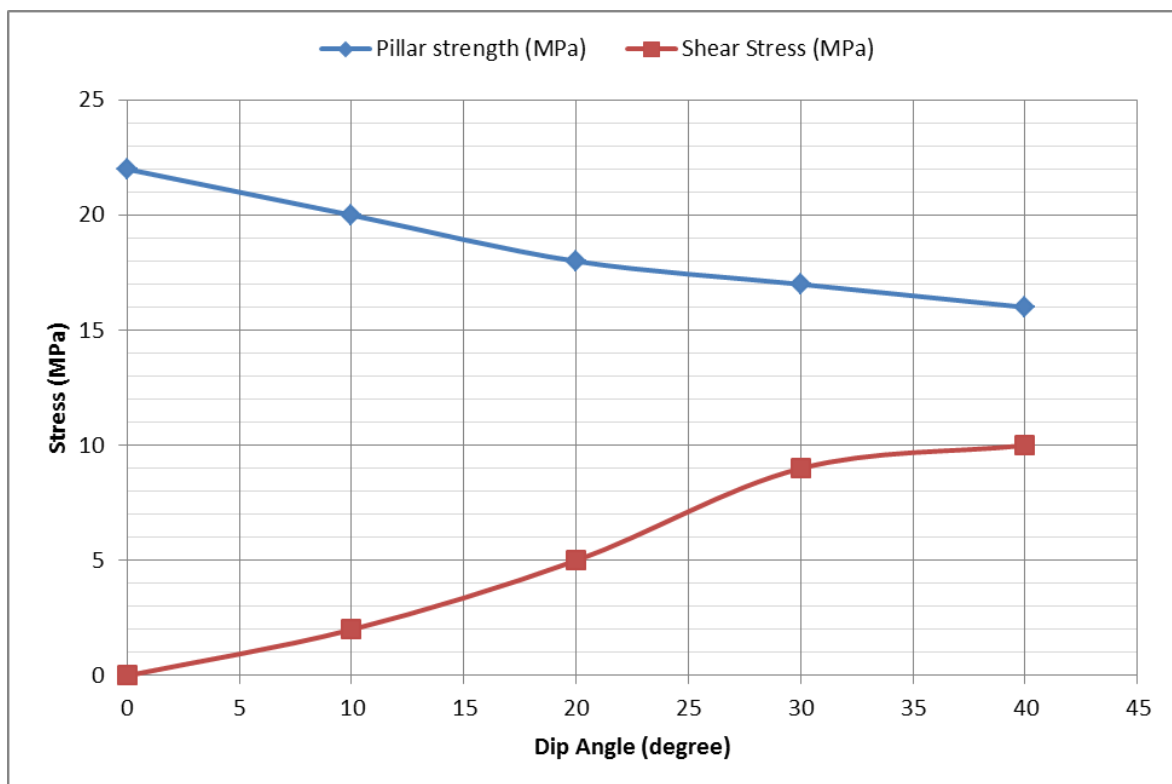
vii. Shear failure is predicted to occur between the two reefs, above and below the excavations, for all cases from 0° to 40°.

viii. The stress vectors indicate that only at the steeper dips would shear failure be possible between the pillars on the different reefs. The normal stress direction between the pillars on the different reefs, for shallow reef dips, remains vertical which reduces the potential for middling failure.

ix.   The shear stress between the excavations on the two reefs increase with an increase in reef dip angle. Shear failure of the area underneath the top pillar and above the bottom pillar is predicted at a steep dip of 40° (foundation failure of the pillars is predicted). Thus, even though the pillars are predicted to remain stable, the footwall foundation of the pillars on the top reef and the hangingwall foundation of the pillars on the bottom reef are predicted to become unstable.

The general conclusion from the analysis is that the loading on the pillar system is somewhat affected by dip due to the minor magnitude of the shear component, it does not indicate any instability in the pillar itself.

The inelastic numerical modelling conducted for this study contradicts the assumption that only normal stresses need to be considered in the factor of safety calculations and suggests that the pillar strength decreases to the same magnitude as the shear stress component increases. This statement is only true for the special conditions that were modelled, though. It nevertheless emphasises the statement made earlier that should one of the factors influencing the pillar strength be present, more and special treatment should be considered in the design of room-and-pillar layouts.

5 CONCLUSIONS

The actual loading environment for pillars on any mine is a highly complex scenario with combinations of normal and shear stresses within the working environment. It is also understood that with an active and advancing work face, consistent redistribution of stresses will occur to maintain equilibrium within the rockmass. It could therefore be expected that a pillar, which is planned and designed to only experience normal loading conditions, will not always be in this "ideal" environment, and during some stages of mining, shear stresses would also form part of the loading system.

Theory suggests that when a rock sample is placed under uniaxial loading conditions, failure will occur in either indirect tension or shear. When the ends have a low friction angle and the sample can expand based on the sample's Poisson's ratio, indirect tension failure is observed, whiles shear failure occurs when the ends are confined. In practice, a pillar in the underground mining environment would experience the same failure mechanisms. However, as "confinement" is created at the pillar and hanging wall or footwall contacts, shear failure is commonly observed in failed pillars.

Dating as far back as the 1960's, a number of equations had been derived, each trying to correctly calculate pillar strength. These early attempts argued that the strength is only governed by the width of the pillar in relation to the mining height as well as a certain pillar "strength" constant (K-value). Based on coal research, hard rock design methodologies adapted the formulae with adjustments to the constants. This has been applied in industry with relatively good success.

The loading environment on the other hand can be determined by either adopting the tributary area theory, assuming an infinitely large area has been mined, in estimating, with some degree of overestimation, the predicted maximum load acting on the pillars or by numerical modelling analysis.

As the major and minor loading directions are greatly dependent on the k-ratio, a change in the reef dip angle will results in a change to the normal load acting on the pillar. In a shallow environment (k > 1) the normal load would increase as the dip increase, whereas in a deep environment (k < 1) the opposites holds true. This

change in normal stress values has a direct effect on the shear stress value for the given reef orientation.

The TEXAN code was used to simulate an actual multi-reef chrome mine layout in the Eastern Bushveld. The results illustrated the extremely complex stress interactions when pillars of irregular shapes are not superimposed. This highlights the facts that the coal mine rules of superimposing of pillars should be treated with caution and that routine numerical modelling and underground monitoring of pillars are considered vital to ensure safe mining conditions.

Orientation of stability pillars in deep mining environments appears to be crucial in the sense that stress conditions, particularly shear stresses, are greatly affected by the direction of dip. First indications showed that dip stability pillars are "stressed" less in both normal and shear orientations.

Results from inelastic modelling of pillars forcing changes in normal and shear stresses acting on the pillars indicates a reduction in the normal stresses as the shear stress increases. Traditional factors of safety calculations would present a higher value since the LOAD on the pillar decreases with a constant strength parameter. The modelling results suggest a decrease in the pillar STRENGTH value in the same proportion as shear stress value increase.

It is thus concluded that should one of the factors influencing the pillar strength be present to a degree that is outside the initial range of assumed conditions when the standard equations had been derived, more and special treatment should be considered in the design of room-and-pillar layouts.

6 RECOMMENDATIONS

Two methodologies could be followed during the design process, whether it be a currently producing mine or a newly found ore body, to determine the expected loading conditions at the point of interest. The first would be to employ the empirical formulae to determine the loading on the pillars with the second being an analysis using numerical models. Scenarios are grouped for easy reference in the below.

Table 6-1: Load determination methodologies

Empirical methods	Numerical Modelling Methods
Greenfields projects (Standard room-and-pillar)	Adverse stress conditions and design adjustments
Multi-reef conditions with middling greater that pillar centres	Multi-reef conditions with middling less than pillar centre
Flat dipping deposits (0 – 10°)	Deposits dipping steeper than 10°

For calculating the FoS for a given scenario, the following flowchart is suggested:

Pillar Strength

Hedley & Grant (hard rock)
Salamon & Munro (coal)
Squat pillar equation
Inelastic numerical modelling (at the presence of shear stresses)

Pillar Load

Empirical methods
Numerical modelling methods

$$\frac{Pillar\ Strenght}{Pillar\ Load} = FoS$$
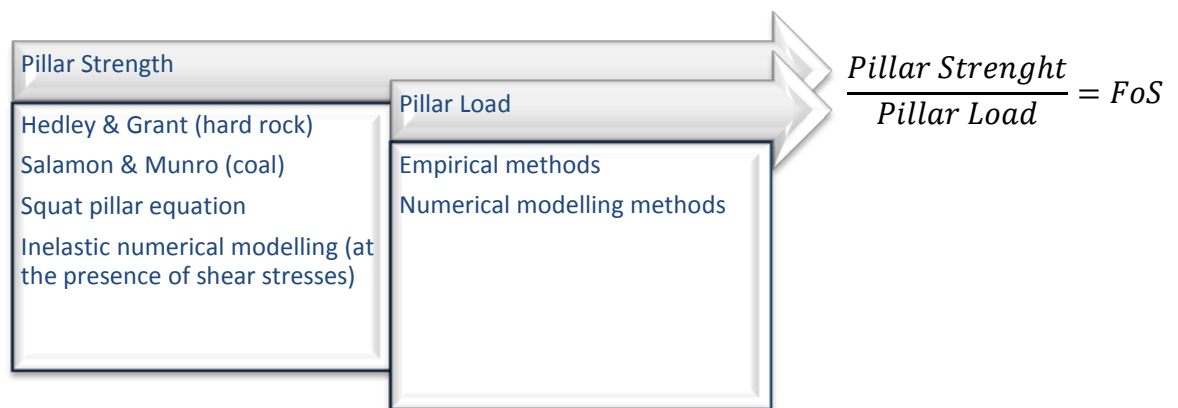
Figure 6-1: Determining the Factor of Safety in Room-and-Pillar designs.

7 SUGGESTIONS FOR FURTHER WORK

A list of suggestions for further work is presented below

    i.   Actual measurements in pillars considered to be in an adverse environment with both normal and shear stress conditions.

    ii.   A more detailed analysis into why dip stability pillars prove to be a better option than strike stability pillars in a deep, high stress environment.

    iii.   Determining the effect of shear stresses on pillars by means of physical models.

```
New
;define original boundary of modelled region
block 0,0 200,0 200,-1000 0,-1000
round 0.05
;
; Horizontal cracks defining stratigraphy
;Stope
crack 0,-397 200,-397
crack 0,-400 200,-400
crack 0,-410 200,-410
crack 0,-413 200,-413
crack 0,-450 200,-450
crack 0,-350 200,-350
; Defining the pillars - Top Seam
crack 4 -397 4 -400
crack 12 -397 12 -400
crack 20 -397 20 -400
crack 28 -397 28 -400
crack 36 -397 36 -400
crack 44 -397 44 -400
crack 52 -397 52 -400
crack 60 -397 60 -400
crack 68 -397 68 -400
crack 76 -397 76 -400
crack 84 -397 84 -400
crack 92 -397 92 -400
crack 100 -397 100 -400
crack 108 -397 108 -400
crack 116 -397 116 -400
crack 124 -397 124 -400
crack 132 -397 132 -400
crack 140 -397 140 -400
crack 148 -397 148 -400
crack 156 -397 156 -400
crack 164 -397 164 -400
crack 172 -397 172 -400
crack 180 -397 180 -400
crack 188 -397 188 -400
crack 196 -397 196 -400
crack 4 -410 4 -413
crack 12 -410 12 -413
crack 20 -410 20 -413
crack 28 -410 28 -413
crack 36 -410 36 -413
crack 44 -410 44 -413
crack 52 -410 52 -413
crack 60 -410 60 -413
crack 68 -410 68 -413
crack 76 -410 76 -413
crack 84 -410 84 -413
crack 92 -410 92 -413
crack 100 -410 100 -413
crack 108 -410 108 -413
crack 116 -410 116 -413
crack 124 -410 124 -413
crack 132 -410 132 -413
crack 140 -410 140 -413
crack 148 -410 148 -413
crack 156 -410 156 -413
crack 164 -410 164 -413
crack 172 -410 172 -413
crack 180 -410 180 -413
crack 188 -410 188 -413
crack 196 -410 196 -413
crack 190 -413 190 -410
; joint sets
;jset ang 0 0 gap 0 0 spac 0.5 0 tra 60 0 range 0 60 -
120 -118
; Discretization
gen quad 5 range 0,200 -350,0
gen quad 1 range 0,200 -450,-350
gen quad 5 range 0,200 -1000,-450
; Define properties
prop   mat=1 d=2800 shear=10e9 bulk=8e9
prop   mat=2 d=3000 shear=3.92e9 bulk=3.72e9
prop   mat=3 d=4000 shear=1e9 bulk=1e9
; Assign properties
change mat=1 range 0,200 -397,0
change mat=2 range 0,200 -400,-397
change mat=1 range 0,200 -410,-400
change mat=3 range 0,200 -413,-410
change mat=1 range 0,200 -1000,-413
prop   jmat=1 jkn=1e11 jks=1e11 jcoh=1e10 jtens=1e10
jfric=60
change jmat=1 range 0 200 -1000 0
; initial stress state
insit stres 0 0 0 szz -45e6 ygra 45000 0 30000 range
0,200 -1000,0
gravity 0 -9.81
; Boundary conditions
bound -0.1 0.1  -1000 0 xvel=0.0
bound 0 200 -1000.1 -999.9 xvel=0 yvel=0.0
bound 199.9 200.1 -1000 0 xvel=0.0
;Define histories
hist unbal
hist syy 96,-398.5
hist syy 112,-398.5
hist yd 96,-398.5
hist yd 112,-398.5
hist sxy 96,-398.5
hist sxy 112,-398.5
hist syy 96,-411.5
hist syy 112,-411.5
hist yd 96,-411.5
hist yd 112,-411.5
hist sxy 96,-411.5
hist sxy 112,-411.5
solve force 1e4
save Janel1.sav
; Reset displacement and velocities
initial xdisp=0 xvel=0
initial ydisp=0 yvel=0
; Mohr Coulomb constitutive model
change cons 3
; Define properties
prop    mat=4 d=2800  shear=10e9 bulk=8e9  coh=6e6
fric=35 &
TENS=1e6
prop      mat=5  d=3000  shear=3.92e9  bulk=3.72e9
coh=10e6 fric=40 &
TENS=1e6
```

113

```
prop    mat=6 d=4000 shear=1e9 bulk=1e9 coh=10e6
fric=50 &
TEnS=0.75e6
; Assign properties
change mat=4 range 0,200 -397,0
change mat=5 range 0,200 -400,-397
change mat=4 range 0,200 -620,-400
change mat=6 range 0,200 -413,-410
change mat=4 range 0,200 -1000,-413
hist syy 96,-398.5
hist syy 112,-398.5
hist eyy 96,-398.5
hist eyy 112,-398.5
hist sxy 96,-398.5
hist sxy 112,-398.5
; mohr coulomb joint properties
change jcons=2
prop   jmat=2   jkn=1e11   jks=1e11   jcoh=1e6   jfric=40
jTENS=1e6
change jmat=2 RANGE 0 200 -1000 0
hist syy 96,-398.5
hist syy 112,-398.5
hist eyy 96,-398.5
hist eyy 112,-398.5
hist sxy 96,-398.5
hist sxy 112,-398.5
;excavate Middle Seam - also use null zones
del range 4 12 -400 -397
del range 20 28 -400 -397
del range 36 44 -400 -397
del range 52 60 -400 -397
del range 68 76 -400 -397
del range 84 92 -400 -397
del range 100 108 -400 -397
del range 116 124 -400 -397
del range 132 140 -400 -397
del range 148 156 -400 -397
del range 164 172 -400 -397
del range 180 188 -400 -397
del range 196 200 -400 -397
solve force 1e4
save Janpl1s.sav
del range 4 12 -413 -410
del range 20 28 -413 -410
del range 36 44 -413 -410
del range 52 60 -413 -410
del range 68 76 -413 -410
del range 84 92 -413 -410
del range 100 108 -413 -410
del range 116 124 -413 -410
del range 132 140 -413 -410
del range 148 156 -413 -410
del range 164 172 -413 -410
del range 180 188 -413 -410
del range 196 200 -413 -410
solve force 1e4
save Janpl1m.sav
```